Electronic Supplementary Material (ESI) for Chemical Science.

Supporting Information

The Inversion of Tetrahedral *p*-Block Element Compounds: General Trends and the Relation to the Second-Order Jahn-Teller Effect

Lukas M. Sigmund, Rouven Maier, Lutz Greb*

Correspondence to: greb@uni-heidelberg.de

Table of Contents

S1. Computational details

The Orca quantum chemistry program package[1, 2], version 4.2.1, was used throughout the entire project. Energy decomposition analyses were done with the Amsterdam Modeling suite (ADF 2019.304).[3] Computational resources were provided by the Baden-Württemberg High Performance Computing program through the bwForCluster JUSTUS2 at Ulm University. Ball and stick representations and isodensity surfaces were rendered with Chemcraft 1.8.[4]

Calculated energies and xyz coordinates of all considered compounds are given in a separate file.

Structure optimization and numerical frequency calculations at the density functional theory level

Structure optimizations with density functional theory (DFT) were done with the DFT-D3(BJ)[5, 6] version of the B97M-V functional[7] (B97M-D3(BJ))) as it was extended by Najibi and Goerigk[8]. The cc-pVTZ basis set was used (H, B, C, N, O, F[9]; Al, Si, P, Cl[10]; Ga, Ge, As, Br[11]). For iodine, the ECP-based version with weighted core functions, that is cc-pwCVTZ-PP along with the SK-MCDHF-RSC pseudo potential was employed.[12] The integration grid was set to the `Grid7 NoFinalGrid` option and SCF convergence was achieved with `VeryTightSCF` and `ConvCheckMode = 0`. For the structural convergence criteria, the parameters of the `VeryTightOpt` keyword were used (`TolE 2e-7`, `TolRMSG 8e-6`, `TolMaxG 3e-5`, `TolRMSD 1e-4`, and `TolMaxD 2e-4`). All optimizations were carried out with redundant internal coordinates. For the optimizations of the planar structures (inversion transition states), the two *trans*-valence angles of the central element were added manually (with an initial value of 180 °) to allow for a proper description of the planar states and of the inversion mode.

All obtained structures were evaluated by means of numerical frequency calculations. The numerical increment was decreased to 0.0005 Bohr and `VeryTight` SCF convergence criteria were applied.

Intrinsic reaction coordinate calculations

Calculations of the intrinsic reaction coordinate (IRC) of the inversion process were done on the exact same level of theory as applied for the structural optimizations (see above). Both directions of the IRC were investigated. The convergence criteria were significantly tightened to `TolRMSG 8e-6` and `TolMaxG 3e-5`. Except for that, the default settings for IRC calculations as implemented in Orca were used. All silicon-containing structures were investigated (46 inversion transition states).

Single point calculations at the DLPNO-CCSD(T) level

The molecular structures obtained from the DFT structure optimizations were used for single point calculations with domain-based local pair natural orbital coupled cluster theory (DLPNO-CCSD(T)).[13-16] `TightPNO` settings were chosen throughout. The cc-pVQZ basis set was used and required auxiliary basis functions were generated with the `AutoAux` keyword.[17] For iodine, the ECP-based version with weighted core functions, that is cc-pwCVQZ-PP along with the SK-MCDHF-RSC pseudo potential was employed.[12] SCF convergence was achieved with `VeryTightSCF` and `ConvCheckMode = 0`.

Time-dependent density functional calculations

Time-dependent density functional theory (TDDFT) calculations were done for a subset of the investigated inversion transition structures to compare the differences between the first vertical excitation energy (obtained from TDDFT) and the HOMO-LUMO gap (obtained from the structure optimizations). The results are shown in Chapter S12. The B97M-D3(BJ) functional and the cc-pVTZ basis set was used as described above. The same integration grid and identical SCF settings were used as for the structure optimizations. The `MaxDim` and the `NRoots` parameter were both set to 5. It was ensured that lowest-energy excited singlet state predominantly (> 95%) resulted from an electronic excitation from the b_{1g} (HOMO) to the a_{2u} (LUMO) molecular orbital.

Natural bond orbital analyses

Natural bond orbital (NBO) analyses were done with the NBO7 program (NBO 7.0. E. D. Glendening, J. K. Badenhoop, A. E. Reed, J. E. Carpenter, J. A. Bohmann, C. M. Morales, P. Karafiloglou, C. R. Landis, and F. Weinhold, Theoretical Chemistry Institute, University of Wisconsin, Madison, WI (2018)), which is applicable within Orca. The PBE0 functional[18] and the def2-TZVPP[19] (for all elements) was used. All default settings were applied. NBO analyses were carried out for all ground and inversion transition states of $\mathbf{ER_4^n}$ with $\mathbf{E^n}$ = Al^-, Si, P^+, Ga^-, Ge, As^+ and **R** = F, Cl, Br, I, OH, NH_2, CH_3, CN, CCH (see Chapter S14).

Energy decomposition analyses

For energy decomposition analyses (EDA)[20-22], the BP86[23] functional with D3(BJ) correction was used together with the TZ2P basis set[24] as implemented in ADF. The ZORA formalism was applied.[25] The frozen core approximation was turned off and the numerical quality was set to `good`. A strictly closed-shell fragmentation scheme was chosen as illustrated in Figure S29. EDAs were carried out for all ground and inversion transition states of $\mathbf{ER_4^n}$ with $\mathbf{E^n}$ = Al^-, Si, P^+, Ga^-, Ge, As^+ and **R** = H, F, Cl, Br, I, OH, NH_2, CH_3, CN, CCH.

For SiH_4 and SiF_4, the EDA was repeated with the QZ4P basis set, and a numerical quality of `very good`. The individual energy contributions into an angular and radial portion were dissected, as it is illustrated in the main article in Table 2. The results are given in Chapter S15.

Quantum theory of atoms in molecules calculations

Quantum theory of atoms in molecules (QTAIM) topological analyses was performed on the electron densities computed with the PBE0 functional and a def2-TZVPP basis set, `Grid6` and `TightSCF`, and were analyzed with AIMAll, Version 19.10.12, using the default settings.[26]

Complete active space self-consistent field and N-electron valence state perturbation theory calculations

It was not possible to calculate proper inversion transition structures for PH_4^+ and AsH_4^+ with the applied DFT method. So, these molecules were further explored with *ab initio* calculations. The ground and inversion transition structure were reoptimized with the complete active space self-consistent field (CASSCF[27]) method. The cc-pVTZ basis set was used. The same SCF and structural convergence criteria as for the DFT optimizations were applied. The same holds for the numerical increment of the frequency calculations. The final single point energies were calculated based on the strongly contracted version of the N-electron valence state perturbation theory (NEVPT2[28-31]). For those calculations, the larger cc-pVQZ basis set was used. The same SCF convergence criteria as for the CASSCF calculations were applied. Except for the mentioned changes, the default CASSCF and NEVPT2 settings of Orca were used.

For all calculations, the active space comprised the entire valence space of the compounds, that is the (highest energy) *s*- and three *p*-orbitals of the central element and the four *s*-orbitals of the hydrogen atoms (CAS(8e,8o)). As initial guess for the CASSCF structural optimizations, orbitals from a Hartree-Fock single point energy calculation (cc-pVTZ basis set) were used. With that computational procedure, it was found that the open-shell singlet configuration (singly occupied a_{2u} and b_{1g} molecular orbitals) of PH_4^+ and AsH_4^+ in the square-planar state are valid inversion transition states with only a single imaginary frequency of B_{2u} symmetry. Inversion barrier heights of 499.5 (PH_4^+) and 498.2 kJ mol^{-1} (AsH_4^+) were obtained. The active space composition is exemplarily shown for PH_4^+ in Figure S1.

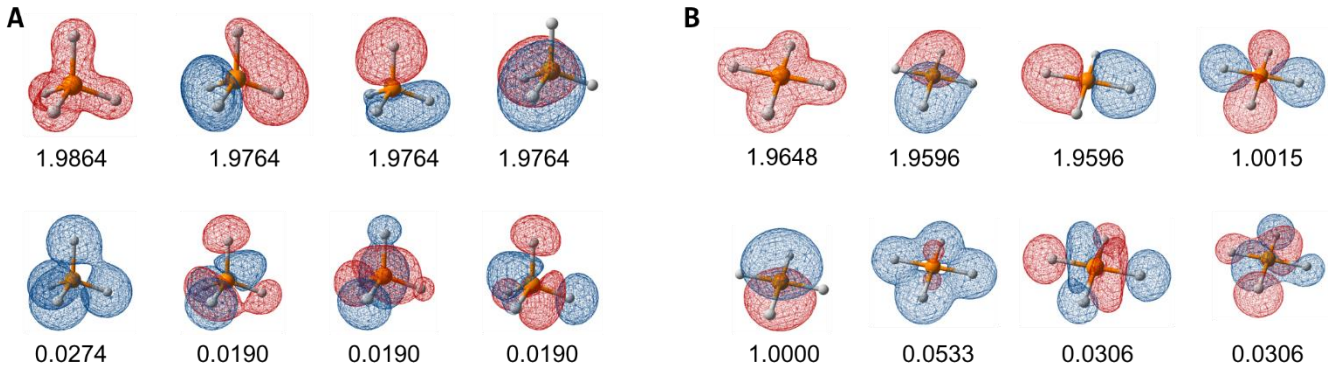

Figure S1: Isodensity surface representations and natural orbital occupation numbers of the active molecular orbitals of PH_4^+ for **A)** its ground und **B)** its inversion transition state, obtained on the CASSCF/cc-pVTZ level of theory.

S2. Inversion barriers and frontier molecular orbital energies

Table S1: Inversion barriers, frontier molecular orbital energies, and energy differences of ground and transition state of all considered compounds $EH_{4-y}R_y^n$ with E^n = Al^-, Si, P^+, Ga^-, Ge, As^+, **R** = F, Cl, Br, I, OH, NH_2, CH_3, CN, CCH, and y = 0, 1, 2, 3, 4 calculated at the B97M-D3(BJ)/cc-pVTZ and the DLPNO-CCSD(T)/cc-pVQZ//B97M-D3(BJ)/cc-pVTZ level of theory. The orbital energies were obtained from the DFT calculations. For further discussions on the structure optimizations, see Chapter S5.

Compound	Inversion barrier [kJ mol^{-1}] (B97M-D3(BJ)/ cc-pVTZ)	Inversion barrier [kJ mol^{-1}] (DLPNO-CCSD(T)/ cc-pVQZ)	Ground state HOMO energy [eV]	Ground state LUMO energy [eV]	Ground state HOMO-LUMO gap [eV]	Transition state HOMO energy [eV]	Transition state LUMO energy [eV]	Transition state HOMO-LUMO gap [eV]
Aluminum								
AlH_4^-	219.14	224.75	-1.5524	5.5542	7.1066	0.6246	2.7112	2.0866
AlH_3F^-	176.66	181.74	-1.4291	4.9834	6.4125	-0.1389	3.2283	3.3672
AlH_3Cl^-	179.05	180.00	-1.7738	4.6916	6.4654	-0.5745	2.6227	3.1972
AlH_3Br^-	174.28	172.82	-1.8369	4.4055	6.2424	-0.7786	2.3727	3.1513
AlH_3I^-	170.44	161.20	-1.6981	4.2042	5.9023	-0.8454	2.0992	2.9446
$AlH_3(OH)^-$	155.84	161.26	-0.9833	4.7460	5.7293	-0.0368	3.4201	3.4569
$AlH_3(NH_2)^-$	144.89	150.28	-0.5322	4.6824	5.2146	0.1610	3.6960	3.5350
$AlH_3(CH_3)^-$	208.00	213.24	-1.4338	4.7184	6.1522	0.4584	2.9629	2.5045
$AlH_3(CN)^-$	204.10	205.43	-2.2858	4.3674	6.6532	-0.5965	1.9790	2.5755
$AlH_3(CCH)^-$	206.52	210.33	-1.676	4.5918	6.2678	-0.0655	2.4305	2.4960
$AlH_2F_2^-$ *(cis)*	173.05	179.94	-1.4066	5.3920	6.7986	-0.4062	3.6549	4.0611
$AlH_2F_2^-$ *(trans)*	155.37	161.90	-1.4066	5.3920	6.7986	-0.8908	3.8287	4.7195
$AlH_2Cl_2^-$ *(cis)*	176.04	179.76	-2.0442	4.7932	6.8374	-1.0813	2.6706	3.7519
$AlH_2Cl_2^-$ *(trans)*	147.48	144.83	-2.0442	4.7932	6.8374	-1.7388	2.6466	4.3854
$AlH_2Br_2^-$ *(cis)*	172.06	175.40	-2.1738	4.4039	6.5777	-1.2539	2.3265	3.5804
$AlH_2Br_2^-$ *(trans)*	139.33	134.28	-2.1738	4.4039	6.5777	-1.8570	2.2587	4.1157
$AlH_2I_2^-$ *(cis)*	169.31	170.00	-2.0891	3.8974	5.9865	-1.2431	1.9734	3.2165
$AlH_2I_2^-$ *(trans)*	135.22	124.29	-2.0891	3.8974	5.9865	-1.7327	1.8702	3.6029
$AlH_2(OH)_2^-$ *(cis)*	136.64	141.27	-1.0693	4.9675	6.0368	-0.2508	4.0158	4.2666
$AlH_2(OH)_2^-$ *(trans)*	123.73	128.53	-1.0693	4.9675	6.0368	-0.7183	4.2422	4.9605
$AlH_2(NH_2)_2^-$ *(cis)*	124.59	126.18	-0.4512	4.8474	5.2986	0.0307	4.4971	4.4664
$AlH_2(NH_2)_2^-$ *(trans)*	101.46	103.42	-0.4512	4.8474	5.2986	-0.5075	4.8015	5.3090
$AlH_2(CH_3)_2^-$ *(cis)*	205.67	209.20	-1.3379	4.7504	6.0883	0.3912	3.2315	2.8403
$AlH_2(CH_3)_2^-$ *(trans)*	199.62	205.30	-1.3379	4.7504	6.0883	0.2944	3.2564	2.9620
$AlH_2(CN)_2^-$ *(cis)*	194.37	196.63	-2.9582	3.4117	6.3699	-1.6335	1.2807	2.9142
$AlH_2(CN)_2^-$ *(trans)*	185.49	182.23	-2.9582	3.4117	6.3699	-2.0851	1.2834	3.3685
$AlH_2(CCH)_2^-$ *(cis)*	197.79	202.24	-1.8096	4.0837	5.8933	-0.6207	2.1994	2.8201
$AlH_2(CCH)_2^-$ *(trans)*	194.39	195.62	-1.8096	4.0837	5.8933	-1.0394	2.1898	3.2292
$AlHF_3^-$	167.84	176.60	-2.2136	5.9064	8.1200	-1.3779	4.2268	5.6047
$AlHCl_3^-$	165.36	167.77	-2.7986	5.0759	7.8745	-2.0433	2.7489	4.7922
$AlHBr_3^-$	158.88	160.34	-2.8331	4.2843	7.1174	-2.1040	2.2641	4.3681
$AlHI_3^-$	155.02	153.41	-2.3759	3.3577	5.7336	-1.8652	1.7666	3.6318
$AlH(OH)_3^-$	117.72	121.88	-1.2726	5.0327	6.3053	-0.8917	4.7257	5.6174
$AlH(NH_2)_3^-$	109.97	107.10	-0.4055	4.7666	5.1721	-0.0237	4.6882	4.7119
$AlH(CH_3)_3^-$	205.24	208.54	-1.2996	4.5647	5.8643	0.3344	3.4682	3.1338
$AlH(CN)_3^-$	180.89	181.95	-3.9004	2.6620	6.5624	-2.9388	0.6260	3.5648

$AlH(CCH)_3^-$	189.46	193.03	-2.2514	3.7645	6.0159	-1.4264	1.9934	3.4198
AlF_4^-	180.52	191.17	-3.7330	5.2939	9.0269	-2.4367	3.9009	6.3376
$AlCl_4^-$	178.09	182.70	-3.3874	4.5367	7.9241	-2.3214	2.6057	4.9271
$AlBr_4^-$	171.61	175.78	-3.1292	3.6576	6.7868	-2.1450	1.9474	4.0924
AlI_4^-	167.74	169.34	-2.6343	2.6865	5.3208	-1.7244	1.3072	3.0316
$Al(OH)_4^-$	113.11	116.07	-1.4628	4.7418	6.2046	-1.0658	4.3609	5.4267
$Al(NH_2)_4^-$	120.64	115.78	-0.1811	4.4931	4.6742	0.1363	4.3751	4.2388
$Al(CH_3)_4^-$	211.40	213.25	-1.2804	4.2899	5.5703	0.3400	3.7306	3.3906
$Al(CN)_4^-$	173.03	175.86	-5.1094	1.9873	7.0967	-4.2702	0.0228	4.2930
$Al(CCH)_4^-$	185.30	189.64	-2.668	3.5292	6.1972	-2.0846	1.8181	3.9027
Gallium								
GaH_4^-	261.95	290.62	-1.4344	5.8583	7.2927	1.0023	2.5329	1.5306
GaH_3F^-	193.87	209.49	-1.4405	5.0239	6.4644	0.0371	2.9374	2.9003
GaH_3Cl^-	187.30	188.99	-1.7221	4.5991	6.3212	-0.6529	2.0455	2.6984
GaH_3Br^-	173.98	158.65	-1.7184	4.3032	6.0216	-0.4043	1.3008	1.7051
GaH_3I^-	162.52	131.45	-1.5124	4.0878	5.6002	-0.2437	0.9756	1.2193
$GaH_3(OH)^-$	179.07	198.56	-0.7744	4.8613	5.6357	0.2765	3.1479	2.8714
$GaH_3(NH_2)^-$	180.43	201.03	-0.4449	4.7943	5.2392	0.4812	3.4775	2.9963
$GaH_3(CH_3)^-$	243.99	271.02	-1.2977	4.8301	6.1278	0.8381	2.7208	1.8827
$GaH_3(CN)^-$	237.22	232.84	-2.2657	4.7453	7.0110	-0.4518	1.0803	1.5321
$GaH_3(CCH)^-$	246.50	271.25	-1.5984	4.9204	6.5188	0.1705	2.2109	2.0404
$GaH_2F_2^-$ *(cis)*	173.68	189.86	-1.6407	5.2753	6.9160	-0.5473	3.2646	3.8119
$GaH_2F_2^-$ *(trans)*	146.13	157.35	-1.6407	5.2753	6.9160	-1.4139	3.3537	4.7676
$GaH_2Cl_2^-$ *(cis)*	187.06	202.91	-2.1427	4.5329	6.6756	-1.1521	2.2799	3.4320
$GaH_2Cl_2^-$ *(trans)*	134.01	137.28	-2.1427	4.5329	6.6756	-1.9173	2.1311	4.0484
$GaH_2Br_2^-$ *(cis)*	186.13	200.77	-2.1809	3.9746	6.1555	-1.2697	1.9656	3.2353
$GaH_2Br_2^-$ *(trans)*	129.24	128.55	-2.1809	3.9746	6.1555	-1.9228	1.7808	3.7036
$GaH_2I_2^-$ *(cis)*	187.41	196.57	-2.0041	3.4000	5.4041	-1.1912	1.6774	2.8686
$GaH_2I_2^-$ *(trans)*	131.75	119.59	-2.0041	3.4000	5.4041	-1.6899	1.4623	3.1522
$GaH_2(OH)_2^-$ *(cis)*	143.65	161.30	-1.048	4.9820	6.0300	-0.1515	3.6595	3.8110
$GaH_2(OH)_2^-$ *(trans)*	133.76	149.18	-1.048	4.9820	6.0300	-0.423	3.7938	4.2168
$GaH_2(NH_2)_2^-$ *(cis)*	152.81	168.26	-0.524	4.8236	5.3476	0.3009	4.005	3.7041
$GaH_2(NH_2)_2$ *(trans)*	136.54	151.43	-0.524	4.8236	5.3476	0.1361	4.2766	4.1405
$GaH_2(CH_3)_2$ *(cis)*	237.09	260.53	-1.2047	4.7971	6.0018	0.7989	2.9583	2.1594
$GaH_2(CH_3)_2^-$ *(trans)*	228.15	256.95	-1.2047	4.7971	6.0018	0.6869	2.9643	2.2774
$GaH_2(CN)_2^-$ *(cis)*	235.99	258.82	-3.0303	3.7631	6.7934	-1.4494	1.0506	2.5000
$GaH_2(CN)_2^-$ *(trans)*	212.12	225.83	-3.0303	3.7631	6.7934	-2.0168	1.0092	3.0260
$GaH_2(CCH)_2^-$ *(cis)*	238.39	264.94	-1.797	4.3699	6.1669	-0.4037	1.962	2.3657
$GaH_2(CCH)_2^-$ *(trans)*	228.09	249.27	-1.797	4.3699	6.1669	-0.9308	1.9278	2.8586
$GaHF_3^-$	147.31	163.21	-2.6070	5.1707	7.7777	-1.7588	3.6708	5.4296
$GaHCl_3^-$	157.58	169.94	-2.9203	3.9922	6.9125	-2.2178	2.2563	4.4741
$GaHBr_3^-$	156.02	165.78	-2.8031	3.2509	6.0540	-2.1954	1.8338	4.0292
$GaHI_3^-$	158.79	161.31	-2.3469	2.5220	4.8689	-1.9216	1.4325	3.3541
$GaH(OH)_3^-$	114.87	130.83	-1.2529	4.7510	6.0039	-0.7567	4.2779	5.0346
$GaH(NH_2)_3^-$	130.49	142.86	-0.5722	4.6346	5.2068	0.0646	4.4313	4.3667
$GaH(CH_3)_3^-$	230.11	254.66	-1.1686	4.5804	5.7490	0.7481	3.195	2.4469
$GaH(CN)_3^-$	217.97	239.04	-3.9914	2.9759	6.9673	-2.7860	0.3386	3.1246
$GaH(CCH)_3^-$	226.12	252.01	-2.2563	3.9988	6.2551	-1.3251	1.7204	3.0455
GaF_4^-	142.44	161.07	-3.8408	4.1008	7.9416	-2.7590	3.1673	5.9263
$GaCl_4^-$	164.09	179.54	-3.4693	3.1434	6.6127	-2.5014	1.6436	4.1450

$GaBr_4^-$	163.84	176.39	-3.1902	2.3811	5.5713	-2.2857	1.0381	3.3238
GaI_4^-	168.02	173.25	-2.6680	1.6841	4.3521	-1.8209	0.5219	2.3428
$Ga(OH)_4^-$	92.08	108.12	-1.5904	4.2569	5.8473	-1.2225	3.9222	5.1447
$Ga(NH_2)_4^-$	126.63	137.33	-0.3440	4.2387	4.5827	-0.0428	4.0808	4.1236
$Ga(CH_3)_4^-$	235.45	256.81	-1.1406	4.2897	5.4303	0.8320	3.3589	2.5269
$Ga(CN)_4^-$	212.04	235.08	-5.0401	2.1958	7.2359	-3.8630	-0.3009	3.5621
$Ga(CCH)_4^-$	221.51	247.74	-2.7237	3.6927	6.4164	-2.1953	1.5238	3.7191
Silicon								
SiH_4	364.28	380.08	-9.0306	0.3463	9.3769	-5.5586	-4.4689	1.0897
SiH_3F	265.84	280.76	-8.8366	-0.7443	8.0923	-6.9366	-3.8247	3.1119
SiH_3Cl	280.01	292.80	-8.2103	-0.7207	7.4896	-6.7627	-4.2307	2.5320
SiH_3Br	278.69	291.22	-7.7418	-0.9693	6.7725	-6.6453	-4.3037	2.3416
SiH_3I	279.05	290.46	-7.0145	-1.2743	5.7402	-6.3170	-4.2922	2.0248
$SiH_3(OH)$	245.90	261.65	-7.7538	-0.5188	7.2350	-6.4275	-3.2606	3.1669
$SiH_3(NH_2)$	220.06	235.74	-6.5771	-0.2191	6.3580	-5.9551	-2.6767	3.2784
$SiH_3(CH_3)$	344.74	361.58	-8.4250	0.0902	8.5152	-5.4075	-3.7674	1.6401
$SiH_3(CN)$	332.83	347.47	-8.8911	-1.4644	7.4267	-6.7433	-5.0817	1.6616
$SiH_3(CCH)$	328.68	347.88	-7.4547	-0.8725	6.5822	-5.9002	-4.2028	1.6974
SiH_2F_2 *(cis)*	249.87	267.56	-8.8776	-0.2541	8.6235	-7.4541	-3.3517	4.1024
SiH_2F_2 *(trans)*	212.10	225.12	-8.8776	-0.2541	8.6235	-8.1524	-3.0833	5.0691
SiH_2Cl_2 *(cis)*	262.20	276.29	-8.2472	-0.5550	7.6922	-7.0229	-3.9948	3.0281
SiH_2Cl_2 *(trans)*	219.07	228.07	-8.2472	-0.5550	7.6922	-7.5561	-3.9432	3.6129
SiH_2Br_2 *(cis)*	257.91	271.93	-7.8254	-1.1798	6.6456	-6.7606	-4.1100	2.6506
SiH_2Br_2 *(trans)*	215.97	224.90	-7.8254	-1.1798	6.6456	-7.1945	-4.0784	3.1161
SiH_2I_2 *(cis)*	253.52	267.86	-6.9619	-1.8303	5.1316	-6.2178	-4.1288	2.0890
SiH_2I_2 *(trans)*	218.02	225.54	-6.9619	-1.8303	5.1316	-6.5680	-4.1022	2.4658
$SiH_2(OH)_2$ *(cis)*	213.34	229.97	-7.8666	0.0018	7.8684	-6.6818	-2.3525	4.3293
$SiH_2(OH)_2$ *(trans)*	186.98	198.16	-7.8666	0.0018	7.8684	-7.6153	-1.959	5.6563
$SiH_2(NH_2)_2$ *(cis)*	184.09	196.74	-6.3522	0.4962	6.8484	-6.0499	-1.4143	4.6356
$SiH_2(NH_2)_2$ *(trans)*	143.40	152.50	-6.3522	0.4962	6.8484	-6.6294	-0.9126	5.7168
$SiH_2(CH_3)_2$ *(cis)*	340.03	355.56	-7.9863	0.4322	8.4185	-5.2333	-3.2126	2.0207
$SiH_2(CH_3)_2$ *(trans)*	330.78	347.35	-7.9863	0.4322	8.4185	-5.3175	-3.1141	2.2034
$SiH_2(CN)_2$ *(cis)*	306.78	325.77	-9.2935	-2.3937	6.8998	-7.7146	-5.6022	2.1124
$SiH_2(CN)_2$ *(trans)*	297.31	309.94	-9.2935	-2.3937	6.8998	-8.0462	-5.6075	2.4387
$SiH_2(CCH)_2$ *(cis)*	302.90	326.21	-7.3294	-1.1557	6.1737	-6.1721	-4.0196	2.1525
$SiH_2(CCH)_2$ *(trans)*	298.65	317.17	-7.3294	-1.1557	6.1737	-6.5979	-4.0108	2.5871
$SiHF_3$	234.43	251.78	-10.0852	0.5486	10.6338	-8.8799	-2.6673	6.2126
$SiHCl_3$	240.49	252.27	-8.5182	-0.6794	7.8388	-7.7101	-3.7607	3.9494
$SiHBr_3$	232.81	245.14	-7.7892	-1.5634	6.2258	-7.1805	-3.9469	3.2336
$SiHI_3$	226.71	238.85	-6.8245	-2.3423	4.4822	-6.3347	-4.0205	2.3142
$SiH(OH)_3$	183.64	196.60	-7.9388	0.2543	8.1931	-7.5506	-1.2143	6.3363
$SiH(NH_2)_3$	159.02	166.48	-5.8591	0.5389	6.3980	-5.6291	0.0378	5.6669
$SiH(CH_3)_3$	339.64	353.20	-7.6716	0.4548	8.1264	-5.1158	-2.7085	2.4073
$SiH(CN)_3$	278.61	298.85	-9.8366	-3.1289	6.7077	-8.7850	-6.0576	2.7274
$SiH(CCH)_3$	282.13	305.86	-7.2659	-1.3467	5.9192	-6.6111	-3.8885	2.7226
SiF_4	258.26	277.58	-11.2712	-0.1021	11.1691	-9.6745	-2.9337	6.7408
$SiCl_4$	259.83	271.54	-8.6563	-1.1219	7.5344	-7.4324	-3.5838	3.8486
$SiBr_4$	246.88	261.40	-7.8752	-2.0590	5.8162	-6.7822	-3.8816	2.9006
SiI_4	236.37	250.18	-6.8488	-2.8050	4.0438	-5.8760	-4.0996	1.7764
$Si(OH)_4$	183.59	195.49	-7.8362	-0.0440	7.7922	-7.4387	-1.1225	6.3162

$Si(NH_2)_4$	184.84	188.12	-5.6957	0.3405	6.0362	-5.0370	-0.1091	4.9279
$Si(CH_3)_4$	356.82	365.68	-7.4099	0.2558	7.6657	-4.9453	-2.4186	2.5267
$Si(CN)_4$	260.03	283.52	-10.2224	-3.6606	6.5618	-9.6103	-6.4548	3.1555
$Si(CCH)_4$	271.49	296.30	-7.2216	-1.3481	5.8735	-6.5625	-3.8036	2.7589
Germanium								
GeH_4	394.14	426.93	-8.8564	0.5531	9.4095	-5.2909	-4.6273	0.6636
GeH_3F	273.52	296.03	-8.7293	-0.9154	7.8139	-6.8364	-4.1923	2.6441
GeH_3Cl	286.50	308.49	-7.9513	-0.9886	6.9627	-6.6659	-4.5414	2.1245
GeH_3Br	286.08	308.06	-7.5090	-1.2306	6.2784	-6.5073	-4.5796	1.9277
GeH_3I	288.80	307.55	-6.8478	-1.4934	5.3544	-6.1452	-4.5112	1.6340
$GeH_3(OH)$	261.63	288.32	-7.4031	-0.6101	6.7930	-6.2224	-3.6432	2.5792
$GeH_3(NH_2)$	248.16	275.00	-6.4695	-0.2552	6.2143	-5.7611	-3.0115	2.7496
$GeH_3(CH_3)$	370.99	403.68	-8.1264	0.1765	8.3029	-5.1203	-4.0649	1.0554
$GeH_3(CN)$	356.49	386.58	-8.7230	-1.0401	7.6829	-6.5892	-5.2333	1.3559
$GeH_3(CCH)$	355.73	391.77	-7.2786	-0.5076	6.7710	-5.7311	-4.3905	1.3406
GeH_2F_2 *(cis)*	236.86	259.97	-9.0274	-0.7312	8.2962	-7.6455	-3.8947	3.7508
GeH_2F_2 *(trans)*	192.17	209.93	-9.0274	-0.7312	8.2962	-8.5163	-3.7584	4.7579
GeH_2Cl_2 *(cis)*	258.52	281.23	-8.1800	-1.3301	6.8499	-7.1118	-4.3295	2.7823
GeH_2Cl_2 *(trans)*	206.67	223.09	-8.1800	-1.3301	6.8499	-7.6623	-4.3386	3.3237
GeH_2Br_2 *(cis)*	256.77	280.39	-7.7311	-1.7966	5.9345	-6.8096	-4.3680	2.4416
GeH_2Br_2 *(trans)*	208.03	224.54	-7.7311	-1.7966	5.9345	-7.2611	-4.3875	2.8736
GeH_2I_2 *(cis)*	255.89	278.05	-6.8871	-2.2418	4.6453	-6.2478	-4.2934	1.9544
GeH_2I_2 *(trans)*	216.21	229.38	-6.8871	-2.2418	4.6453	-6.6118	-4.3029	2.3089
$GeH_2(OH)_2$ *(cis)*	208.87	234.65	-7.6032	-0.2129	7.3903	-6.7167	-2.9186	3.7981
$GeH_2(OH)_2$ *(trans)*	187.09	206.89	-7.6032	-0.2129	7.3903	-7.1088	-2.6887	4.4201
$GeH_2(NH_2)_2$ *(cis)*	197.79	220.17	-6.3278	0.1494	6.4772	-6.0122	-1.8891	4.1231
$GeH_2(NH_2)_2$ *(trans)*	167.27	185.33	-6.3278	0.1494	6.4772	-6.2314	-1.5847	4.6467
$GeH_2(CH_3)_2$ *(cis)*	359.36	389.92	-7.7017	0.4674	8.1691	-4.9371	-3.5804	1.3567
$GeH_2(CH_3)_2$ *(trans)*	351.15	383.06	-7.7017	0.4674	8.1691	-4.9843	-3.5294	1.4549
$GeH_2(CN)_2$ *(cis)*	330.86	365.25	-9.1977	-1.9911	7.2066	-7.5524	-5.7411	1.8113
$GeH_2(CN)_2$ *(trans)*	312.54	341.05	-9.1977	-1.9911	7.2066	-7.8504	-5.7722	2.0782
$GeH_2(CCH)_2$ *(cis)*	327.62	367.88	-7.2549	-0.8489	6.4060	-6.0933	-4.2222	1.8711
$GeH_2(CCH)_2$ *(trans)*	320.33	355.87	-7.2549	-0.8489	6.4060	-6.5008	-4.2287	2.2721
$GeHF_3$	193.47	216.32	-10.1936	-1.2712	8.9224	-9.1438	-3.5069	5.6369
$GeHCl_3$	217.85	236.87	-8.4938	-2.0305	6.4633	-7.8533	-4.1503	3.7030
$GeHBr_3$	216.08	236.10	-7.8003	-2.5210	5.2793	-7.2528	-4.2166	3.0362
$GeHI_3$	217.40	234.97	-6.8607	-2.9283	3.9324	-6.4084	-4.1598	2.2486
$GeH(OH)_3$	159.56	182.09	-7.7178	-0.3993	7.3185	-7.4473	-2.0782	5.3691
$GeH(NH_2)_3$	166.01	180.61	-6.2022	0.1864	6.3886	-5.7655	-0.845	4.9205
$GeH(CH_3)_3$	350.53	378.52	-7.4398	0.4352	7.8750	-4.7719	-3.1415	1.6304
$GeH(CN)_3$	297.11	332.65	-9.7620	-2.7592	7.0028	-8.5883	-6.2124	2.3759
$GeH(CCH)_3$	301.85	342.40	-7.2771	-1.0968	6.1803	-8.5883	-6.2124	2.3759
GeF_4	185.76	212.36	-11.2093	-2.5464	8.6629	-9.9339	-4.0681	5.8658
$GeCl_4$	218.45	236.91	-8.7530	-2.8138	5.9392	-7.6709	-4.4844	3.1865
$GeBr_4$	214.39	235.03	-7.9687	-3.2522	4.7165	-6.9864	-4.6562	2.3302
GeI_4	213.94	231.36	-6.9336	-3.5335	3.4001	-6.0403	-4.6485	1.3918
$Ge(OH)_4$	133.77	156.28	-7.9387	-0.9222	7.0165	-7.5995	-1.9533	5.6462
$Ge(NH_2)_4$	173.56	185.40	-5.8926	-0.1025	5.7901	-5.6307	-0.7029	4.9278
$Ge(CH_3)_4$	356.12	378.05	-7.2216	0.2210	7.4426	-4.5537	-2.8587	1.6950
$Ge(CN)_4$	275.20	313.95	-10.2320	-3.4008	6.8312	-9.3596	-6.6180	2.7416

$Ge(CCH)_4$	285.89	327.45	-7.2999	-1.1724	6.1275	-6.6934	-4.0282	2.6652
Phosphorus								
PH_3F^+	393.19	407.91	-17.5408	-8.5796	8.9612	-15.2010	-13.1155	2.0855
PH_3Cl^+	407.51	419.46	-15.0939	-8.0064	7.0875	-13.9576	-12.6513	1.3063
PH_3Br^+	396.89	407.96	-14.1207	-8.1289	5.9918	-13.4493	-12.3195	1.1298
PH_3I^+	381.52	387.48	-12.8630	-8.2218	4.6412	-12.6248	-11.7526	0.8722
$PH_3(OH)^+$	364.48	376.99	-15.4914	-7.6143	7.8771	-14.1330	-11.9683	2.1647
$PH_3(NH_2)^+$	312.70	319.05	-13.5878	-6.7973	6.7905	-13.2327	-10.9095	2.3232
$PH_3(CH_3)^+$	528.33	540.49	-16.2382	-6.1668	10.0714	-12.5019	-11.1223	1.3796
$PH_3(CN)^+$	495.63	520.38	-15.3083	-8.3758	6.9325	-13.7514	-13.4800	0.2714
$PH_3(CCH)^+$	462.62	487.06	-13.569	-7.3679	6.2011	-12.5284	-12.015	0.5134
$PH_2F_2^+$ *(cis)*	347.59	368.00	-17.5742	-8.1063	9.4679	-15.8402	-12.6125	3.2277
$PH_2F_2^+$ *(trans)*	271.82	288.03	-17.5742	-8.1063	9.4679	-16.6360	-12.2685	4.3675
$PH_2Cl_2^+$ *(cis)*	356.07	373.67	-14.8192	-7.8926	6.9266	-13.6032	-11.9045	1.6987
$PH_2Cl_2^+$ *(trans)*	288.10	304.81	-14.8192	-7.8926	6.9266	-14.0187	-11.7104	2.3083
$PH_2Br_2^+$ *(cis)*	340.43	361.30	-13.7026	-8.1956	5.5070	-12.8157	-11.5007	1.3150
$PH_2Br_2^+$ *(trans)*	280.38	300.15	-13.7026	-8.1956	5.5070	-13.1296	-11.2981	1.8315
$PH_2I_2^+$ *(cis)*	320.23	344.38	-12.2077	-8.3310	3.8767	-11.6819	-10.8187	0.8632
$PH_2I_2^+$ *(trans)*	273.96	297.68	-12.2077	-8.3310	3.8767	-11.8995	-10.5950	1.3045
$PH_2(OH)_2^+$ *(cis)*	304.89	323.59	-15.4834	-6.5790	8.9044	-14.2713	-10.7033	3.5680
$PH_2(OH)_2^+$ *(trans)*	242.23	255.48	-15.4834	-6.5790	8.9044	-15.2684	-10.1731	5.0953
$PH_2(NH_2)_2^+$ *(cis)*	250.44	262.45	-13.0896	-5.4726	7.6170	-13.1675	-9.1169	4.0506
$PH_2(NH_2)_2^+$ *(trans)*	173.99	180.79	-13.0896	-5.4726	7.6170	-13.4995	-8.4647	5.0348
$PH_2(CH_3)_2^+$ *(cis)*	519.07	540.95	-15.3097	-5.4241	9.8856	-11.7984	-11.0366	0.7618
$PH_2(CH_3)_2^+$ *(trans)*	499.00	520.28	-15.3097	-5.4241	9.8856	-11.8694	-10.7678	1.1016
$PH_2(CN)_2^+$ *(cis)*	422.44	460.63	-15.3930	-9.0294	6.3636	-14.3141	-13.3056	1.0085
$PH_2(CN)_2^+$ *(trans)*	402.81	438.80	-15.3930	-9.0294	6.3636	-14.5489	-13.2326	1.3163
$PH_2(CCH)_2^+$ *(cis)*	394.13	432.82	-12.9933	-7.2357	5.7576	-12.2023	-10.9788	1.2235
$PH_2(CCH)_2^+$ *(trans)*	376.65	412.10	-12.9933	-7.2357	5.7576	-12.638	-10.8758	1.7622
PHF_3^+	304.49	327.50	-18.9268	-7.2759	11.6509	-17.4288	-11.9180	5.5108
$PHCl_3^+$	308.09	326.54	-14.4428	-7.9300	6.5128	-13.7474	-11.2791	2.4683
$PHBr_3^+$	289.95	313.25	-13.1601	-8.3246	4.8355	-12.6102	-10.8643	1.7459
PHI_3^+	271.15	298.64	-11.5991	-8.4276	3.1715	-11.1812	-10.1606	1.0206
$PH(OH)_3^+$	248.98	267.21	-15.24	-5.4458	9.7942	-15.0719	-9.291	5.7809
$PH(NH_2)_3^+$	207.99	217.66	-12.3159	-4.5027	7.8132	-12.1562	-7.3223	4.8339
$PH(CH_3)_3^+$	510.48	531.77	-14.6592	-4.7573	9.9019	-11.3352	-10.1785	1.1567
$PH(CN)_3^+$	356.69	403.65	-15.4976	-9.5123	5.9853	-14.8950	-13.2139	1.6811
$PH(CCH)_3^+$	346.27	391.80	-12.4238	-7.0360	5.3878	-12.045	-10.2611	1.7839
PF_4^+	337.21	365.73	-19.6448	-7.6412	12.0036	-17.8545	-11.7707	6.0838
PCl_4^+	325.56	344.59	-14.3108	-8.1799	6.1309	-13.0133	-10.9193	2.0940
PBr_4^+	298.58	326.85	-12.9486	-8.5420	4.4066	-11.8308	-10.5339	1.2969
PI_4^+	276.07	308.26	-11.3166	-8.5369	2.7797	-10.3475	-9.8603	0.4872
$P(OH)_4^+$	257.16	277.97	-14.8981	-5.5703	9.3278	-14.4783	-8.3539	6.1244
$P(NH_2)_4^+$	249.58	258.21	-11.9683	-4.4011	7.5672	-11.4697	-6.4147	5.0550
$P(CH_3)_4^+$	540.99	558.68	-14.1379	-4.2067	9.9312	-10.8642	-9.8706	0.9936
$P(CN)_4^+$	316.55	369.69	-15.6347	-9.7759	5.8588	-15.0105	-13.2157	1.7948
$P(CCH)_4^+$	327.32	376.35	-12.1087	-6.6829	5.4258	-11.4122	-9.8006	1.6116
Arsenic								
AsH_3F^+	365.36	392.78	-16.8303	-8.5398	8.2905	-14.7618	-12.9234	1.8384
AsH_3Cl^+	380.22	405.97	-14.6059	-8.1430	6.4629	-13.6517	-12.4105	1.2412

AsH_3Br^+	373.67	397.20	-13.7536	-8.2356	5.5180	-13.1683	-12.0565	1.1118
AsH_3I^+	364.94	379.94	-12.6250	-8.2619	4.3631	-12.4007	-11.4796	0.9211
$AsH_3(OH)^+$	346.47	372.44	-14.7582	-7.6009	7.1573	-13.7244	-11.8757	1.8487
$AsH_3(NH_2)^+$	308.34	326.73	-13.2228	-6.7408	6.4820	-12.9286	-10.8317	2.0969
$AsH_3(CN)^+$	466.44	516.34	-14.9162	-7.8112	7.1050	-13.7047	-12.6213	1.0834
$AsH_3(CCH)^+$	447.65	494.78	-13.2076	-6.9006	6.3070	-12.3297	-11.792	0.5377
$AsH_2F_2^+$ *(cis)*	303.18	331.19	-17.1600	-8.4185	8.7415	-15.6391	-12.6130	3.0261
$AsH_2F_2^+$ *(trans)*	236.07	259.58	-17.1600	-8.4185	8.7415	-16.4443	-12.4094	4.0349
$AsH_2Cl_2^+$ *(cis)*	322.45	350.83	-14.5357	-8.4259	6.1098	-13.5206	-11.7702	1.7504
$AsH_2Cl_2^+$ *(trans)*	262.19	288.84	-14.5357	-8.4259	6.1098	-13.8932	-11.6179	2.2753
$AsH_2Br_2^+$ *(cis)*	313.52	344.40	-13.4780	-8.5566	4.9214	-12.7359	-11.3270	1.4089
$AsH_2Br_2^+$ *(trans)*	261.51	290.10	-13.4780	-8.5566	4.9214	-13.0249	-11.1554	1.8695
$AsH_2I_2^+$ *(cis)*	301.96	332.93	-12.0967	-8.5047	3.5920	-11.6246	-10.6309	0.9937
$AsH_2I_2^+$ *(trans)*	264.08	292.86	-12.0967	-8.5047	3.5920	-11.8307	-10.4294	1.4013
$AsH_2(OH)_2^+$ *(cis)*	269.52	297.98	-14.7695	-6.8736	7.8959	-14.1062	-10.8554	3.2508
$AsH_2(OH)_2^+$ *(trans)*	223.85	246.04	-14.7695	-6.8736	7.8959	-14.5492	-10.5075	4.0417
$AsH_2(NH_2)_2^+$ *(cis)*	231.33	254.25	-12.7267	-5.7518	6.9749	-12.7098	-9.2513	3.4585
$AsH_2(NH_2)_2^+$ *(trans)*	176.03	193.17	-12.7267	-5.7518	6.9749	-12.836	-8.8276	4.0084
$AsH_2(CH_3)_2^+$ *(cis)*	500.16	540.72	-14.8027	-5.3413	9.4614	-11.3952	-11.1877	0.2075
$AsH_2(CH_3)_2^+$ *(trans)*	486.75	527.34	-14.8027	-5.3413	9.4614	-11.4147	-11.039	0.3757
$AsH_2(CN)_2^+$ *(cis)*	407.77	465.56	-15.0772	-8.4978	6.5794	-14.0516	-13.0511	1.0005
$AsH_2(CN)_2^+$ *(trans)*	385.22	442.28	-15.0772	-8.4978	6.5794	-14.2061	-12.9834	1.2227
$AsH_2(CCH)_2^+$ *(cis)*	384.07	442.85	-12.7787	-6.8660	5.9127	-12.1535	-10.8657	1.2878
$AsH_2(CCH)_2^+$ *(trans)*	367.97	424.43	-12.7787	-6.8660	5.9127	-12.5073	-10.7722	1.7351
$AsHF_3^+$	236.12	264.31	-18.3714	-9.3368	9.0346	-17.2123	-12.2198	4.9925
$AsHCl_3^+$	264.12	289.59	-14.3334	-8.8924	5.4410	-13.6983	-11.2090	2.4893
$AsHBr_3^+$	257.00	286.18	-13.1218	-8.9225	4.1993	-12.5975	-10.7270	1.8705
$AsHI_3^+$	250.35	280.65	-11.6109	-8.7067	2.9042	-11.1949	-9.9938	1.2011
$AsH(OH)_3^+$	196.58	222.30	-14.7724	-6.8979	7.8745	-14.6827	-9.7758	4.9069
$AsH(NH_2)_3^+$	190.32	205.82	-12.1577	-5.2409	6.9168	-11.9419	-7.7603	4.1816
$AsH(CH_3)_3^+$	484.04	522.07	-14.1975	-4.6453	9.5522	-10.8986	-10.3774	0.5212
$AsH(CN)_3^+$	344.20	407.60	-15.3085	-9.0392	6.2693	-14.6009	-13.0142	1.5867
$AsH(CCH)_3^+$	337.00	399.34	-12.3673	-6.7423	5.6250	-12.0081	-10.2172	1.7909
AsF_4^+	225.55	257.95	-19.1540	-10.8338	8.3202	-17.7647	-12.6699	5.0948
$AsCl_4^+$	260.23	283.27	-14.3197	-9.4353	4.8844	-13.1828	-11.0809	2.1019
$AsBr_4^+$	249.64	279.32	-12.9838	-9.3138	3.6700	-11.9802	-10.6289	1.3513
AsI_4^+	242.67	273.51	-11.3666	-8.8995	2.4671	-10.4750	-9.8907	0.5843
$As(OH)_4^+$	169.96	197.22	-14.7818	-7.2906	7.4912	-14.4042	-9.2122	5.1920
$As(NH_2)_4^+$	206.12	217.70	-11.9567	-5.1742	6.7825	-11.4305	-6.8674	4.5631
$As(CH_3)_4^+$	493.22	525.68	-13.7115	-4.1724	9.5391	-10.4111	-9.9535	0.4576
$As(CN)_4^+$	303.12	369.80	-15.5171	-9.4075	6.1096	-14.9358	-13.0522	1.8836
$As(CCH)_4^+$	313.65	376.56	-12.1282	-6.4528	5.6754	-11.4827	-9.7834	1.6993

S3. T1 diagnostics

Table S2: T1 diagnostics of all considered compounds $EH_{4-y}R_y^n$ with E^n = Al^-, Si, P^+, Ga^-, Ge, As^+, **R** = F, Cl, Br, I, OH, NH_2, CH_3, CN, CCH, and y = 0, 1, 2, 3, 4 calculated at the DLPNO-CCSD(T)/cc-pVQZ level of theory.

Compound	Ground state	Inversion transition state	Compound	Ground state	Inversion transition state
Aluminum			**Gallium**		
AlH_4^-	0.01009231	0.00896273	GaH_4^-	0.01536578	0.01419500
AlH_3F^-	0.01016018	0.01204583	GaH_3F^-	0.01369242	0.01496438
AlH_3Cl^-	0.00711487	0.00846520	GaH_3Cl^-	0.01241114	0.01268891
AlH_3Br^-	0.00635317	0.00694931	GaH_3Br^-	0.01078985	0.01033029
AlH_3I^-	0.00823962	0.00852681	GaH_3I^-	0.01163943	0.01124518
$AlH_3(OH)^-$	0.01022205	0.01306864	$GaH_3(OH)^-$	0.01385952	0.01613993
$AlH_3(NH_2)^-$	0.00932166	0.01196227	$GaH_3(NH_2)^-$	0.01351100	0.01552136
$AlH_3(CH_3)^-$	0.00939141	0.00977811	$GaH_3(CH_3)^-$	0.01345779	0.01325302
$AlH_3(CN)^-$	0.01314306	0.01332283	$GaH_3(CN)^-$	0.01524918	0.01477962
$AlH_3(CCH)^-$	0.01282137	0.01315291	$GaH_3(CCH)^-$	0.01510147	0.01471305
$AlH_2F_2^-$ *(cis)*	0.01065204	0.01187185	$GaH_2F_2^-$ *(cis)*	0.01310791	0.01443041
$AlH_2F_2^-$ *(trans)*	0.01065204	0.01253178	$GaH_2F_2^-$ *(trans)*	0.01310791	0.01479198
$AlH_2Cl_2^-$ *(cis)*	0.00631287	0.00782332	$GaH_2Cl_2^-$ *(cis)*	0.01080841	0.01184685
$AlH_2Cl_2^-$ *(trans)*	0.00631287	0.00790256	$GaH_2Cl_2^-$ *(trans)*	0.01080841	0.01175365
$AlH_2Br_2^-$ *(cis)*	0.00570971	0.00642165	$GaH_2Br_2^-$ *(cis)*	0.00893522	0.00946635
$AlH_2Br_2^-$ *(trans)*	0.00570971	0.00640345	$GaH_2Br_2^-$ *(trans)*	0.00893522	0.00936463
$AlH_2I_2^-$ *(cis)*	0.00799490	0.00842527	$GaH_2I_2^-$ *(cis)*	0.01022087	0.01060671
$AlH_2I_2^-$ *(trans)*	0.00799490	0.00846786	$GaH_2I_2^-$ *(trans)*	0.01022087	0.01062361
$AlH_2(OH)_2^-$ *(cis)*	0.01091957	0.01245980	$GaH_2(OH)_2^-$ *(cis)*	0.01337299	0.01518488
$AlH_2(OH)_2^-$ *(trans)*	0.01091957	0.01326520	$GaH_2(OH)_2^-$ *(trans)*	0.01337299	0.01572757
$AlH_2(NH_2)_2^-$ *(cis)*	0.00958915	0.01061763	$GaH_2(NH_2)_2^-$ *(cis)*	0.01259241	0.01402123
$AlH_2(NH_2)_2^-$ *(trans)*	0.00958915	0.01125548	$GaH_2(NH_2)_2$ *(trans)*	0.01259241	0.01434787
$AlH_2(CH_3)_2^-$ *(cis)*	0.00921247	0.00977630	$GaH_2(CH_3)_2$ *(cis)*	0.01226503	0.01239254
$AlH_2(CH_3)_2^-$ *(trans)*	0.00921247	0.00998230	$GaH_2(CH_3)_2^-$ *(trans)*	0.01226503	0.01254598
$AlH_2(CN)_2^-$ *(cis)*	0.01390048	0.01433545	$GaH_2(CN)_2^-$ *(cis)*	0.01509213	0.01507472
$AlH_2(CN)_2^-$ *(trans)*	0.01390048	0.01437915	$GaH_2(CN)_2^-$ *(trans)*	0.01509213	0.01509137
$AlH_2(CCH)_2^-$ *(cis)*	0.01353382	0.01408958	$GaH_2(CCH)_2^-$ *(cis)*	0.01490521	0.01486683
$AlH_2(CCH)_2^-$ *(trans)*	0.01353382	0.01421702	$GaH_2(CCH)_2^-$ *(trans)*	0.01490521	0.01492191
$AlHF_3^-$	0.01079339	0.01199223	$GaHF_3^-$	0.01271276	0.01412604
$AlHCl_3^-$	0.00611428	0.00753690	$GaHCl_3^-$	0.00985499	0.01100801
$AlHBr_3^-$	0.00552288	0.00617940	$GaHBr_3^-$	0.00796162	0.00855865
$AlHI_3^-$	0.00793330	0.00833535	$GaHI_3^-$	0.00946384	0.00991850
$AlH(OH)_3^-$	0.01101102	0.01233360	$GaH(OH)_3^-$	0.01304438	0.01457143
$AlH(NH_2)_3^-$	0.00966443	0.01039650	$GaH(NH_2)_3^-$	0.01196857	0.01321626
$AlH(CH_3)_3^-$	0.00919511	0.00983357	$GaH(CH_3)_3^-$	0.01145309	0.01183377
$AlH(CN)_3^-$	0.01419367	0.01474720	$GaH(CN)_3^-$	0.01496159	0.01515386
$AlH(CCH)_3^-$	0.01381135	0.01449580	$GaH(CCH)_3^-$	0.01474695	0.01488103
AlF_4^-	0.01056424	0.01143835	GaF_4^-	0.01224954	0.01348801
$AlCl_4^-$	0.00596427	0.00709237	$GaCl_4^-$	0.00913839	0.01032087
$AlBr_4^-$	0.00542689	0.00594022	$GaBr_4^-$	0.00732552	0.00796818
AlI_4^-	0.00781917	0.00809386	GaI_4^-	0.00893492	0.00934331
$Al(OH)_4^-$	0.01086671	0.01168363	$Ga(OH)_4^-$	0.01258408	0.01380224
$Al(NH_2)_4^-$	0.00955732	0.01006414	$Ga(NH_2)_4^-$	0.01153083	0.01246649

$Al(CH_3)_4^-$	0.00923787	0.00977889	$Ga(CH_3)_4^-$	0.01090273	0.01131380
$Al(CN)_4^-$	0.01436861	0.01494258	$Ga(CN)_4^-$	0.01487815	0.01517579
$Al(CCH)_4^-$	0.01395565	0.01461473	$Ga(CCH)_4^-$	0.01460450	0.01479753
Silicon			**Germanium**		
SiH_4	0.01101788	0.00935514	GeH_4	0.01236853	0.01171574
SiH_3F	0.01027243	0.01345484	GeH_3F	0.01173078	0.01474601
SiH_3Cl	0.00835016	0.01301035	GeH_3Cl	0.01038254	0.01411311
SiH_3Br	0.00725684	0.01003205	GeH_3Br	0.00915334	0.01149120
SiH_3I	0.00889577	0.01197386	GeH_3I	0.01004217	0.01290726
$SiH_3(OH)$	0.01014070	0.01507140	$GeH_3(OH)$	0.01168963	0.01654636
$SiH_3(NH_2)$	0.00932546	0.01467884	$GeH_3(NH_2)$	0.01116208	0.01636222
$SiH_3(CH_3)$	0.00969076	0.01030849	$GeH_3(CH_3)$	0.01104835	0.01150399
$SiH_3(CN)$	0.01328243	0.01419131	$GeH_3(CN)$	0.01322136	0.01360579
$SiH_3(CCH)$	0.01271539	0.01426101	$GeH_3(CCH)$	0.01286808	0.01355227
SiH_2F_2 *(cis)*	0.01062779	0.01280507	GeH_2F_2 *(cis)*	0.01177784	0.01428127
SiH_2F_2 *(trans)*	0.01062779	0.01370005	GeH_2F_2 *(trans)*	0.01177784	0.01481383
SiH_2Cl_2 *(cis)*	0.00790899	0.01174797	GeH_2Cl_2 *(cis)*	0.00949561	0.01288801
SiH_2Cl_2 *(trans)*	0.00790899	0.01233749	GeH_2Cl_2 *(trans)*	0.00949561	0.01319877
SiH_2Br_2 *(cis)*	0.00668668	0.00909123	GeH_2Br_2 *(cis)*	0.00797075	0.01017554
SiH_2Br_2 *(trans)*	0.00668668	0.00925100	GeH_2Br_2 *(trans)*	0.00797075	0.01039520
SiH_2I_2 *(cis)*	0.00869271	0.01101456	GeH_2I_2 *(cis)*	0.00926815	0.01158526
SiH_2I_2 *(trans)*	0.00869271	0.01132096	GeH_2I_2 *(trans)*	0.00926815	0.01188351
$SiH_2(OH)_2$ *(cis)*	0.01049995	0.01341716	$GeH_2(OH)_2$ *(cis)*	0.01164656	0.01517824
$SiH_2(OH)_2$ *(trans)*	0.01049995	0.01425452	$GeH_2(OH)_2$ *(trans)*	0.01164656	0.01581164
$SiH_2(NH_2)_2$ *(cis)*	0.00907770	0.01215124	$GeH_2(NH_2)_2$ *(cis)*	0.01068763	0.01402260
$SiH_2(NH_2)_2$ *(trans)*	0.00907770	0.01247812	$GeH_2(NH_2)_2$ *(trans)*	0.01068763	0.01439664
$SiH_2(CH_3)_2$ *(cis)*	0.00922616	0.01026419	$GeH_2(CH_3)_2$ *(cis)*	0.01022652	0.01103583
$SiH_2(CH_3)_2$ *(trans)*	0.00922616	0.01056080	$GeH_2(CH_3)_2$ *(trans)*	0.01022652	0.01137465
$SiH_2(CN)_2$ *(cis)*	0.01321342	0.01509182	$GeH_2(CN)_2$ *(cis)*	0.01310384	0.01419406
$SiH_2(CN)_2$ *(trans)*	0.01321342	0.01530572	$GeH_2(CN)_2$ *(trans)*	0.01310384	0.01421061
$SiH_2(CCH)_2$ *(cis)*	0.01396698	0.01544467	$GeH_2(CCH)_2$ *(cis)*	0.01370462	0.01465588
$SiH_2(CCH)_2$ *(trans)*	0.01396698	0.01541147	$GeH_2(CCH)_2$ *(trans)*	0.01370462	0.01439662
$SiHF_3$	0.01064859	0.01263543	$GeHF_3$	0.01176694	0.01405227
$SiHCl_3$	0.00797173	0.01126544	$GeHCl_3$	0.00909206	0.01220800
$SiHBr_3$	0.00660792	0.00850191	$GeHBr_3$	0.00743940	0.00928202
$SiHI_3$	0.00872941	0.01048584	$GeHI_3$	0.00892358	0.01081985
$SiH(OH)_3$	0.01040613	0.01271295	$GeH(OH)_3$	0.01147005	0.01435547
$SiH(NH_2)_3$	0.00894616	0.01071536	$GeH(NH_2)_3$	0.01028947	0.01260458
$SiH(CH_3)_3$	0.00902870	0.01025665	$GeH(CH_3)_3$	0.00969320	0.01077963
$SiH(CN)_3$	0.01432165	0.01596500	$GeH(CN)_3$	0.01402776	0.01516141
$SiH(CCH)_3$	0.01344553	0.01540384	$GeH(CCH)_3$	0.01323331	0.01446077
SiF_4	0.01027897	0.01177708	GeF_4	0.01153751	0.01359743
$SiCl_4$	0.00797937	0.01053360	$GeCl_4$	0.00882010	0.01150282
$SiBr_4$	0.00655025	0.00796854	$GeBr_4$	0.00711238	0.00859123
SiI_4	0.00870562	0.00989391	GeI_4	0.00870497	0.01008864
$Si(OH)_4$	0.01006089	0.01174199	$Ge(OH)_4$	0.01124944	0.01348288
$Si(NH_2)_4$	0.00872115	0.00974539	$Ge(NH_2)_4$	0.00990569	0.01183284
$Si(CH_3)_4$	0.00893376	0.01004997	$Ge(CH_3)_4$	0.00931091	0.01042830
$Si(CN)_4$	0.01455105	0.01627027	$Ge(CN)_4$	0.01428267	0.01558312
$Si(CCH)_4$	0.01357184	0.01540996	$Ge(CCH)_4$	0.01331345	0.01456146

Phosphorus			Arsenic		
PH_3F^+	0.01109429	0.01962760	AsH_3F^+	0.01098899	0.01973910
PH_3Cl^+	0.00977562	0.02818503	AsH_3Cl^+	0.00947635	0.02635618
PH_3Br^+	0.00830403	0.02391464	AsH_3Br^+	0.00841101	0.02304878
PH_3I^+	0.00986833	0.02429335	AsH_3I^+	0.00937801	0.02247257
$PH_3(OH)^+$	0.01083589	0.02143819	$AsH_3(OH)^+$	0.01074252	0.02263098
$PH_3(NH_2)^+$	0.00992520	0.01913185	$AsH_3(NH_2)^+$	0.01006418	0.01973047
$PH_3(CH_3)^+$	0.00994744	0.01358831	$AsH_3(CN)^+$	0.01259943	0.02146373
$PH_3(CN)^+$	0.01396638	0.02082534	$AsH_3(CCH)^+$	0.01184296	0.01729212
$PH_3(CCH)^+$	0.01306799	0.02006296	$AsH_2F_2^+$ *(cis)*	0.01180258	0.01734932
$PH_2F_2^+$ *(cis)*	0.01193306	0.01690552	$AsH_2F_2^+$ *(trans)*	0.01180258	0.01823023
$PH_2F_2^+$ *(trans)*	0.01193306	0.01794104	$AsH_2Cl_2^+$ *(cis)*	0.00951192	0.01912430
$PH_2Cl_2^+$ *(cis)*	0.01022198	0.02037292	$AsH_2Cl_2^+$ *(trans)*	0.00951192	0.01937635
$PH_2Cl_2^+$ *(trans)*	0.01022198	0.02058994	$AsH_2Br_2^+$ *(cis)*	0.00792787	0.01565904
$PH_2Br_2^+$ *(cis)*	0.00814333	0.01591829	$AsH_2Br_2^+$ *(trans)*	0.00792787	0.01489648
$PH_2Br_2^+$ *(trans)*	0.00814333	0.01527686	$AsH_2I_2^+$ *(cis)*	0.00919272	0.01687348
$PH_2I_2^+$ *(cis)*	0.00991292	0.01799801	$AsH_2I_2^+$ *(trans)*	0.00919272	0.01545169
$PH_2I_2^+$ *(trans)*	0.00991292	0.01615354	$AsH_2(OH)_2^+$ *(cis)*	0.01156192	0.01888420
$PH_2(OH)_2^+$ *(cis)*	0.01157556	0.01771646	$AsH_2(OH)_2^+$ *(trans)*	0.01156192	0.01921073
$PH_2(OH)_2^+$ *(trans)*	0.01157556	0.01777395	$AsH_2(NH_2)_2^+$ *(cis)*	0.01032579	0.01718927
$PH_2(NH_2)_2^+$ *(cis)*	0.01007938	0.01622979	$AsH_2(NH_2)_2^+$ *(trans)*	0.01032579	0.01688632
$PH_2(NH_2)_2^+$ *(trans)*	0.01007938	0.01545020	$AsH_2(CH_3)_2^+$ *(cis)*	0.00911176	0.01292634
$PH_2(CH_3)_2^+$ *(cis)*	0.00945489	0.01442860	$AsH_2(CH_3)_2^+$ *(trans)*	0.00911176	0.01371297
$PH_2(CH_3)_2^+$ *(trans)*	0.00945489	0.01444085	$AsH_2(CN)_2^+$ *(cis)*	0.01379727	0.01782942
$PH_2(CN)_2^+$ *(cis)*	0.01493802	0.02073279	$AsH_2(CN)_2^+$ *(trans)*	0.01379727	0.01807458
$PH_2(CN)_2^+$ *(trans)*	0.01493802	0.02127791	$AsH_2(CCH)_2^+$ *(cis)*	0.01244305	0.01660603
$PH_2(CCH)_2^+$ *(cis)*	0.01353375	0.01907630	$AsH_2(CCH)_2^+$ *(trans)*	0.01244305	0.01704198
$PH_2(CCH)_2^+$ *(trans)*	0.01353375	0.01976179	$AsHF_3^+$	0.01225826	0.01651519
PHF_3^+	0.01209319	0.01574186	$AsHCl_3^+$	0.00977036	0.01662376
$PHCl_3^+$	0.01072245	0.01743272	$AsHBr_3^+$	0.00780520	0.01267796
$PHBr_3^+$	0.00823046	0.01285853	$AsHI_3^+$	0.00920792	0.01366042
PHI_3^+	0.01004127	0.01438940	$AsH(OH)_3^+$	0.01164764	0.01679144
$PH(OH)_3^+$	0.01139100	0.01553363	$AsH(NH_2)_3^+$	0.01023062	0.01434619
$PH(NH_2)_3^+$	0.00993399	0.01321400	$AsH(CH_3)_3^+$	0.00878648	0.01254721
$PH(CH_3)_3^+$	0.00922436	0.01352094	$AsH(CN)_3^+$	0.01460301	0.01819702
$PH(CN)_3^+$	0.01548765	0.02050255	$AsH(CCH)_3^+$	0.01275776	0.01622365
$PH(CCH)_3^+$	0.01373466	0.01828347	AsF_4^+	0.01226979	0.01565288
PF_4^+	0.01151319	0.01432474	$AsCl_4^+$	0.00984911	0.01487170
PCl_4^+	0.01082095	0.01551362	$AsBr_4^+$	0.00771094	0.01094768
PBr_4^+	0.00821452	0.01123844	AsI_4^+	0.00916779	0.01206099
PI_4^+	0.01004701	0.01281314	$As(OH)_4^+$	0.01153155	0.01539917
$P(OH)_4^+$	0.01090809	0.01414399	$As(NH_2)_4^+$	0.00993927	0.01304862
$P(NH_2)_4^+$	0.00954831	0.01234834	$As(CH_3)_4^+$	0.00857964	0.01171813
$P(CH_3)_4^+$	0.00908654	0.01277140	$As(CN)_4^+$	0.01521947	0.01854467
$P(CN)_4^+$	0.01585233	0.02018824	$As(CCH)_4^+$	0.01294368	0.01583818
$P(CCH)_4^+$	0.01380563	0.01750091			

S4. Bond lengths

Table S3: Bond lengths of all considered ER_4^n with E^n = Al^-, Si, P^+, Ga^-, Ge, As^+ and **R** = H, F, Cl, Br, I, OH, NH_2, CH_3, CN, CCH of the tetrahedral (GS) and the planar inversion transition structure (TS), calculated at the B97M-D3(BJ)/cc-pVTZ level of theory. In all cases, the bond lengths of the transition structure are longer than those of the ground state.

Com-pound	R_{GS} [pm]	R_{TS} [pm]	Difference [pm]	Com-pound	R_{GS} [pm]	R_{TS} [pm]	Difference [pm]
Aluminum				**Gallium**			
AlH_4^-	164.56	170.50	5.94	GaH_4^-	163.01	173.24	10.23
AlF_4^-	169.03	172.26	3.23	GaF_4^-	178.33	180.70	2.37
$AlCl_4^-$	214.75	220.35	5.60	$GaCl_4^-$	219.20	224.93	5.73
$AlBr_4^-$	230.01	236.25	6.24	$GaBr_4^-$	233.39	239.98	6.58
AlI_4^-	250.66	257.92	7.26	GaI_4^-	252.47	260.58	8.11
$Al(OH)_4^-$	176.90	179.97	3.08	$Ga(OH)_4^-$	185.36	188.01	2.66
$Al(NH_2)_4^-$	186.49	188.55	2.05	$Ga(NH_2)_4^-$	193.36	196.20	2.84
$Al(CH_3)_4^-$	201.74	207.30	5.56	$Ga(CH_3)_4^-$	203.95	212.07	8.12
$Al(CN)_4^-$	196.49	199.94	3.45	$Ga(CN)_4^-$	197.39	204.20	6.80
$Al(CCH)_4^-$	196.23	199.46	3.23	$Ga(CCH)_4^-$	197.29	203.59	6.30
Silicon				**Germanium**			
SiH_4	148.19	154.60	6.41	GeH_4	152.95	162.64	9.69
SiF_4	156.37	160.06	3.69	GeF_4	168.76	171.45	2.69
$SiCl_4$	201.92	208.22	6.29	$GeCl_4$	210.91	216.85	5.94
$SiBr_4$	218.22	225.09	6.87	$GeBr_4$	226.37	233.03	6.66
SiI_4	240.17	247.92	7.75	GeI_4	247.06	254.90	7.84
$Si(OH)_4$	163.25	167.10	3.85	$Ge(OH)_4$	175.25	178.27	3.02
$Si(NH_2)_4$	171.83	173.90	2.06	$Ge(NH_2)_4$	182.91	185.10	2.19
$Si(CH_3)_4$	187.06	193.32	6.26	$Ge(CH_3)_4$	195.12	203.02	7.90
$Si(CN)_4$	181.91	185.14	3.23	$Ge(CN)_4$	189.28	194.71	5.43
$Si(CCH)_4$	181.04	184.05	3.02	$Ge(CCH)_4$	188.36	193.26	4.91
Phosphorus				**Arsenic**			
PF_4^+	148.50	152.94	4.44	AsF_4^+	162.88	165.90	3.02
PCl_4^+	194.35	201.72	7.37	$AsCl_4^+$	205.93	212.26	6.34
PBr_4^+	211.87	219.88	8.01	$AsBr_4^+$	222.43	229.32	6.88
PI_4^+	235.15	243.78	8.63	AsI_4^+	244.24	251.92	7.69
$P(OH)_4^+$	154.46	159.36	4.91	$As(OH)_4^+$	168.72	172.32	3.59
$P(NH_2)_4^+$	162.78	165.95	3.17	$As(NH_2)_4^+$	176.28	177.61	1.33
$P(CH_3)_4^+$	178.66	184.86	6.19	$As(CH_3)_4^+$	190.30	197.24	6.93
$P(CN)_4^+$	172.64	175.84	3.20	$As(CN)_4^+$	183.80	188.38	4.58
$P(CCH)_4^+$	170.92	174.15	3.23	$As(CCH)_4^+$	181.77	186.04	4.27

S5. Further comments on the structure optimizations and on the IRC calculations

Structure optimizations

The transition structure optimizations for GaH_3R^-, R = Br, I, CN converged to dissociative structures ($GaH_3 + R^-$). In all three cases, the frequency analysis revealed a single imaginary frequency corresponding to an inversion process. However, due the significant structural differences, the data of GaH_3R^-, R = Br, I, CN cannot be compared with that of all other compounds.

The lowest-energy square planar states of PH_4^+ and AsH_4^+ have an open-shell singlet electronic configuration. They are valid inversion transition states. Structure optimizations and frequency analyses for those two compounds were done on the CASSCF(8,8)/cc-pVTZ level of theory followed by single point calculations with NEVPT2/cc-pVQZ (see Chapter S1 for further details).

It was not possible to locate an inversion transition state of $AsH_3(CH_3)^+$ with the applied DFT method. This is ascribed to the significant multiconfigurational character of the compound. For all other molecules of the type AsH_3R^+, the transition structure optimization with DFT was successful.

The frequency analysis of the optimized inversion transition structure of *trans*-$GeH_2(CH_3)_2$ consistently gave two imaginary frequencies – despite several structure optimizations: the inversion mode (1335i cm^{-1}) and an additional mode (29i cm^{-1}). The second imaginary vibration was considered negligible.

IRC calculations

To further verify the located transition structures to correspond to true inversion transition state, IRC calculations were carried out as described in Chapter S1. In all cases, tetrahedral structures were obtained. It should be noted that the extreme tight convergence criteria mentioned above were not met by all calculations. However, the energies of the final IRC structures differed by less than 1 kJ mol^{-1} from the final single point energy of the B97M-D3(BJ)/cc-pVTZ structural optimizations. Only for the *trans*-inversion of $SiH_2(NH_2)_2$ (both directions) and the *cis*-inversion of $SiH_2(OH)_2$ (both directions) larger deviations were obtained (5.0 and 4.5 kJ mol^{-1}, respectively). Those were traced back to rotations around the Si-N and Si-O bond respectively and are hence not of relevance. Therefore, the IRC calculations verified the located first order saddle points as valid inversion transition states.

S6. Influence of diffuse basis functions

The inversion barrier heights obtained on the DLPNO-CCSD(T)/cc-pVQZ level were compared to those from DLPNO-CCSD(T)/aug-cc-pVQZ for the elements of group 13 and 14 (Al, Ga, Si, Ge). For that, nine randomly chosen inversion barriers were recomputed by reoptimizing the structures on the B97M-D3(BJ)/aug-cc-pVTZ level and subsequent final single point energy calculation with DLPNO-CCSD(T)/aug-cc-pVQZ. The chosen cases are: $\mathbf{EH_4^n}$, $\mathbf{EF_4^n}$, $\mathbf{EHF_3^n}$, $\mathbf{EH_2Cl_2^n}$ (*cis* and *trans*), $\mathbf{EH_3Br^n}$, $\mathbf{EH_2(CN)_2^n}$ (*cis* and *trans*), $\mathbf{EH_3(CCH)^n}$, with $\mathbf{E^n}$ = Al^-, Si, Ga^-, Ge. The dissociative structure of GaH_3Br^- was also found with the aug-basis set (see Chapter S5). In all cases, the barrier calculated with the aug-cc-pVQZ basis set was lower by an overall average value of 2.2 kJ mol^{-1}. This means that no significant influence of diffuse basis functions on the inversion barriers heights was found.

Table S4: Comparison of the inversion barrier heights with respect to the use of diffuse basis functions for a selected class of compounds.

Compound	Inversion barrier [kJ mol^{-1}]		Difference in the inversion barrier height [kJ mol^{-1}]
	DLPNO-CCSD(T)/cc-pVQZ//B97M-D3(BJ)/cc-pVTZ	DLPNO-CCSD(T)/aug-cc-pVQZ//B97M-D3(BJ)/aug-cc-pVTZ	
Aluminum			
AlH_4^-	224.75	221.01	-3.74
AlF_4^-	191.17	187.07	-4.10
$AlHF_3^-$	176.60	172.95	-3.65
$AlH_2Cl_2^-$ *(cis)*	179.76	177.16	-2.60
$AlH_2Cl_2^-$ *(trans)*	144.83	142.35	-2.48
AlH_3Br^-	172.82	170.01	-2.81
$AlH_2(CN)_2^-$ *(cis)*	196.63	194.81	-1.82
$AlH_2(CN)_2^-$ *(trans)*	182.23	180.29	-1.94
$AlH_3(CCH)^-$	210.33	207.77	-2.56

Gallium			
GaH_4^-	290.62	287.05	-3.57
GaF_4^-	161.07	157.13	-3.94
$GaHF_3^-$	163.21	159.59	-3.62
$GaH_2Cl_2^-$ *(cis)*	202.91	199.94	-2.97
$GaH_2Cl_2^-$ *(trans)*	137.28	133.33	-3.95
GaH_3Br^-	158.65	155.35	-3.30
$GaH_2(CN)_2^-$ *(cis)*	258.82	257.79	-1.03
$GaH_2(CN)_2^-$ *(trans)*	225.83	224.16	-1.67
$GaH_3(CCH)^-$	271.25	269.68	-1.57
Silicon			
SiH_4	380.08	379.07	-1.01
SiF_4	277.58	275.14	-2.44
$SiHF_3$	251.78	249.69	-2.09
SiH_2Cl_2 *(cis)*	276.29	274.86	-1.43
SiH_2Cl_2 *(trans)*	228.07	226.94	-1.13
SiH_3Br	291.22	290.55	-0.67
$SiH_2(CN)_2$ *(cis)*	325.77	324.98	-0.79
$SiH_2(CN)_2$ *(trans)*	309.94	309.20	-0.74
$SiH_3(CCH)$	347.47	346.92	-0.55
Germanium			
GeH_4	426.93	426.91	-0.02
GeF_4	212.36	210.03	-2.33
$GeHF_3$	216.32	214.06	-2.26
GeH_2Cl_2 *(cis)*	281.23	277.62	-3.61
GeH_2Cl_2 *(trans)*	223.09	220.38	-2.71
GeH_3Br	308.06	306.21	-1.85
$GeH_2(CN)_2$ *(cis)*	365.25	363.98	-1.27
$GeH_2(CN)_2$ *(trans)*	341.05	339.53	-1.52
$GeH_3(CCH)$	391.77	390.48	-1.29

S7. Final single point energy benchmark

Various computational methods for the calculation of the final single point energies and hence of the inversion barrier heights were benchmarked against CCSD(T) data extrapolated toward the complete basis set limit. The two-point extrapolation was done with the cc-pVTZ and the cc-pVQZ basis set (Table S5). The extrapolated SCF ($^{\infty}E_{SCF}$) and correlation energy ($^{\infty}E_{corr}$) were calculated by

$$^{\infty}E = {}^{\infty}E_{SCF} + {}^{\infty}E_{corr} = \frac{{}^{X}E_{SCF} \cdot e^{-\alpha\sqrt{Y}} - {}^{Y}E_{SCF} \cdot e^{-\alpha\sqrt{X}}}{e^{-\alpha\sqrt{Y}} - e^{-\alpha\sqrt{X}}} + \frac{{}^{X}E_{corr} \cdot X^{\beta} - {}^{Y}E_{corr} \cdot Y^{\beta}}{X^{\beta} - Y^{\beta}}, \quad (1)$$

with

$X = 3, Y = 4, \alpha = 5.46, \beta = 3.05$.[13, 32]

A subclass of all investigated molecules was used: $\mathbf{EH_{4-y}R_y^n}$, with $\mathbf{E^n}$ = Al^-, Si, Ga^-, Ge for y = 0 and Al^-, Si, P^+, Ga^-, Ge, As^+ for y = 4 and **R** = F, CN.

Data evaluation was done with respect to the mean signed (relative) deviation (MSD and MSD_{rel}) and the mean absolute (relative) deviation (MAD and MAD_{rel}). "IB" stands for inversion barrier in the following formulas. The number of considered barriers is given by n (n = 16).

$$MSD = \frac{1}{n} \cdot \sum_{i=0}^{n} IB_i - {}^{\infty}IB \tag{2}$$

$$MSD_{rel} = \frac{1}{n} \cdot \sum_{i=0}^{n} \frac{IB_i - {}^{\infty}IB}{{}^{\infty}IB} \tag{3}$$

$$MAD = \frac{1}{n} \cdot \sum_{i=0}^{n} \left| IB_i - {}^{\infty}IB \right| \tag{4}$$

$$MAD_{rel} = \frac{1}{n} \cdot \sum_{i=0}^{n} \left| \frac{IB_i - {}^{\infty}IB}{{}^{\infty}IB} \right| \tag{5}$$

Table S5: Two-point extrapolation to the complete basis set limit of selected inversion barrier heights using the cc-pVTZ and the cc-pVQZ basis set together with the CCSD(T) method.

	CCSD(T)/cc-pVTZ, X = 3				CCSD(T)/cc-pVQZ, Y = 4				CCSD(T)/CBS			
	$^{X}E_{SCF}$ [Eh]	$^{X}E_{corr}$ [Eh]	^{X}E [Eh]	I. barrier [kJ mol^{-1}]	$^{Y}E_{SCF}$ [Eh]	$^{Y}E_{corr}$ [Eh]	^{Y}E [Eh]	I. barrier [kJ mol^{-1}]	$^{\infty}E_{SCF}$ [Eh]	$^{\infty}E_{corr}$ [Eh]	$^{\infty}E$ [Eh]	I. barrier [kJ mol^{-1}]
AlH_4^-	-244.24736847	-0.16201095	-244.40937943		-244.25238253	-0.16868107	-244.42106360		-244.25389329	-0.17342945	-244.42732274	
	-244.15951991	-0.16398512	-244.32350503	**225.46**	-244.16457227	-0.17088715	-244.33545942	**224.75**	-244.16609456	-0.17580064	-244.34189520	**224.29**
AlF_4^-	-640.22917019	-1.12942551	-641.35859570		-640.27911291	-1.23594315	-641.51505606		-640.29416085	-1.31177193	-641.60593278	
	-640.15355684	-1.13488218	-641.28843902	**184.20**	-640.20017843	-1.24225392	-641.44243235	**190.67**	-640.21422569	-1.31869074	-641.53291643	**191.70**
$Al(CN)_4^-$	-611.50675479	-1.48178096	-612.98853576		-611.53672211	-1.56640225	-613.10312435		-611.54575138	-1.62664325	-613.17239463	
	-611.43452508	-1.48697843	-612.92150351	**175.99**	-611.46390165	-1.57242173	-613.03632338	**175.39**	-611.47275292	-1.63324792	-613.10600085	**174.32**
GaH_4^-	-1925.59526050	-0.25338049	-1925.84864099		-1925.60018955	-0.32184245	-1925.92203200		-1925.60167470	-0.37057979	-1925.97225449	
	-1925.49224011	-0.24481679	-1925.73705691	**292.96**	-1925.49752392	-0.31386459	-1925.81138851	**290.49**	-1925.49911595	-0.36301900	-1925.86213495	**289.12**
GaF_4^-	-2321.46904166	-1.21341049	-2322.68245215		-2321.51377876	-1.37940527	-2322.89318403		-2321.52725823	-1.49757521	-2323.02483344	
	-2321.40517910	-1.21604802	-2322.62122712	**160.75**	-2321.44845947	-1.38361566	-2322.83207513	**160.44**	-2321.46150001	-1.50290530	-2322.96440532	**158.65**
$Ga(CN)_4^-$	-2292.82747455	-1.57791600	-2294.40539055		-2292.85686276	-1.72342035	-2294.58028311		-2292.86571754	-1.82700336	-2294.69272090	
	-2292.74319147	-1.57397210	-2294.31716357	**231.64**	-2292.77196148	-1.71891684	-2294.49087832	**234.73**	-2292.78062999	-1.82210147	-2294.60273147	**236.27**
SiH_4	-291.26055229	-0.17679719	-291.43734948		-291.26600851	-0.18470312	-291.45071163		-291.26765249	-0.19033127	-291.45798376	
	-291.11304884	-0.17955977	-291.29260861	**380.02**	-291.11882845	-0.18714743	-291.30597588	**380.00**	-291.12056987	-0.19254900	-291.31311887	**380.34**
SiF_4	-687.14759118	-1.13885492	-688.28644610		-687.19759321	-1.24326947	-688.44086268		-687.21265901	-1.31760110	-688.53026011	
	-687.03606145	-1.14901299	-688.18507444	**266.15**	-687.08073658	-1.25470336	-688.33543994	**276.79**	-687.09419737	-1.32994323	-688.42414060	**278.62**
$Si(CN)_4$	-658.33223324	-1.51247823	-659.84471147		-658.36226907	-1.59724301	-659.95951208		-658.37131899	-1.65758616	-660.02890515	
	-658.21448030	-1.52311220	-659.73759250	**281.24**	-658.24381059	-1.60830646	-659.85211705	**281.97**	-658.25264792	-1.66895537	-659.92160328	**281.72**
GeH_4	-2077.71800288	-0.25685068	-2077.97485356		-2077.72215923	-0.32107891	-2078.04323815		-2077.72341156	-0.36680231	-2078.09021387	
	-2077.56086896	-0.25274542	-2077.81361439	**423.33**	-2077.56510777	-0.31559696	-2077.88070473	**426.73**	-2077.56638494	-0.36034031	-2077.92672525	**429.24**
GeF_4	-2473.48091636	-1.22042838	-2474.70134474		-2473.52573250	-1.37820935	-2474.90394185		-2473.53923578	-1.49053197	-2475.02976775	
	-2473.39372263	-1.22877789	-2474.62250052	**207.01**	-2473.43610078	-1.38723779	-2474.82333857	**211.62**	-2473.44886948	-1.50004372	-2474.94891320	**212.28**
$Ge(CN)_4$	-2444.76750129	-1.59369825	-2446.36119954		-2444.79530617	-1.73371018	-2446.52901635		-2444.80368389	-1.83338320	-2446.63706709	
	-2444.64415020	-1.59997111	-2446.24412131	**307.39**	-2444.67136328	-1.73865291	-2446.41001619	**312.43**	-2444.67956269	-1.83737902	-2446.51694171	**315.39**
PF_4^+	-738.49542835	-1.16308342	-739.65851177		-738.54669094	-1.26657215	-739.81326309		-738.56213655	-1.34024469	-739.90238124	
	-738.33982258	-1.18418420	-739.52400678	**353.14**	-738.38595334	-1.28861519	-739.67456852	**364.14**	-738.39985271	-1.36295850	-739.76281122	**366.44**
$P(CN)_4^+$	-709.69721295	-1.55449617	-711.25170912		-709.72864524	-1.63971198	-711.36835722		-709.73811591	-1.70037622	-711.43849213	
	-709.53354979	-1.57904581	-711.11259559	**365.24**	-709.56503703	-1.66401875	-711.22905578	**365.74**	-709.57452425	-1.72451010	-711.29903435	**366.15**
AsF_4^+	-2631.86292770	-1.23637446	-2633.09930216		-2631.90930017	-1.39136202	-2633.30066219		-2631.92327237	-1.50169603	-2633.42496841	
	-2631.74905159	-1.25463672	-2633.00368831	**251.03**	-2631.79285209	-1.41020902	-2633.20306111	**256.25**	-2631.80604936	-1.52095930	-2633.32700866	**257.19**
$As(CN)_4^+$	-2603.16298303	-1.61768288	-2604.78066591		-2603.19047391	-1.75660109	-2604.94707500		-2603.19875702	-1.85549550	-2605.05425252	
	-2603.00321989	-1.63955323	-2604.64277311	**362.04**	-2603.03004011	-1.77767850	-2604.80771862	**365.88**	-2603.03812115	-1.87600843	-2604.91412959	**367.89**

Table S6: Selected inversion barrier heights calculated at various levels of theory and their deviations to the CCSD(T)/CBS data given in Table S5.

	CCSD(T)/ cc-pVTZ		CCSD(T)/ cc-pVQZ		DLPNO-CCSD(T)/ cc-pVQZ		B97M-D3(BJ)/ cc-pVTZ		B97M-D3(BJ)/ cc-pVQZ		B3LYP-D3(BJ)/cc-pVQZ		PW6B95-D3(BJ)/cc-pVQZ		TPSS-D3(BJ)/ cc-pVQZ		DSD-BLYP/ cc-pVQZ	
	I. barrier [kJ mol^{-1}]	Dev. [kJ mol^{-1}]	I. barrier [kJ mol^{-1}]	Dev. [kJ mol^{-1}]	I. barrier [kJ mol^{-1}]	Dev. [kJ mol^{-1}]	I. barrier [kJ mol^{-1}]	Dev. [kJ mol^{-1}]	I. barrier [kJ mol^{-1}]	Dev. [kJ mol^{-1}]	I. barrier [kJ mol^{-1}]	Dev. [kJ mol^{-1}]	I. barrier [kJ mol^{-1}]	Dev. [kJ mol^{-1}]	I. barrier [kJ mol^{-1}]	Dev. [kJ mol^{-1}]	I. barrier [kJ mol^{-1}]	Dev. [kJ mol^{-1}]
AlH_4^-	225.46	1.17	224.75	0.46	224.75	0.46	219.14	-5.15	219.94	-4.35	221.06	-3.23	221.38	-2.91	218.28	-6.01	226.75	2.46
AlF_4^-	184.20	-7.51	190.67	-1.03	191.17	-0.53	180.52	-11.19	185.34	-6.36	185.25	-6.45	180.09	-11.62	174.20	-17.50	189.13	-2.57
$Al(CN)_4^-$	175.99	1.68	175.39	1.07	175.86	1.54	173.03	-1.28	172.69	-1.62	173.44	-0.88	170.19	-4.13	164.60	-9.71	175.87	1.55
GaH_4^-	292.96	3.85	290.49	1.38	290.62	1.50	261.95	-27.17	262.27	-26.85	268.15	-20.97	270.34	-18.78	264.92	-24.20	289.72	0.60
GaF_4^-	160.75	2.09	160.44	1.79	161.07	2.42	142.44	-16.21	141.94	-16.71	145.96	-12.70	144.68	-13.97	135.28	-23.38	156.40	-2.26
$Ga(CN)_4^-$	231.64	-4.63	234.73	-1.53	235.08	-1.19	212.04	-24.23	212.37	-23.90	214.39	-21.88	213.49	-22.77	204.89	-31.38	230.71	-5.55
SiH_4	380.02	-0.33	380.00	-0.34	380.08	-0.26	364.28	-16.06	363.61	-16.73	374.32	-6.02	378.48	-1.86	375.29	-5.06	383.89	3.55
SiF_4	266.15	-12.47	276.79	-1.83	277.58	-1.04	258.26	-20.36	268.04	-10.57	264.50	-14.12	261.02	-17.60	249.11	-29.51	274.15	-4.47
$Si(CN)_4$	281.24	-0.48	281.97	0.24	283.52	1.79	260.03	-21.69	261.39	-20.33	268.20	-13.52	268.38	-13.34	253.06	-28.66	280.86	-0.86
GeH_4	423.33	-5.91	426.73	-2.51	426.93	-2.30	394.14	-35.10	393.36	-35.88	402.30	-26.94	406.39	-22.85	398.52	-30.72	429.02	-0.22
GeF_4	207.01	-5.28	211.62	-0.66	212.36	0.08	185.76	-26.52	188.45	-23.84	190.42	-21.86	190.63	-21.65	175.15	-37.13	205.87	-6.42
$Ge(CN)_4$	307.39	-8.00	312.43	-2.95	313.95	-1.44	275.20	-40.19	276.22	-39.17	283.73	-31.66	286.87	-28.52	265.66	-49.73	307.76	-7.63
PF_4^+	353.14	-13.30	364.14	-2.30	365.73	-0.71	337.21	-29.23	348.42	-18.03	342.22	-24.22	343.82	-22.62	318.87	-47.57	360.66	-5.78
$P(CN)_4^+$	365.24	-0.90	365.74	-0.41	369.69	3.55	316.55	-49.60	317.70	-48.45	329.60	-36.54	335.12	-31.02	297.19	-68.96	363.25	-2.90
AsF_4^+	251.03	-6.16	256.25	-0.94	257.95	0.76	225.55	-31.64	229.31	-27.88	228.83	-28.36	232.70	-24.49	207.63	-49.56	249.14	-8.06
$As(CN)_4^+$	362.04	-5.86	365.88	-2.01	369.80	1.91	303.12	-64.77	304.82	-63.07	318.23	-49.67	810.84	442.95	657.23	289.33	359.15	-8.75
MSD [kJ mol^{-1}]	**-3.88**		**-0.72**		**0.42**		**-26.27**		**-23.98**		**-19.94**		**11.55**		**-10.61**		**-2.96**	
MSD_{rel}	**-0.0130**		**-0.0018**		**0.0020**		**-0.0893**		**-0.0810**		**-0.0681**		**0.0159**		**-0.0554**		**-0.0108**	
MAD [kJ mol^{-1}]	**4.97**		**1.34**		**1.34**		**26.27**		**23.98**		**19.94**		**43.82**		**46.78**		**3.98**	
MAD_{rel}	**0.0181**		**0.0050**		**0.0050**		**0.0893**		**0.0810**		**0.0681**		**0.1346**		**0.1538**		**0.0147**	

S8. *Cis*/*trans*-isomerism for the inversion transition states of $EH_2R_2^n$

The disubstituted compounds $\mathbf{EH_2R_2^n}$ can invert through two diastereomeric transition states – either through the (effectively) C_{2v} symmetric *cis*- or the corresponding *trans*-form, which is of (effective) D_{2h} symmetry. For all considered compounds, both isomers were identified as valid inversion transition states. In all cases, the *trans*-inversion transition state is energetically more favorable. The largest difference was found for $PH_2(NH_2)_2^+$ (82 kJ mol^{-1}), the smallest for $GaH_2(CH_3)_2^-$ (4 kJ mol^{-1}).

Table S7: Energies of the *cis*-configurated inversion transition states of $\mathbf{EH_2R_2^n}$ relative to the *trans*-isomers with $\mathbf{E^n}$ = Al^-, Si, P^+, Ga^-, Ge, As^+ and **R** = F, Cl, Br, I, OH, NH_2, CH_3, CN, CCH.

Compound	Energy of the *cis*- versus the *trans*-inversion transition state [kJ mol^{-1}]	Compound	Energy of the *cis*- versus the *trans*-inversion transition state [kJ mol^{-1}]	Compound	Energy of the *cis*- versus the *trans*-inversion transition state [kJ mol^{-1}]
Aluminum		**Silicon**		**Phosphorus**	
$AlH_2F_2^-$	18.04	SiH_2F_2	42.44	$PH_2F_2^+$	79.97
$AlH_2Cl_2^-$	34.93	SiH_2Cl_2	48.22	$PH_2Cl_2^+$	68.86
$AlH_2Br_2^-$	41.12	SiH_2Br_2	47.03	$PH_2Br_2^+$	61.15
$AlH_2I_2^-$	45.71	SiH_2I_2	42.32	$PH_2I_2^+$	46.7
$AlH_2(OH)_2^-$	12.74	$SiH_2(OH)_2$	31.81	$PH_2(OH)_2^+$	68.11
$AlH_2(NH_2)_2^-$	22.76	$SiH_2(NH_2)_2$	44.24	$PH_2(NH_2)_2^+$	81.66
$AlH_2(CH_3)_2^-$	3.9	$SiH_2(CH_3)_2$	8.21	$PH_2(CH_3)_2^+$	20.67
$AlH_2(CN)_2^-$	14.4	$SiH_2(CN)_2$	15.83	$PH_2(CN)_2^+$	21.83
$AlH_2(CCH)_2^-$	6.62	$SiH_2(CCH)_2$	9.04	$PH_2(CCH)_2^+$	20.72
average	*22.2*	***average***	*32.1*	***average***	*52.2*
Gallium		**Germanium**		**Arsenic**	
$GaH_2F_2^-$	32.51	GeH_2F_2	50.04	$AsH_2F_2^+$	71.61
$GaH_2Cl_2^-$	65.63	GeH_2Cl_2	58.14	$AsH_2Cl_2^+$	61.99
$GaH_2Br_2^-$	72.22	GeH_2Br_2	55.85	$AsH_2Br_2^+$	54.3
$GaH_2I_2^-$	76.98	GeH_2I_2	48.67	$AsH_2I_2^+$	40.07
$GaH_2(OH)_2^-$	12.12	$GeH_2(OH)_2$	27.76	$AsH_2(OH)_2^+$	51.94
$GaH_2(NH_2)_2^-$	16.83	$GeH_2(NH_2)_2$	34.84	$AsH_2(NH_2)_2^+$	61.08
$GaH_2(CH_3)_2^-$	3.58	$GeH_2(CH_3)_2$	6.86	$AsH_2(CH_3)_2^+$	13.38
$GaH_2(CN)_2^-$	32.99	$GeH_2(CN)_2$	24.2	$AsH_2(CN)_2^+$	23.28
$GaH_2(CCH)_2^-$	15.67	$GeH_2(CCH)_2$	12.01	$AsH_2(CCH)_2^+$	18.42
average	*36.5*	***average***	*35.4*	***average***	*44.0*

S9. Trends in the inversion barrier height along the degree of substitution

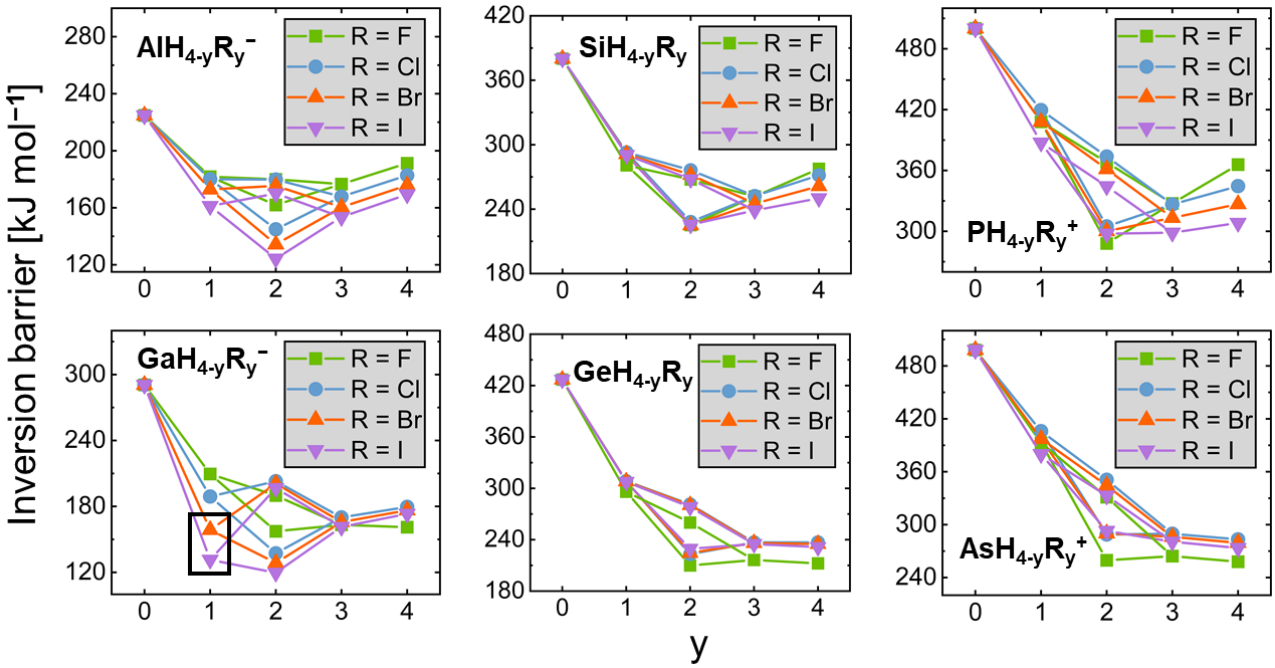

Figure S2: Trends in the inversion barrier height for $EH_{4-y}R_y^n$ with E^n = Al^-, Si, P^+, Ga^-, Ge, As^+ and y = 0, 1, 2, 3, 4, R = F, Cl, Br, I. The transition structure optimization of GaH_3Br^- and GaH_3I^- converged to a dissociative structure (GaH_3 + Br/I^-) and can thus not be compared with the other data points (marked with black box).

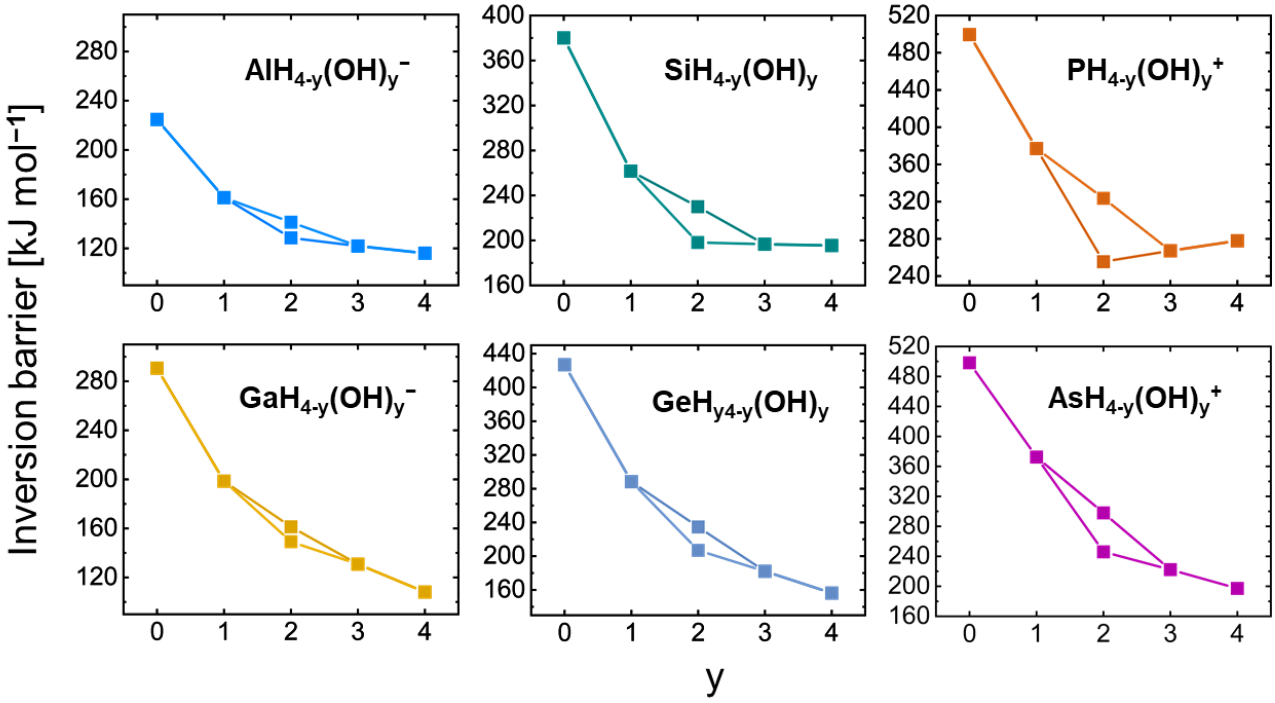

Figure S3: Trends in the inversion barrier height for $EH_{4-y}R_y^n$ with E^n = Al^-, Si, P^+, Ga^-, Ge, As^+ and y = 0, 1, 2, 3, 4, R = OH.

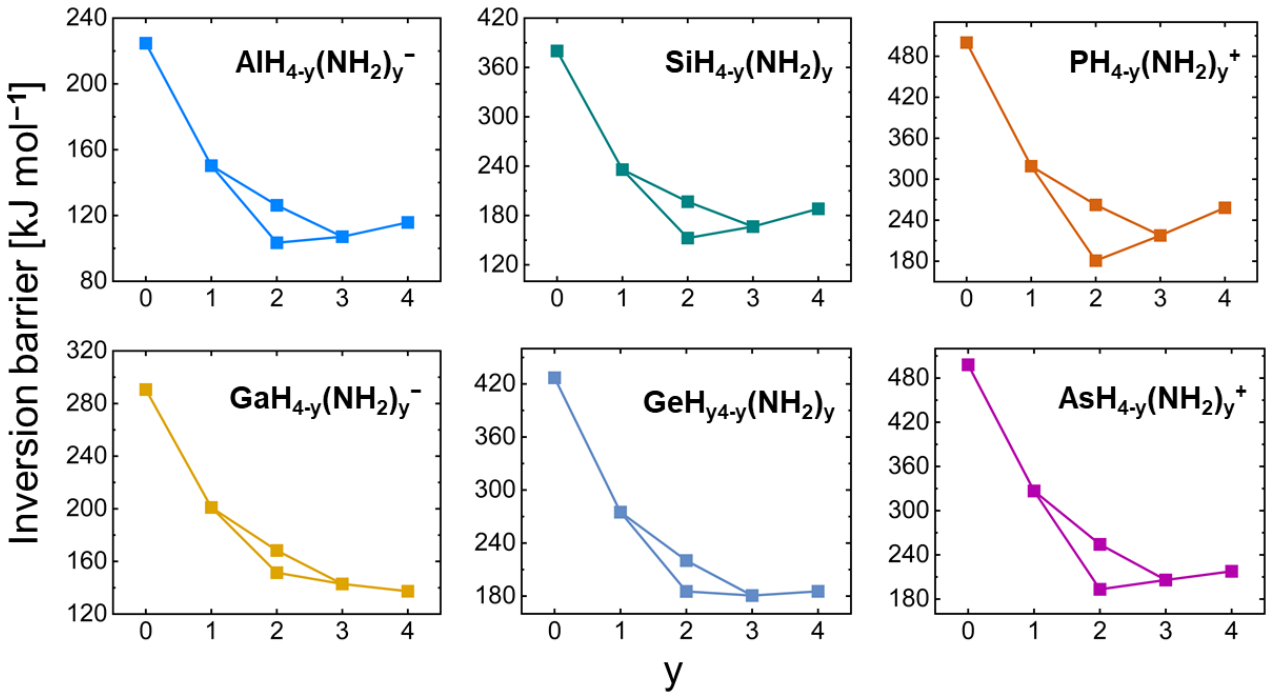

Figure S4: Trends in the inversion barrier height for $\mathbf{EH_{4-y}R_y^n}$ with $\mathbf{E^n}$ = Al^-, Si, P^+, Ga^-, Ge, As^+ and y = 0, 1, 2, 3, 4, **R** = NH_2.

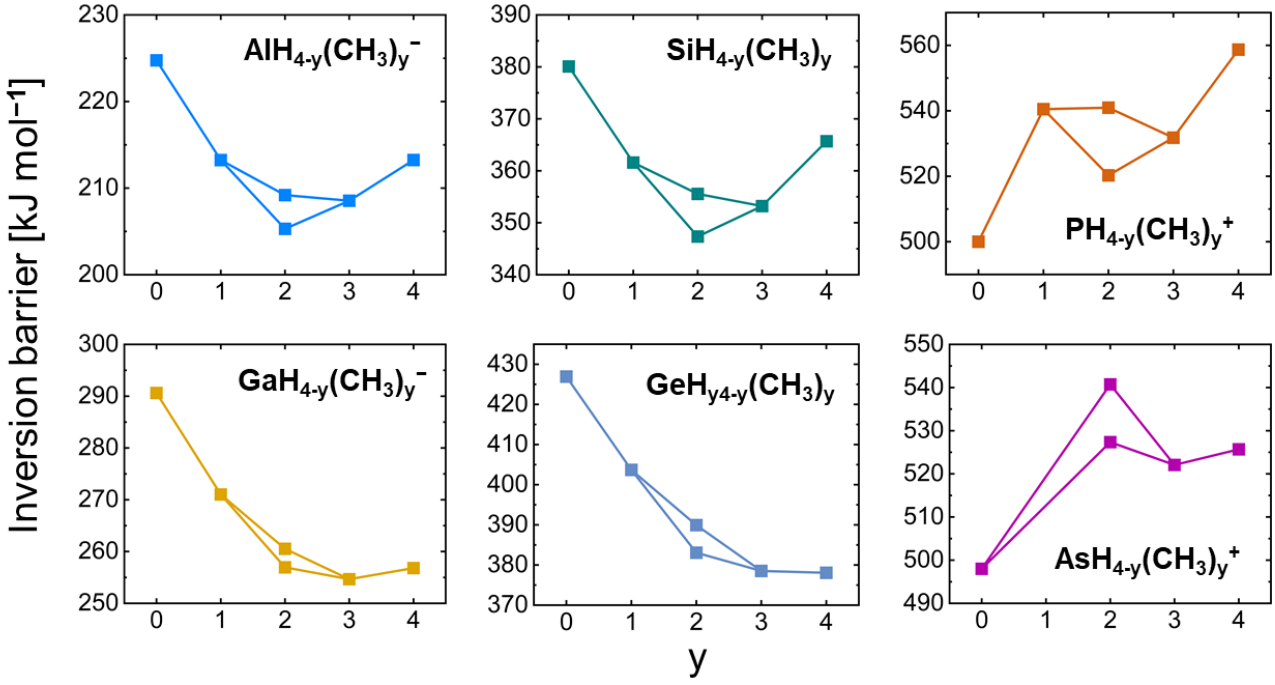

Figure S5: Trends in the inversion barrier height for $\mathbf{EH_{4-y}R_y^n}$ with $\mathbf{E^n}$ = Al^-, Si, P^+, Ga^-, Ge, As^+ and y = 0, 1, 2, 3, 4, **R** = CH_3. For $AsH_3(CH_3)^+$, no inversion transition state was found with the applied computational methodology.

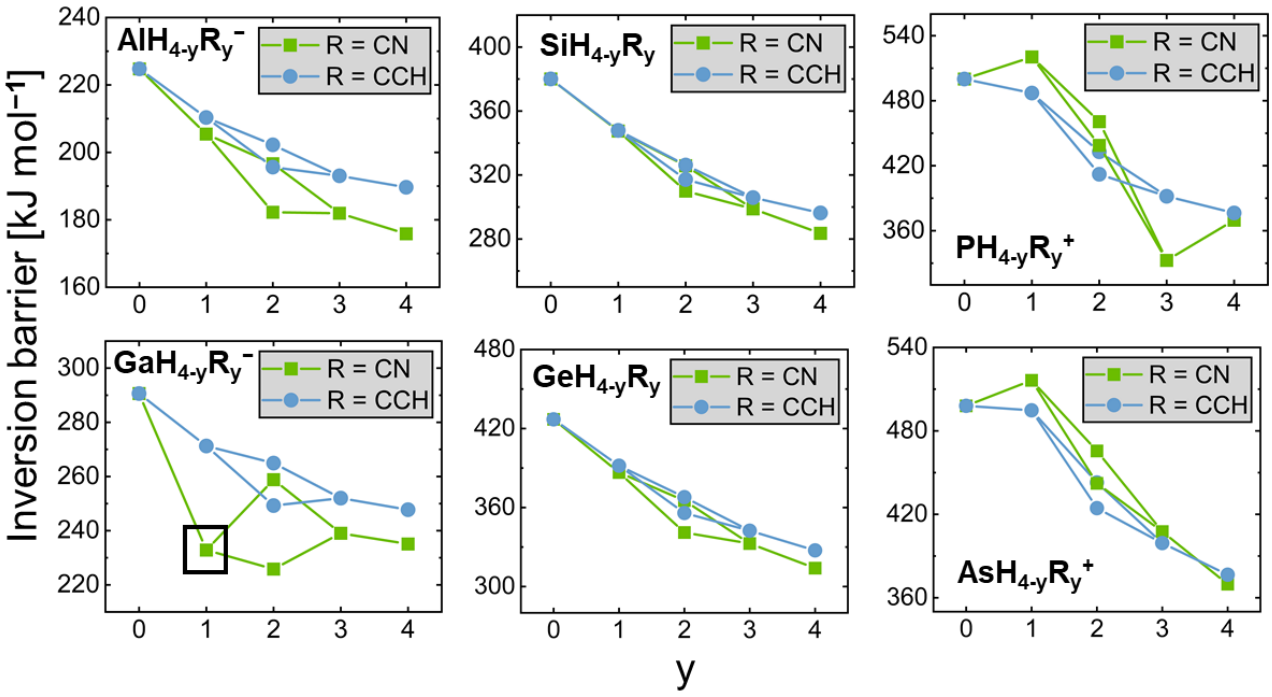

Figure S6: Trends in the inversion barrier height for $\mathbf{EH_{4-y}R_y^n}$ with $\mathbf{E^n}$ = Al^-, Si, P^+, Ga^-, Ge, As^+ and y = 0, 1, 2, 3, 4, **R** = CN, CCH. The transition structure optimization of GaH_3CN^- converged to a dissociative structure (GaH_3 + CN^-) and can thus not be compared with the other data points (marked with black box).

S10. Trends in the inversion barrier height with respect to the central element

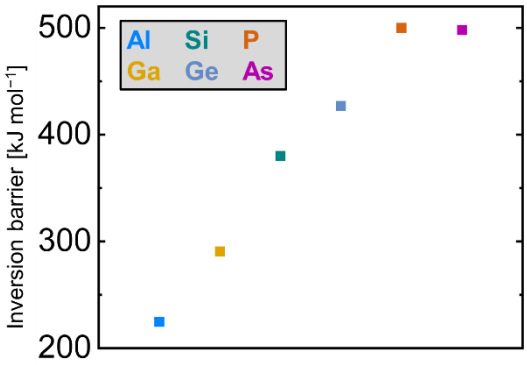

Figure S7: Trend in the inversion barrier height for **EH_4^n** with **E^n** = Al^-, Si, P^+, Ga^-, Ge, As^+. The transition states of PH_4^+ and AsH_4^+ were calculated on the NEVPT2/cc-pVQZ//CASSCF(8,8)/cc-pVTZ level of theory. They have an open-shell singlet electronic configuration ($^1B_{2u}$ state).

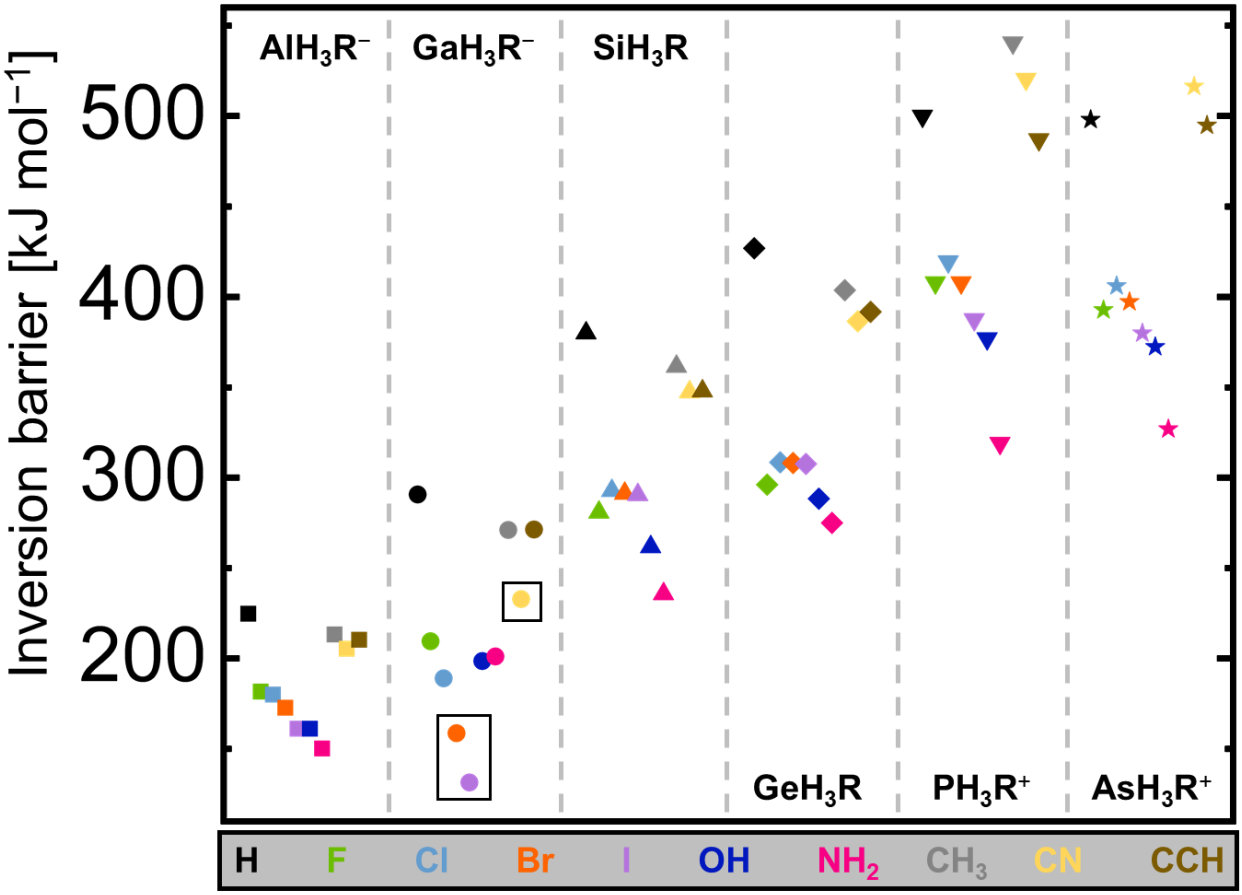

Figure S8: Trends in the inversion barrier height for **EH_3R^n** with **E^n** = Al^-, Si, P^+, Ga^-, Ge, As^+ and **R** = H, F, Cl, Br, I, OH, NH_2, CH_3, CN, CCH. The transition structure optimization of GaH_3Br^-, GaH_3I^-, and GaH_3CN^- converged to a dissociative structure (GaH_3 + $Br/I/CN^-$) and can thus not be compared with the other data points (marked with black box).

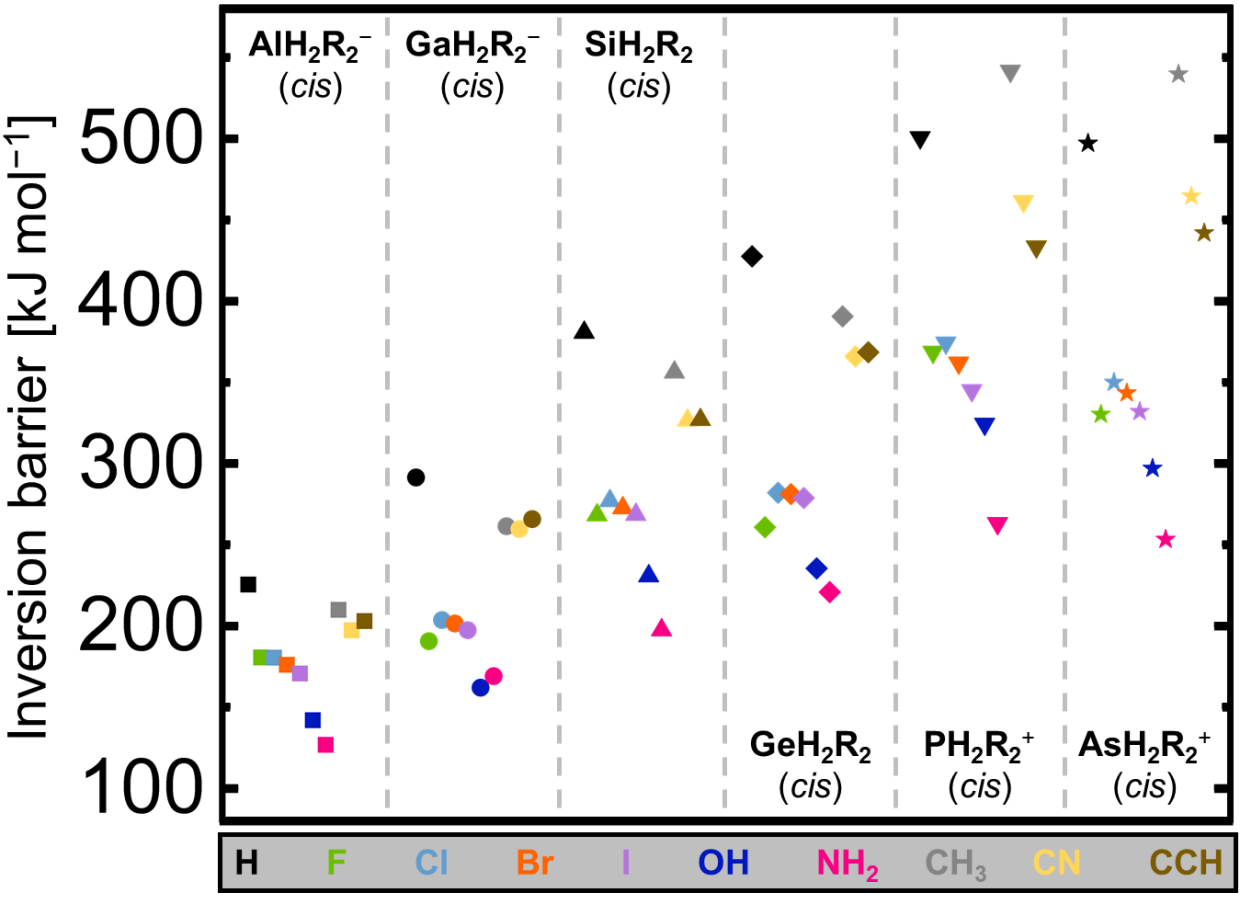

Figure S9: Trends in the inversion barrier height for $\mathbf{EH_2R_2^n}$ with $\mathbf{E^n}$ = Al^-, Si, P^+, Ga^-, Ge, As^+ and **R** = H, F, Cl, Br, I, OH, NH_2, CH_3, CN, CCH considering the *cis*-configurated inversion transition states.

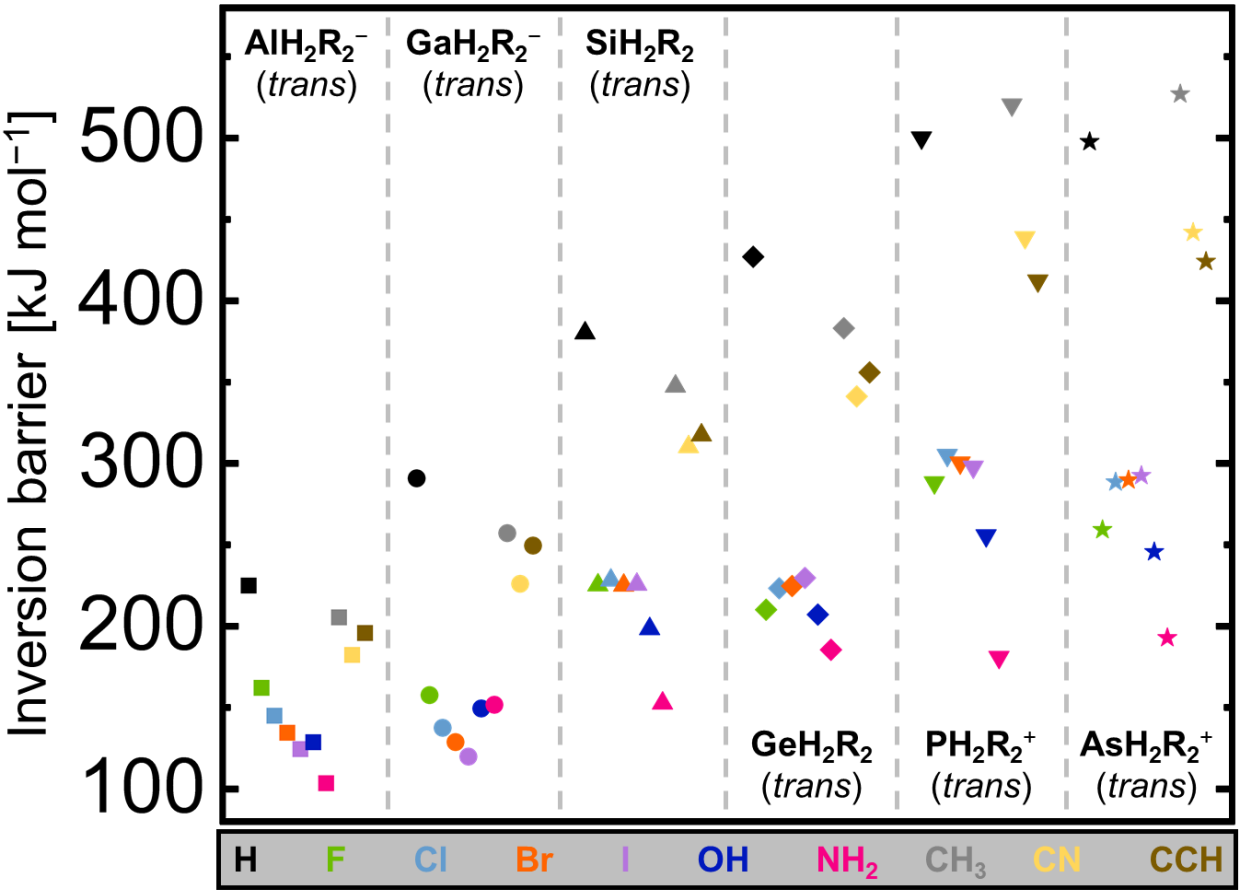

Figure S10: Trends in the inversion barrier height for $\mathbf{EH_2R_2^n}$ with $\mathbf{E^n}$ = Al^-, Si, P^+, Ga^-, Ge, As^+ and **R** = H, F, Cl, Br, I, OH, NH_2, CH_3, CN, CCH considering the *trans*-configurated inversion transition states.

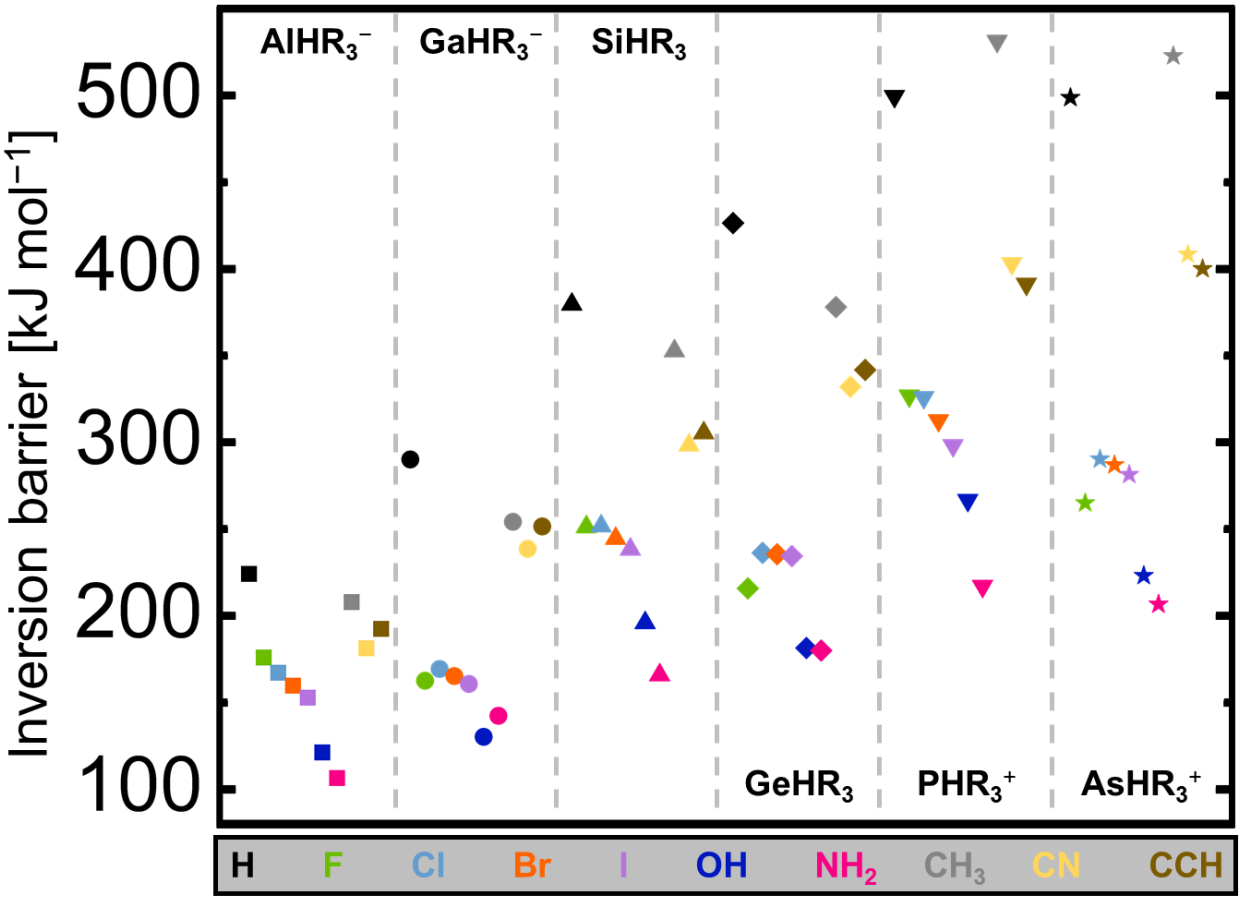

Figure S11: Trends in the inversion barrier height for EHR_3^n with E^n = Al^-, Si, P^+, Ga^-, Ge, As^+ and **R** = H, F, Cl, Br, I, OH, NH_2, CH_3, CN, CCH.

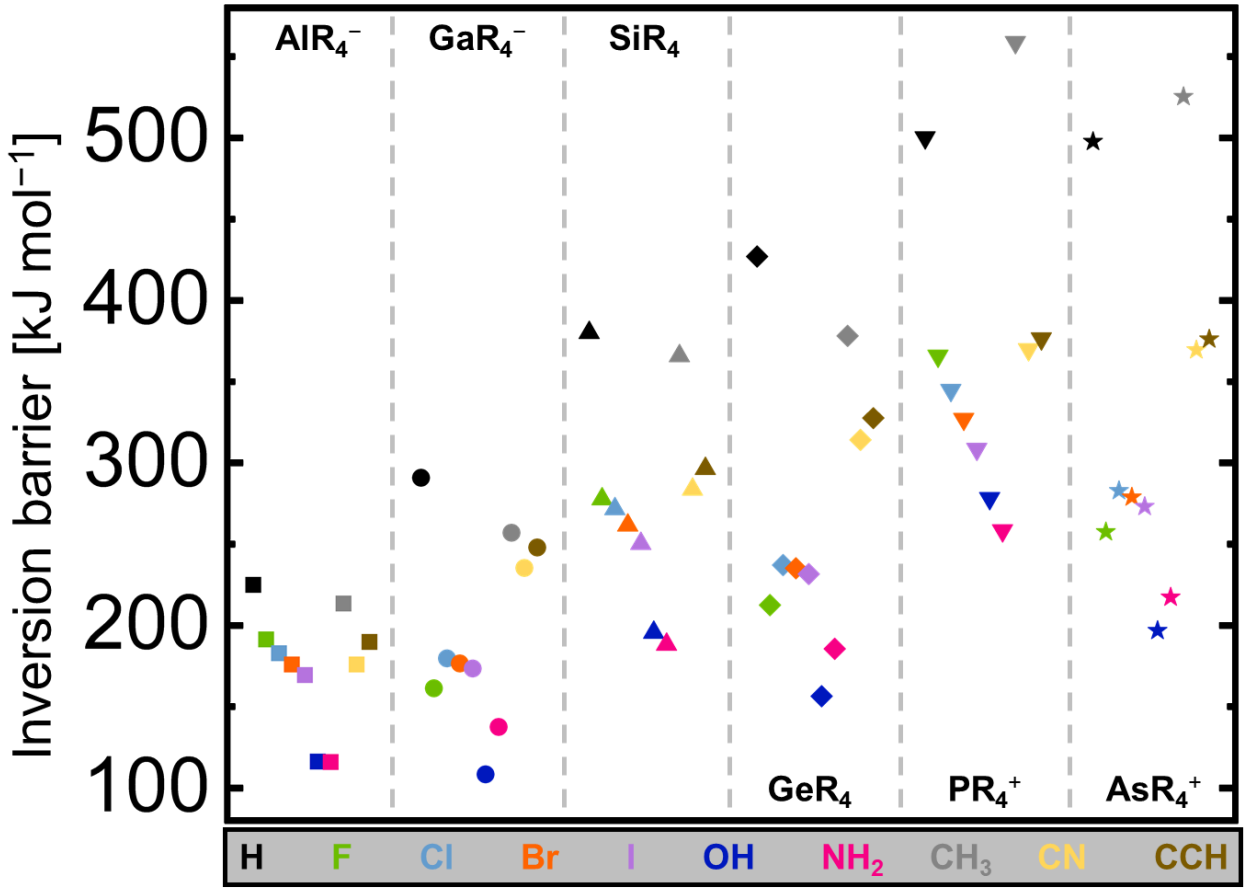

Figure S12: Trends in the inversion barrier height for $\mathbf{ER_4^n}$ with $\mathbf{E^n}$ = Al^-, Si, P^+, Ga^-, Ge, As^+ and **R** = H, F, Cl, Br, I, OH, NH_2, CH_3, CN, CCH.

S11. Inversion transition structures of $EH_{4-y}(OH)_y^n$

The isomeric inversion transition structures of $\mathbf{EH_{4-y}(OH)_y^n}$ with $\mathbf{E^n}$ = Al^-, Si, P^+, Ga^-, Ge, As^+ and y = 0, 1, 2, 3, 4 were investigated. For the transition structures of $\mathbf{EH_{4-y}(OH)_y^n}$ with *cis*-configuration, three conformers were considered (Figure S13A) whereas for the corresponding *trans*-isomers, two conformers were of relevance (Figure S13B). Regarding $\mathbf{EH_{4-y}(OH)_y^n}$, four different transition structures were investigated (Figure S13C). All conformers were obtained through transition structure optimization and were confirmed as valid inversion transition states by frequency calculations.

The two possible *trans*-structures are essentially isoenergetic (Table S8). The *cis*-structures which possess a hydrogen bond (*cis*-TS1-$\mathbf{EH_2(OH)_2^n}$) are favored over the two others without a hydrogen bond (Table S8). Comparing *cis* and *trans*-transition states, the *trans*-version is favored, as it is for all other substituents, too (see Table S7). To estimate the influence of hydrogen bonding, the $\mathbf{EH(OH)_3^n}$ class of compounds was used. TS1-$\mathbf{EH(OH)_3^n}$ was compared with TS2-$\mathbf{EH(OH)_3^n}$ and TS3-$\mathbf{EH(OH)_3^n}$ with TS4-$\mathbf{EH(OH)_3^n}$. It was found that the two energy differences are of comparable size (Table S9). Their mean was thus interpreted as the energetically stabilizing influence of one hydrogen bond.

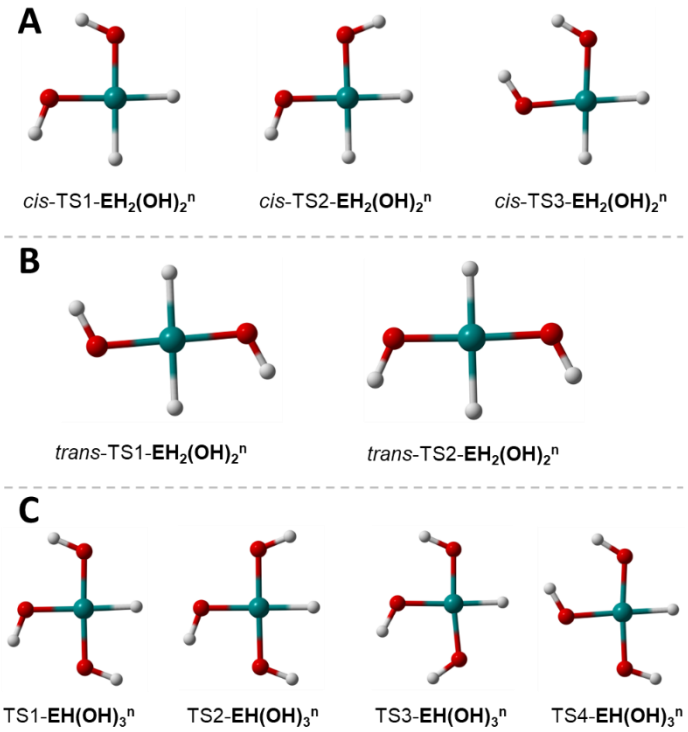

Figure S13: Molecular representations of the possible inversion transition structures of **A, B)** $EH_2(OH)_2^n$ and of **C)** $EH(OH)_3^n$, with E^n = Al^-, Si, P^+, Ga^-, Ge, As^+.

Table S8: Inversion transition state energies of the *cis*/*trans*-$EH_2(OH)_2^n$ class of compounds relative to *trans*-TS1-$EH_2(OH)_2^n$ and *cis*-TS1-$EH_2(OH)_2^n$, with E^n = Al^-, Si, P^+, Ga^-, Ge, As^+.

Element	Compound	Relative energy [kJ mol^{-1}]
	trans-TS-$[EH_2(OH)_2]^{-/0/+}$	
Al	*trans*-TS1-$[AlH_2(OH)_2]^-$	0.0
	trans-TS2-$[AlH_2(OH)_2]^-$	-0.3
Ga	*trans*-TS1-$[GaH_2(OH)_2]^-$	0.0
	trans-TS2-$[GaH_2(OH)_2]^-$	-0.5
Si	*trans*-TS1-$[SiH_2(OH)_2]$	0.0
	trans-TS2-$[SiH_2(OH)_2]$	0.9
Ge	*trans*-TS1-$[GeH_2(OH)_2]$	0.0
	trans-TS2-$[GeH_2(OH)_2]$	0.7
P	*trans*-TS1-$[PH_2(OH)_2]^+$	0.0
	trans-TS2-$[PH_2(OH)_2]^+$	1.7
As	*trans*-TS1-$[AsH_2(OH)_2]^+$	0.0
	trans-TS2-$[AsH_2(OH)_2]^+$	1.2
	cis-TS-$[EH_2(OH)_2]^{-/0/+}$	
Al	*cis*-TS1-$[AlH_2(OH)_2]^-$	0.0
	cis-TS2-$[AlH_2(OH)_2]^-$	3.1
	cis-TS3-$[AlH_2(OH)_2]^-$	19.6
Ga	*cis*-TS1-$[GaH_2(OH)_2]^-$	0.0
	cis-TS2-$[GaH_2(OH)_2]^-$	8.9
	cis-TS3-$[GaH_2(OH)_2]^-$	16.3
Si	*cis*-TS1-$[SiH_2(OH)_2]$	0.0
	cis-TS2-$[SiH_2(OH)_2]$	8.8
	cis-TS3-$[SiH_2(OH)_2]$	18.6
Ge	*cis*-TS1-$[GeH_2(OH)_2]$	0.0

	cis-TS2-[$GeH_2(OH)_2$]	13.7
	cis-TS3-[$GeH_2(OH)_2$]	13.7
P	*cis*-TS1-$[PH_2(OH)_2]^+$	0.0
	cis-TS2-$[PH_2(OH)_2]^+$	14.9
	cis-TS3-$[PH_2(OH)_2]^+$	17.1
As	*cis*-TS1-$[AsH_2(OH)_2]^+$	0.0
	cis-TS2-$[AsH_2(OH)_2]^+$	18.4
	cis-TS3-$[AsH_2(OH)_2]^+$	11.5

Table S9: Inversion transition state energies of the **$EH(OH)_3^n$** class of compounds relative to TS1-**$EH(OH)_3^n$**, with **E^n** = Al^-, Si, P^+, Ga^-, Ge, As^+. The last column gives the difference in energy between TS1 compared to TS2 and TS3 compared to TS4 which was used to estimate the influence of hydrogen bonding.

Element	Compound	Relative energy [kJ mol^{-1}]	Energy difference between TS1/2 and TS3/4 [kJ mol^{-1}]
TS-[**EH(OH)3**]$^{-/0/+}$			
Al	*trans*-TS1-$[AlH(OH)_3]^-$	0.0	5.2
	trans-TS2-$[AlH(OH)_3]^-$	5.2	
	trans-TS3-$[AlH(OH)_3]^-$	17.9	4.7
	trans-TS4-$[AlH(OH)_3]^-$	22.6	
Ga	*trans*-TS1-$[GaH(OH)_3]^-$	0.0	10.3
	trans-TS2-$[GaH(OH)_3]^-$	10.3	
	trans-TS3-$[GaH(OH)_3]^-$	13.2	10.3
	trans-TS4-$[GaH(OH)_3]^-$	23.5	
Si	*trans*-TS1-$[SiH(OH)_3]$	0.0	13.0
	trans-TS2-$[SiH(OH)_3]$	13.0	
	trans-TS3-$[SiH(OH)_3]$	17.8	10.9
	trans-TS4-$[SiH(OH)_3]$	28.7	
Ge	*trans*-TS1-$[GeH(OH)_3]$	0.0	16.1
	trans-TS2-$[GeH(OH)_3]$	16.1	
	trans-TS3-$[GeH(OH)_3]$	12.3	14.6
	trans-TS4-$[GeH(OH)_3]$	26.9	
P	*trans*-TS1-$[PH(OH)_3]^+$	0.0	22.3
	trans-TS2-$[PH(OH)_3]^+$	22.3	
	trans-TS3-$[PH(OH)_3]^+$	16.0	18.8
	trans-TS4-$[PH(OH)_3]^+$	34.8	
As	*trans*-TS1-$[AsH(OH)_3]^+$	0.0	22.7
	trans-TS1-$[AsH(OH)_3]^+$	22.7	
	trans-TS1-$[AsH(OH)_3]^+$	10.1	20.1
	trans-TS1-$[AsH(OH)_3]^+$	30.2	

S12. Comparison of HOMO-LUMO gaps and TDDFT data

TDDFT calculations were carried out as described in Chapter S1. The energy differences between the highest occupied and lowest unoccupied molecular orbital obtained from the B97M-D3(BJ)/cc-pVTZ level were compared to the first vertical excitation energies from TDDFT calculations using the same computational method. This was done for a subset of the investigated inversion transition states, namely for $\mathbf{EH_4^n}$ (4 structures), $\mathbf{EH_{4-y}F_y^n}$, with y = 1, 4 (12 structures), and $\mathbf{EH_{4-y}(CN)_y^n}$, with y = 1, 2, 3, 4 (30 structures). In all cases, the lowest vertical excitation corresponded to more than 95% to the HOMO-LUMO transition. The HOMO-LUMO gaps were found to correlate well with the first vertical excitation energies, and therefore the former were used to analyze the entire set of molecules.

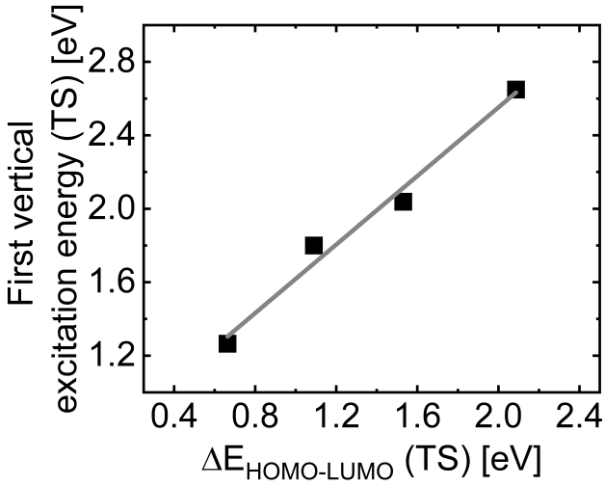

Figure S14: Correlation plot (R^2 = 0.9827) for the first vertical excitation energy *versus* the HOMO-LUMO gap of the inversion transition states of $\mathbf{EH_4^n}$, with $\mathbf{E^n}$ = Al^-, Si, Ga^-, Ge.

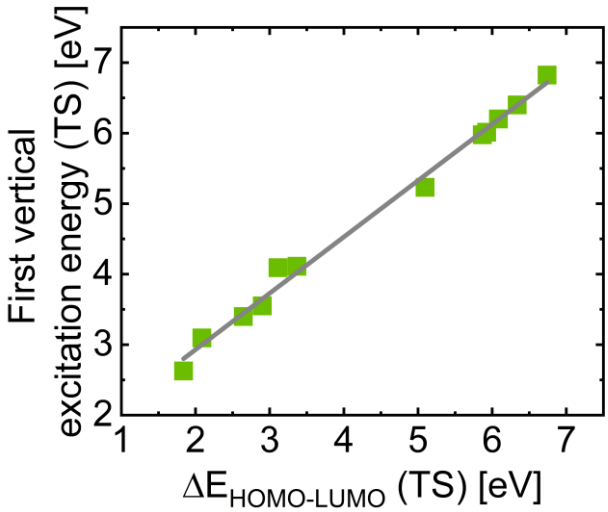

Figure S15: Correlation plot (R^2 = 0.9924) for the first vertical excitation energy *versus* the HOMO-LUMO gap of the inversion transition states of $\mathbf{EH_{4-y}F_y^n}$, with $\mathbf{E^n}$ = Al^-, Si, P^+, Ga^-, Ge, As^+ and y = 1, 4.

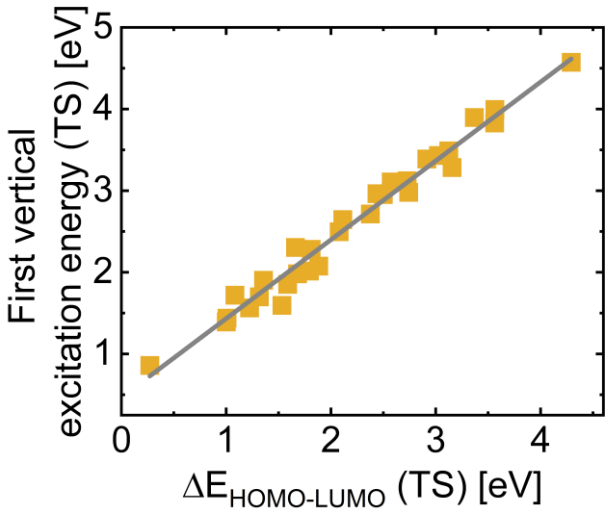

Figure S16: Correlation plot (R^2 = 0.9761) for the first vertical excitation energy *versus* the HOMO-LUMO gap of the inversion transition states of $\mathbf{EH_{4-y}(CN)_y^n}$, with $\mathbf{E^n}$ = Al^-, Si, P^+, Ga^-, Ge, As^+ and y = 1, 2, 3, 4.

S13. Correlation plots of inversion barrier heights against transition state HOMO-LUMO gaps

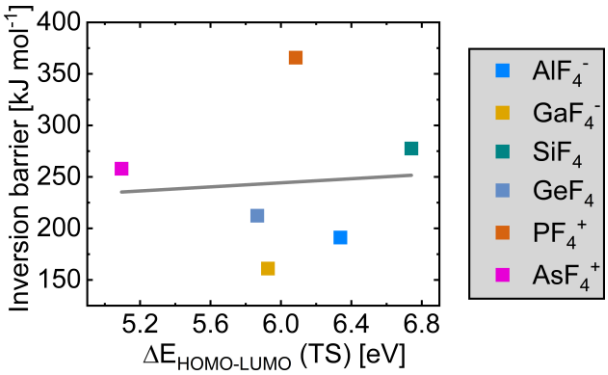

Figure S17: Correlation plot (R^2 = 0.0055) of the inversion barrier heights *versus* the HOMO-LUMO gap in the inversion transition state for $\mathbf{EF_4^n}$, $\mathbf{E^n}$ = Al^-, Si, P^+, Ga^-, Ge, As^+.

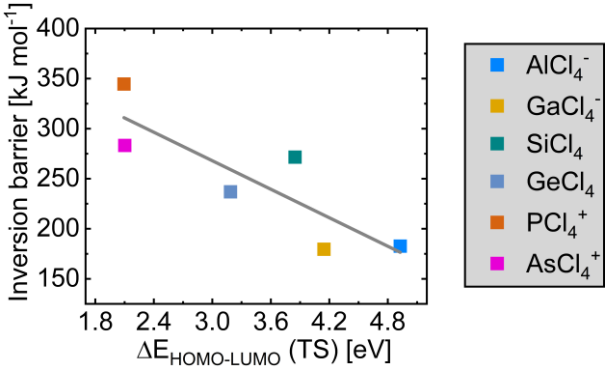

Figure S18: Correlation plot (R^2 = 0.7279) of the inversion barrier heights *versus* the HOMO-LUMO gap in the inversion transition state for $\mathbf{ECl_4^n}$, $\mathbf{E^n}$ = Al^-, Si, P^+, Ga^-, Ge, As^+.

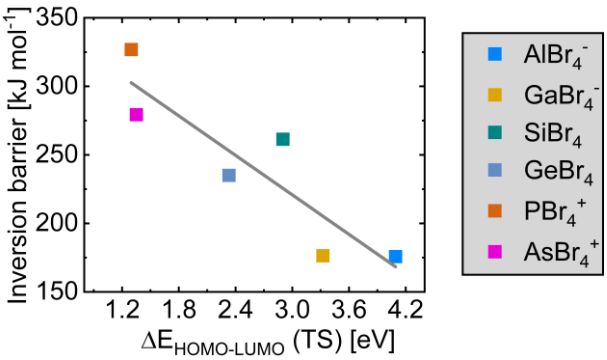

Figure S19: Correlation plot (R^2 = 0.8018) of the inversion barrier heights *versus* the HOMO-LUMO gap in the inversion transition state for **EBr_4^n**, **E^n** = Al^-, Si, P^+, Ga^-, Ge, As^+.

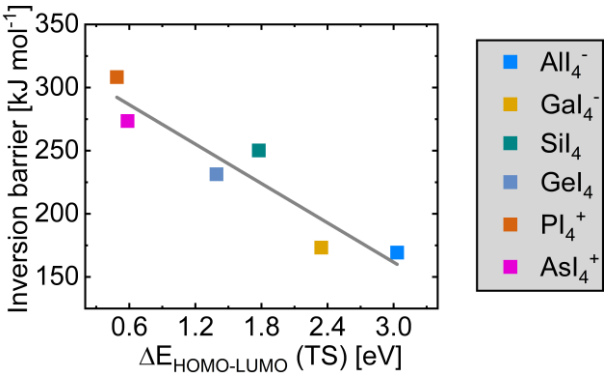

Figure S20: Correlation plot (R^2 = 0.8782) of the inversion barrier heights *versus* the HOMO-LUMO gap in the inversion transition state for **EI_4^n**, **E^n** = Al^-, Si, P^+, Ga^-, Ge, As^+.

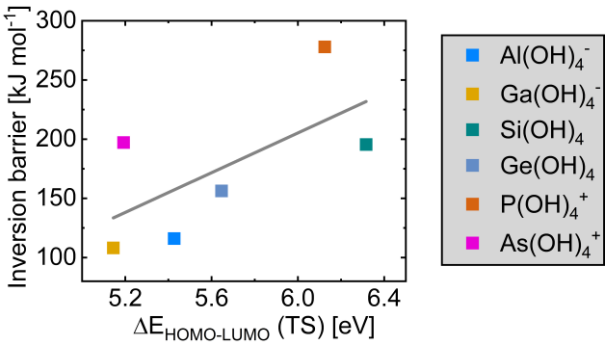

Figure S21: Correlation plot (R^2 = 0.4210) of the inversion barrier heights *versus* the HOMO-LUMO gap in the inversion transition state for **$E(OH)_4^n$**, **E^n** = Al^-, Si, P^+, Ga^-, Ge, As^+.

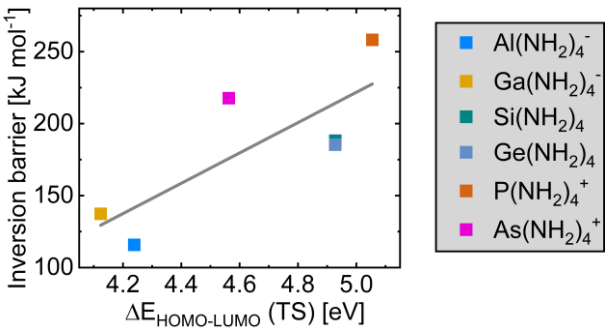

Figure S22: Correlation plot (R^2 = 0.6344) of the inversion barrier heights *versus* the HOMO-LUMO gap in the inversion transition state for **$E(NH_2)_4^n$**, **E^n** = Al^-, Si, P^+, Ga^-, Ge, As^+.

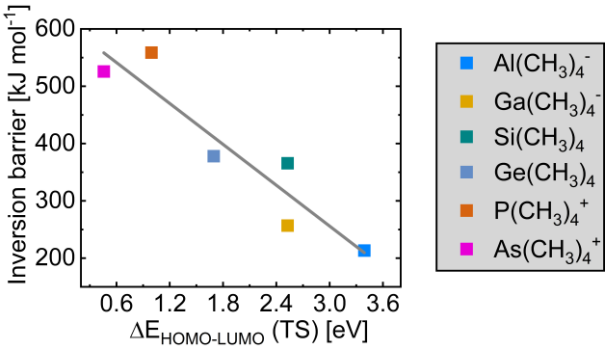

Figure S23: Correlation plot (R^2 = 0.8732) of the inversion barrier heights *versus* the HOMO-LUMO gap in the inversion transition state for **E(CH₃)₄ⁿ**, **Eⁿ** = Al^-, Si, P^+, Ga^-, Ge, As^+.

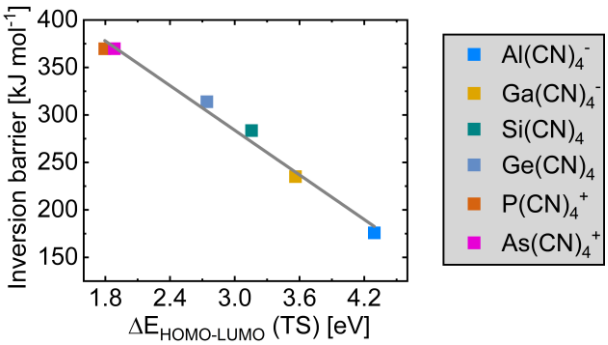

Figure S24: Correlation plot (R^2 = 0.9870) of the inversion barrier heights *versus* the HOMO-LUMO gap in the inversion transition state for **E(CN)₄ⁿ**, **Eⁿ** = Al^-, Si, P^+, Ga^-, Ge, As^+.

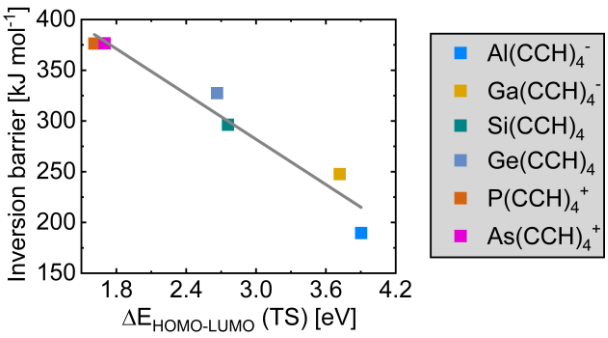

Figure S25: Correlation plot (R^2 = 0.9442) of the inversion barrier heights *versus* the HOMO-LUMO gap in the inversion transition state for **E(CCH)₄ⁿ**, **Eⁿ** = Al^-, Si, P^+, Ga^-, Ge, As^+.

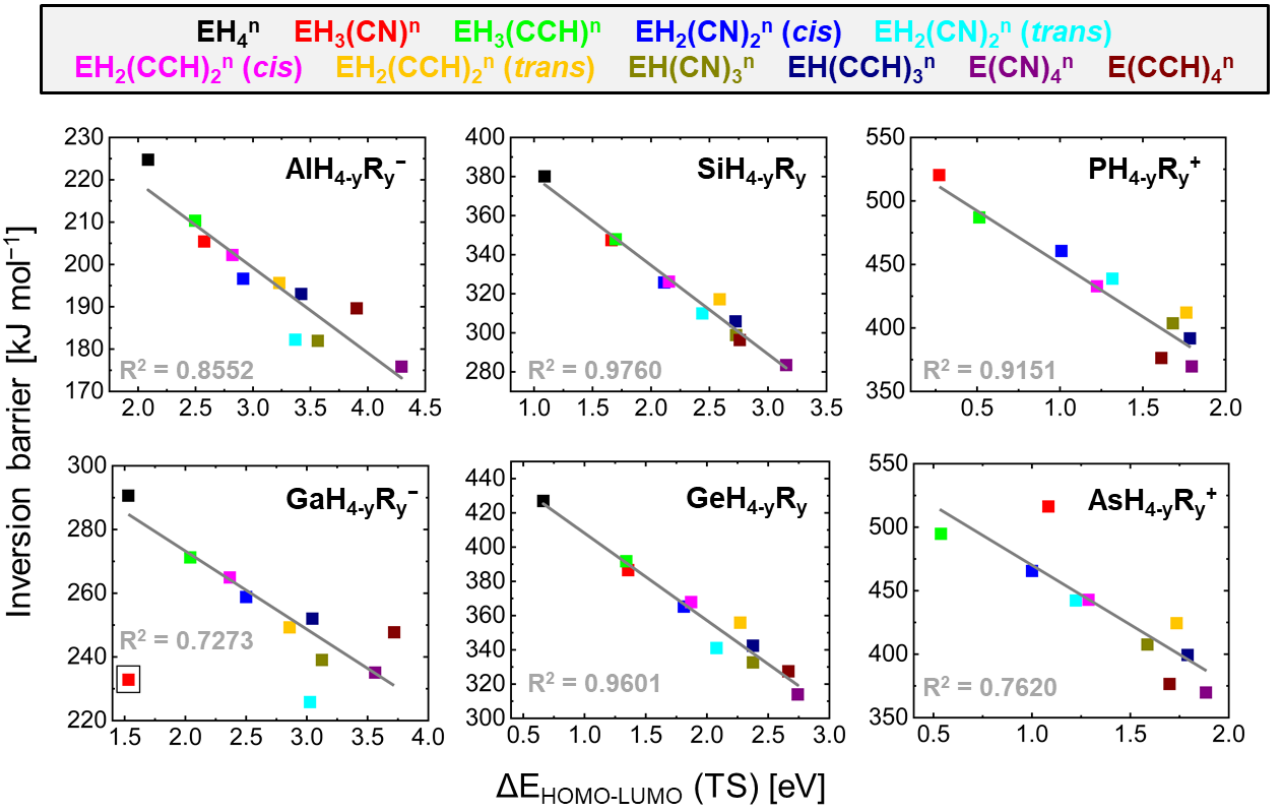

Figure S26: Correlation plots of the inversion barrier height *versus* the Kohn-Sham HOMO-LUMO gap in the inversion transition state for $\mathbf{EH_{4-y}R_y^n}$, $\mathbf{E^n}$ = Al^-, Si, P^+, Ga^-, Ge, As^+ and **R** = CN, CCH, y = 0, 1, 2, 3, 4. The data point for GaH_3CN^- (marked with a box) was not included in the linear regression as the transition structure optimization converged to a dissociative structure.

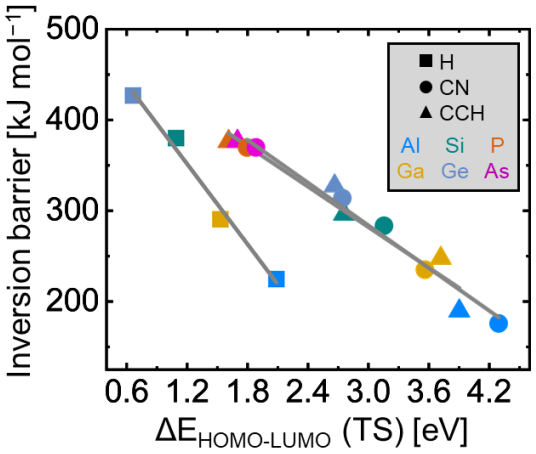

Figure S27: Comparison of the correlation of the inversion barrier height *versus* the Kohn-Sham HOMO-LUMO gap in the inversion transition state for $\mathbf{ER_4^n}$, $\mathbf{E^n}$ = Al^-, Si, P^+, Ga^-, Ge, As^+ and **R** = H, CN, CCH.

S14. Natural bond orbital analyses

Natural bond orbital (NBO) analyses were carried out as described in Chapter S1.

Table S10: Natural charges of the central element of the ground and inversion transition state of ER_4^n with E^n = Al^-, Si, P^+, Ga^-, Ge, As^+ and **R** = H, F, Cl, Br, I, OH, NH_2, CH_3, CN, CCH.

Compound	Natural charge of the central element		
	Ground state	Transition state	Difference
Aluminum			
AlH_4^-	0.57049	0.96899	0.3985
AlF_4^-	2.10855	2.1281	0.01955
$AlCl_4^-$	1.38572	1.46609	0.08037
$AlBr_4^-$	1.1422	1.23628	0.09408
AlI_4^-	0.74907	0.86158	0.11251
$Al(OH)_4^-$	1.99348	2.00423	0.01075
$Al(NH_2)_4^-$	1.82311	1.88261	0.0595
$Al(CH_3)_4^-$	1.58578	1.80524	0.21946
$Al(CN)_4^-$	1.18313	1.39893	0.2158
$Al(CCH)_4^-$	1.35394	1.55337	0.19943
Gallium			
GaH_4^-	0.23335	0.79667	0.56332
GaF_4^-	2.04399	2.04423	0.00024
$GaCl_4^-$	1.27626	1.33871	0.06245
$GaBr_4^-$	0.98371	1.06552	0.08181
GaI_4^-	0.53686	0.6577	0.12084
$Ga(OH)_4^-$	1.9008	1.91452	0.01372
$Ga(NH_2)_4^-$	1.69451	1.79243	0.09792
$Ga(CH_3)_4^-$	1.39484	1.65266	0.25782
$Ga(CN)_4^-$	0.95944	1.28117	0.32173
$Ga(CCH)_4^-$	1.14169	1.44644	0.30475
Silicon			
SiH_4	0.55975	1.13747	0.57772
SiF_4	2.53116	2.52241	-0.00875
$SiCl_4$	1.29647	1.34103	0.04456
$SiBr_4$	0.92104	0.97732	0.05628
SiI_4	0.41609	0.17381	-0.24228
$Si(OH)_4$	2.36362	2.33136	-0.03226
$Si(NH_2)_4$	2.08901	2.08797	-0.00104
$Si(CH_3)_4$	1.60607	1.93719	0.33112
$Si(CN)_4$	1.36167	1.57971	0.21804
$Si(CCH)_4$	1.50369	1.68529	0.1816
Germanium			
GeH_4	0.43832	1.10654	0.66822
GeF_4	2.56446	2.55051	-0.01395
$GeCl_4$	1.39267	1.41089	0.01822
$GeBr_4$	0.96708	1.00118	0.0341
GeI_4	0.41058	0.4718	0.06122
$Ge(OH)_4$	2.3855	2.36829	-0.01721
$Ge(NH_2)_4$	2.09243	2.14433	0.0519
$Ge(CH_3)_4$	1.61307	1.90953	0.29646

$Ge(CN)_4$	1.33518	1.61143	0.27625
$Ge(CCH)_4$	1.49235	1.73036	0.23801
Phosphorus			
PF_4^+	2.78457	2.70771	-0.07686
PCl_4^+	1.13791	1.08996	-0.04795
PBr_4^+	0.67458	0.62727	-0.04731
PI_4^+	0.11388	0.07536	-0.03852
$P(OH)_4^+$	2.57103	2.44756	-0.12347
$P(NH_2)_4^+$	2.20486	2.09288	-0.11198
$P(CH_3)_4^+$	1.5881	1.93523	0.34713
$P(CN)_4^+$	1.4611	1.49097	0.02987
$P(CCH)_4^+$	1.59122	1.57401	-0.01721
Arsenic			
AsF_4^+	2.88387	2.83098	-0.05289
$AsCl_4^+$	1.37078	1.31534	-0.05544
$AsBr_4^+$	0.87939	0.82546	-0.05393
AsI_4^+	0.28951	-0.00365	-0.29316
$As(OH)_4^+$	2.64632	2.56573	-0.08059
$As(NH_2)_4^+$	2.26846	2.237	-0.03146
$As(CH_3)_4^+$	1.64475	2.00717	0.36242
$As(CN)_4^+$	1.55569	1.64065	0.08496
$As(CCH)_4^+$	1.70869	1.73272	0.02403

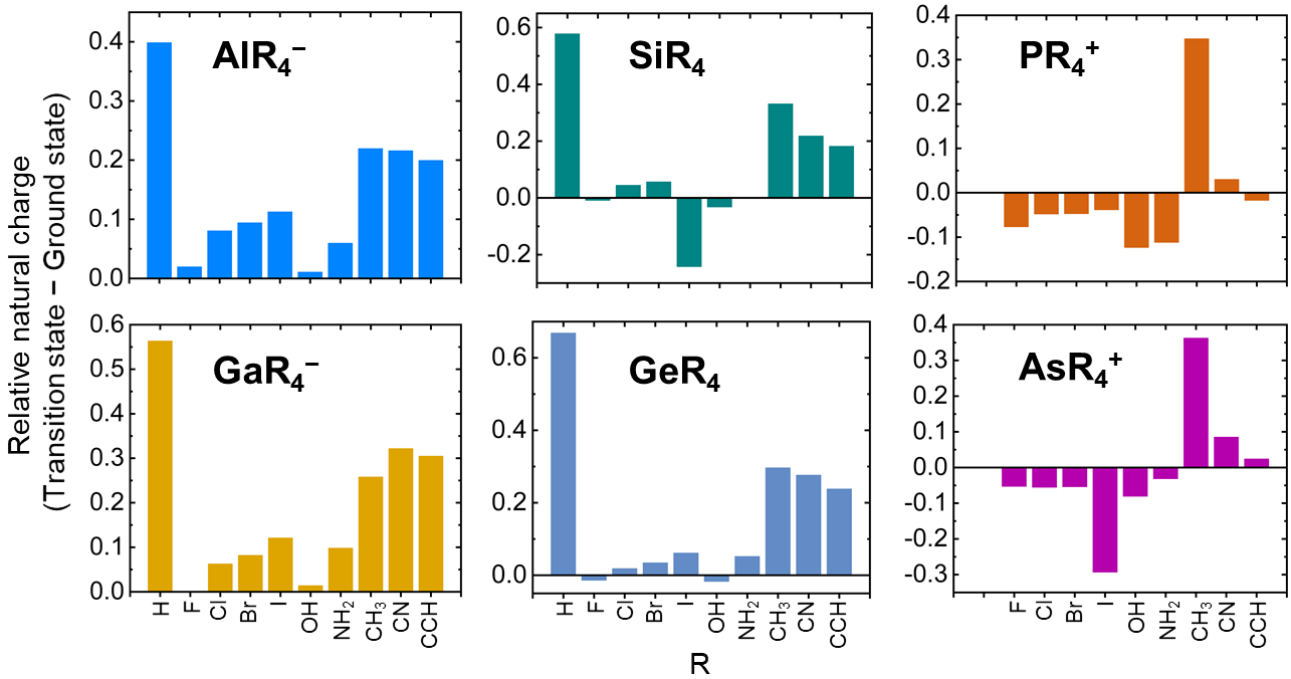

Figure S28: Relative natural charges (Transition state – Ground state) of the central element of ER_4^n with E^n = Al^-, Si, P^+, Ga^-, Ge, As^+ and **R** = H, F, Cl, Br, I, OH, NH_2, CH_3, CN, CCH.

Table S11: Natural electron configuration of the central element of the ground and inversion transition state of ER_4^n with E^n = Al^-, Si, P^+, Ga^-, Ge, As^+ and **R** = H, F, Cl, Br, I, OH, NH_2, CH_3, CN, CCH.

Compound	Natural electron configuration of the central element					
	Ground state			Transition state		
Aluminum						
AlH_4^-	3s 1.000	3p 1.904	3d 0.012	3s 1.000	3p 1.284	3d 0.023
AlF_4^-	3s 1.000	3p 2.000	3d 0.143	3s 1.000	3p 1.893	3d 0.143
$AlCl_4^-$	3s 1.000	3p 1.800	3d 0.091	3s 1.000	3p 1.636	3d 0.091
$AlBr_4^-$	3s 1.000	3p 1.723	3d 0.077	3s 1.000	3p 1.569	3d 0.077
AlI_4^-	3s 1.000	3p 1.688	3d 0.062	3s 1.000	3p 1.519	3d 0.074
$Al(OH)_4^-$	3s 1.000	3p 1.939	4p 0.030	3s 1.000	3p 2.065	4p 0.032
$Al(NH_2)_4^-$	3s 1.000	3p 1.850	3d 0.025	3s 1.000	3p 2.028	3d 0.028
$Al(CH_3)_4^-$	3s 1.000	3p 1.593	3d 0.019	3s 1.000	3p 1.089	3d 0.018
$Al(CN)_4^-$	3s 1.000	3p 1.857	4d 0.016	3s 1.000	3p 1.678	3d 0.017
$Al(CCH)_4^-$	3s 1.000	3p 2.019	3d 0.019	3s 1.000	3p 1.860	3d 0.040
Gallium						
GaH_4^-	4s 1.000	4p 1.936	4d 0.000	4s 1.000	4p 1.095	4d 0.000
GaF_4^-	4s 1.000	4p 1.385	4d 0.026	4s 1.000	4p 1.114	4d 0.045
$GaCl_4^-$	4s 1.000	4p 1.400	4d 0.029	4s 1.000	4p 1.176	4d 0.027
$GaBr_4^-$	4s 1.000	4p 1.420	4d 0.025	4s 1.000	4p 1.186	4d 0.023
GaI_4^-	4s 1.000	4p 1.474	4d 0.021	4s 1.000	4p 1.235	4d 0.020
$Ga(OH)_4^-$	4s 1.000	4p 1.400	5p 0.022	4s 1.000	4p 1.208	5p 0.021
$Ga(NH_2)_4^-$	4s 1.000	4p 1.415	4d 0.019	4s 1.000	4p 1.204	4d 0.019
$Ga(CH_3)_4^-$	4s 1.000	4p 1.409	4d 0.015	4s 1.000	4p 0.773	4d 0.013
$Ga(CN)_4^-$	4s 1.000	4p 1.833	4d 0.000	4s 1.000	4p 1.293	4d 0.000
$Ga(CCH)_4^-$	4s 1.000	4p 1.937	4d 0.000	4s 1.000	4p 1.385	4d 0.000
Silicon						
SiH_4	3s 1.000	3p 2.109	3d 0.018	3s 1.000	3p 1.398	3d 0.025
SiF_4	3s 1.000	3p 2.045	3d 0.205	3s 1.000	3p 1.957	3d 0.196
$SiCl_4$	3s 1.000	3p 2.012	3d 0.129	3s 1.000	3p 1.864	3d 0.125
$SiBr_4$	3s 1.000	3p 1.920	3d 0.110	3s 1.000	3p 1.786	3d 0.107
SiI_4	3s 1.000	3p 1.882	3d 0.092	3s 1.000	3p 0.877	4s 0.015
$Si(OH)_4$	3s 1.000	3p 2.163	3d 0.143	3s 1.000	3p 2.224	3d 0.143
$Si(NH_2)_4$	3s 1.000	3p 2.246	3d 0.070	3s 1.000	3p 2.577	3d 0.096
$Si(CH_3)_4$	3s 1.000	3p 2.078	3d 0.026	3s 1.000	3p 1.446	3d 0.036
$Si(CN)_4$	3s 1.000	3p 2.171	3d 0.037	3s 1.000	3p 2.000	3d 0.051
$Si(CCH)_4$	3s 1.000	3p 2.356	3d 0.041	3s 1.000	3p 2.290	3d 0.058
Germanium						
GeH_4	4s 1.000	4p 2.043	4d 0.009	4s 1.000	4p 1.223	4d 0.008
GeF_4	4s 1.000	4p 1.421	4d 0.070	4s 1.000	4p 1.206	4d 0.063
$GeCl_4$	4s 1.000	4p 1.571	4d 0.051	4s 1.000	4p 1.404	4d 0.048
$GeBr_4$	4s 1.000	4p 1.625	4d 0.045	4s 1.000	4p 1.458	4d 0.042
GeI_4	4s 1.000	4p 1.705	4d 0.039	4s 1.000	4p 1.548	4d 0.044
$Ge(OH)_4$	4s 1.000	4p 1.508	5p 0.016	4s 1.000	4p 1.388	4d 0.030
$Ge(NH_2)_4$	4s 1.000	4p 1.648	5p 0.014	4s 1.000	4p 1.614	5p 0.014
$Ge(CH_3)_4$	4s 1.000	4p 1.663	4d 0.011	4s 1.000	4p 1.050	5p 0.010
$Ge(CN)_4$	4s 1.000	4p 1.891	5d 0.011	4s 1.000	4p 1.505	4d 0.011
$Ge(CCH)_4$	4s 1.000	4p 2.012	4d 0.012	4s 1.000	4p 1.690	5d 0.012
Phosphorus						
PF_4^+	3s 1.000	3p 2.108	3d 0.246	3s 1.000	3p 2.043	3d 0.217

PCl_4^+	3s 1.000	3p 2.121	3d 0.172	3s 1.000	3p 2.058	3d 0.140
PBr_4^+	3s 1.000	3p 2.091	3d 0.144	3s 1.000	3p 2.029	3d 0.123
PI_4^+	3s 1.000	3p 2.134	3d 0.114	3s 1.000	3p 2.105	3d 0.098
$P(OH)_4^+$	3s 1.000	3p 2.304	3d 0.174	3s 1.000	3p 2.347	3d 0.167
$P(NH_2)_4^+$	3s 1.000	3p 2.405	3d 0.101	3s 1.000	3p 2.733	3d 0.120
$P(CH_3)_4^+$	3s 1.000	3p 2.272	3d 0.029	3s 1.000	3p 1.712	3d 0.045
$P(CN)_4^+$	3s 1.000	3p 2.337	3d 0.058	3s 1.000	3p 2.430	3d 0.070
$P(CCH)_4^+$	3s 1.000	3p 2.505	3d 0.074	3s 1.000	3p 2.711	3d 0.078
Arsenic						
AsF_4^+	4s 1.000	4p 1.557	4d 0.089	4s 1.000	4p 1.407	4d 0.081
$AsCl_4^+$	4s 1.000	4p 1.815	4d 0.081	4s 1.000	4p 1.718	4d 0.069
$AsBr_4^+$	4s 1.000	4p 1.863	4d 0.072	4s 1.000	4p 1.793	4d 0.062
AsI_4^+	4s 1.000	4p 1.980	4d 0.065	4s 1.000	4p 1.452	5s 0.005
$As(OH)_4^+$	4s 1.000	4p 1.747	4d 0.060	4s 1.000	4p 1.663	4d 0.056
$As(NH_2)_4^+$	4s 1.000	4p 1.924	4d 0.033	4s 1.000	4p 2.091	4d 0.034
$As(CH_3)_4^+$	4s 1.000	4p 1.956	4d 0.009	4s 1.000	4p 1.376	5p 0.008
$As(CN)_4^+$	4s 1.000	4p 2.062	4d 0.018	4s 1.000	4p 1.947	4d 0.018
$As(CCH)_4^+$	4s 1.000	4p 2.206	4d 0.020	4s 1.000	4p 2.198	4d 0.020

S15. Energy decomposition analyses

Energy decomposition analyses (EDA) were carried out as described in Chapter S1 for the ground and inversion transition states of all $\mathbf{ER_4^n}$ with $\mathbf{E^n}$ = Al^-, Si, P^+, Ga^-, Ge, As^+ and R = H, F, Cl, Br, I, OH, NH_2, CH_3, CN, CCH. For five compounds, $Si(NH_2)_4$, $Si(CH_3)_4$, $P(NH_2)_4^+$, AsI_4^+, and $As(CH_3)_4$), the calculation for the transition structure did not converge and non-aufbau populations were obtained. Therefore, results for those compounds are not shown. PH_4^+ and AsH_4^+ were not analyzed by the EDA due to the open-shell singlet configuration in their inversion transition states. As it is shown in Table S12, unreliably large electrostatic contributions were obtained for R = CCH. They were excluded from the data evaluation.

The following parameters were obtained from the EDA calculations: ΔE_{Pauli} (total Pauli repulsion), ΔE_{Coul} (electrostatic interaction), ΔE_{Orb} (total orbital interaction), ΔE_{Disp} (dispersion energy). They sum up to ΔE_{Int} (total interaction energy).[20]

$$\Delta E^i_{Int} = \Delta E^i_{Pauli} + \Delta E^i_{Coul} + \Delta E^i_{Orb} + \Delta E^i_{Disp}, \tag{6}$$

with i = GS (ground state) or TS (transition state). Moreover, ΔE_{Prep} (preparation energy) is defined as

$$\Delta E^i_{Prep} = E^i_{Region1} - E^{i,0}_{Region1} + E^i_{Region2} - E^{i,0}_{Region2}. \tag{7}$$

Given the chosen fragmentation scheme (Figure S29),

$$E^{GS}_{Region1} = E^{GS,0}_{Region1} = E^{TS}_{Region1} = E^{TS,0}_{Region1}, \tag{8}$$

and

$$E^{GS,0}_{Region2} = E^{TS,0}_{Region2}. \tag{9}$$

Therefore,

$$\Delta\Delta E_{Prep} = \Delta E^{TS}_{Prep} - \Delta E^{GS}_{Prep} = E^{TS}_{Region2} - E^{GS}_{Region2}. \tag{10}$$

The single point energies of region 2 for ground ($E^{GS}_{Region2}$) and transition state ($E^{TS}_{Region2}$) were also obtained from the EDA calculations. In total, the inversion barrier (IB) can then be derived from the EDA parameters,

$$IB = \Delta(\Delta E_{Int} + \Delta E_{Prep}) = \Delta E^{TS}_{Int} - \Delta E^{GS}_{Int} + \Delta\Delta E_{Prep} \quad (11)$$
$$= \Delta\Delta E_{Pauli} + \Delta\Delta E_{Coul} + \Delta\Delta E_{Orb} + \Delta\Delta E_{Disp} + \Delta\Delta E_{Prep}.$$

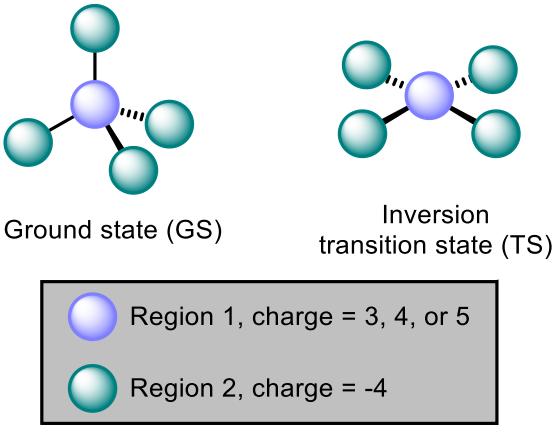

Figure S29: Heterolytic fragmentation scheme which was applied during the EDA analyses.

Table S12: Results of the energy decomposition analyses carried out for **ER$_4^n$** with **E^n** = Al$^-$, Si, P$^+$, Ga$^-$, Ge, As$^+$ and **R** = H, F, Cl, Br, I, OH, NH_2, CH_3, CN, CCH. Calculations were done on the ZORA-BP86-D3(BJ)/TZ2P level of theory. The applied fragmentation scheme is shown in Figure S29.

		ΔE_{Pauli} [kJ mol^{-1}]	**ΔE_{Coul} [kJ mol^{-1}]**	**ΔE_{Orb} [kJ mol^{-1}]**	**ΔE_{Disp} [kJ mol^{-1}]**	**ΔE_{Int} [kJ mol^{-1}]**	**$E_{Region1}$ [kJ mol^{-1}]**	**$E_{Region2}$ [kJ mol^{-1}]**	**Inversion barrier [kJ mol^{-1}]**
Aluminum									
AlH_4^-	*GS*	555.26	-6781.73	-2444.06	-3.44	-8673.97	5158.55	1814.31	
	TS	497.63	-6673.02	-2329.28	-3.63	-8508.30	5158.55	1861.40	
	Δ	-57.63	108.71	114.78	-0.19	165.67	0.00	47.09	212.76
AlF_4^-	*GS*	690.48	-8118.49	-1793.42	-5.25	-9226.68	5158.55	1176.25	
	TS	598.54	-7916.22	-1799.93	-5.30	-9122.91	5158.55	1250.52	
	Δ	-91.94	202.27	-6.51	-0.05	103.77	0.00	74.27	178.04
$AlCl_4^-$	*GS*	522.09	-6365.41	-2069.00	-19.04	-7931.34	5158.55	675.15	
	TS	438.68	-6249.75	-1996.26	-19.04	-7826.36	5158.55	739.34	
	Δ	-83.41	115.66	72.74	0.00	104.98	0.00	64.19	169.17
$AlBr_4^-$	*GS*	469.73	-5515.90	-2448.74	-23.37	-7518.28	5158.55	488.10	
	TS	395.28	-5453.07	-2339.29	-23.23	-7420.29	5158.55	548.62	
	Δ	-74.45	62.83	109.45	0.14	97.99	0.00	60.52	158.51
AlI_4^-	*GS*	410.29	-4733.43	-2751.07	-29.58	-7103.78	5158.55	341.43	
	TS	335.86	-4702.27	-2620.49	-28.88	-7015.74	5158.55	406.85	
	Δ	-74.43	31.16	130.58	0.70	88.04	0.00	65.42	153.46
$Al(OH)_4^-$	*GS*	686.95	-7189.45	-2517.90	-11.30	-9031.70	5158.55	-1114.30	
	TS	597.31	-7067.83	-2455.23	-11.35	-8937.10	5158.55	-1101.21	
	Δ	-89.64	121.62	62.67	-0.05	94.60	0.00	13.09	107.69
$Al(NH_2)_4^-$	*GS*	688.58	-6693.26	-2817.43	-17.08	-8839.19	5158.55	-3049.52	
	TS	598.85	-6609.66	-2766.11	-17.03	-8793.94	5158.55	-2981.70	

	Δ	-89.73	83.60	51.32	0.05	45.25	0.00	67.82	113.07
$Al(CH_3)_4^-$	*GS*	696.38	-6168.76	-3011.99	-19.53	-8503.90	5158.55	-4818.24	
	TS	569.42	-6002.76	-2870.88	-19.38	-8323.61	5158.55	-4792.92	
	Δ	-126.96	166.00	141.11	0.15	180.29	0.00	25.32	205.61
$Al(CN)_4^-$	*GS*	577.59	-6174.99	-2189.99	-16.31	-7803.70	5158.55	-4458.15	
	TS	495.47	-6079.18	-2119.71	-16.08	-7719.49	5158.55	-4379.04	
	Δ	-82.12	95.81	70.28	0.23	84.21	0.00	79.11	163.32
$Al(CCH)_4^-$	*GS*	614.13	-6088.48	-2689.78	-17.78	-8181.92	5158.55	-5103.47	
	TS	550.16	-5807.73	-2758.96	-17.40	-8033.92	5158.55	-5077.94	
	Δ	-63.97	280.75	-69.18	0.38	148.00	0.00	25.53	173.53
Gallium									
GaH_4^-	*GS*	738.26	-7037.85	-2770.10	-3.56	-9073.25	5638.16	1825.19	
	TS	624.71	-6882.89	-2559.09	-3.88	-8821.14	5638.16	1839.51	
	Δ	-113.55	154.96	211.01	-0.32	252.11	0.00	14.32	266.43
GaF_4^-	*GS*	799.17	-8150.40	-1813.11	-5.63	-9169.97	5638.16	1066.99	
	TS	707.86	-7960.77	-1854.69	-5.67	-9113.27	5638.16	1143.81	
	Δ	-91.31	189.63	-41.58	-0.04	56.70	0.00	76.82	133.52
$GaCl_4^-$	*GS*	650.41	-6525.27	-2243.83	-19.29	-8137.97	5638.16	640.49	
	TS	542.82	-6374.73	-2191.02	-19.28	-8042.19	5638.16	697.46	
	Δ	-107.59	150.54	52.81	0.01	95.78	0.00	56.97	152.75
$GaBr_4^-$	*GS*	587.47	-5692.08	-2657.01	-23.42	-7785.03	5638.16	469.30	
	TS	489.03	-5593.32	-2560.91	-23.31	-7688.49	5638.16	522.11	
	Δ	-98.44	98.76	96.10	0.11	96.54	0.00	52.81	149.35
GaI_4^-	*GS*	521.18	-4902.64	-3016.49	-29.42	-7427.38	5638.16	333.54	
	TS	416.73	-4834.91	-2889.14	-28.77	-7336.06	5638.16	390.78	
	Δ	-104.45	67.73	127.35	0.65	91.32	0.00	57.24	148.56
$Ga(OH)_4^-$	*GS*	798.20	-7350.60	-2519.58	-11.84	-9083.82	5638.16	-1199.54	
	TS	707.23	-7203.14	-2511.03	-11.87	-9018.81	5638.16	-1178.91	
	Δ	-90.97	147.46	8.55	-0.03	65.01	0.00	20.63	85.64
$Ga(NH_2)_4^-$	*GS*	818.86	-6845.15	-2936.00	-17.81	-8980.10	5638.16	-3130.24	
	TS	700.69	-6696.46	-2885.14	-17.74	-8898.65	5638.16	-3089.21	
	Δ	-118.17	148.69	50.86	0.07	81.45	0.00	41.03	122.48
$Ga(CH_3)_4^-$	*GS*	896.20	-6453.72	-3252.68	-20.34	-8830.55	5638.16	-4829.55	
	TS	684.33	-6200.89	-3067.38	-20.22	-8604.19	5638.16	-4820.28	
	Δ	-211.87	252.83	185.30	0.12	226.36	0.00	9.27	235.63
$Ga(CN)_4^-$	*GS*	768.68	-6412.60	-2435.39	-16.95	-8096.27	5638.16	-4462.22	
	TS	606.60	-6215.44	-2308.00	-16.78	-7933.61	5638.16	-4413.41	
	Δ	-162.08	197.16	127.39	0.17	162.66	0.00	48.81	211.47
$Ga(CCH)_4^-$	*GS*	813.29	-6344.75	-2923.43	-18.50	-8473.40	5638.16	-5105.79	
	TS	664.40	-6032.89	-2875.02	-18.13	-8261.61	5638.16	-5097.19	
	Δ	-148.89	311.86	48.41	0.37	211.79	0.00	8.60	220.39
Silicon									
SiH_4	*GS*	737.97	-8921.33	-5485.41	-3.61	-13672.37	9928.32	1932.24	
	TS	657.67	-8848.80	-5176.02	-3.82	-13370.97	9928.32	1997.17	
	Δ	-80.30	72.53	309.39	-0.21	301.40	0.00	64.93	366.33
SiF_4	*GS*	1016.43	-11001.48	-4003.78	-5.81	-13994.64	9928.32	1338.11	
	TS	864.90	-10698.48	-3989.83	-5.86	-13829.27	9928.32	1424.79	
	Δ	-151.53	303.00	13.95	-0.05	165.37	0.00	86.68	252.05
$SiCl_4$	*GS*	719.39	-8537.27	-4686.71	-21.11	-12525.70	9928.32	784.71	
	TS	586.58	-8397.88	-4530.00	-21.19	-12362.47	9928.32	865.94	

	Δ	-132.81	139.39	156.71	-0.08	163.23	0.00	81.23	244.46
$SiBr_4$	*GS*	617.57	-7321.35	-5329.08	-26.11	-12058.98	9928.32	560.43	
	TS	505.83	-7264.07	-5126.32	-25.79	-11910.31	9928.32	639.47	
	Δ	-111.74	57.28	202.76	0.32	148.67	0.00	79.04	227.71
SiI_4	*GS*	513.30	-6249.31	-5852.73	-33.01	-11621.75	9928.32	391.72	
	TS	410.62	-6228.53	-5639.55	-32.46	-11489.86	9928.32	475.17	
	Δ	-102.68	20.78	213.18	0.55	131.89	0.00	83.45	215.34
$Si(OH)_4$	*GS*	1010.12	-9574.06	-5361.82	-12.29	-13938.05	9928.32	-984.62	
	TS	852.50	-9419.05	-5201.05	-12.37	-13779.98	9928.32	-967.50	
	Δ	-157.62	155.01	160.77	-0.08	158.07	0.00	17.12	175.19
$Si(CN)_4$	*GS*	840.08	-8364.03	-4820.80	-17.75	-12362.51	9928.32	-4350.18	
	TS	727.85	-8251.69	-4686.32	-17.65	-12227.80	9928.32	-4238.69	
	Δ	-112.23	112.34	134.48	0.10	134.71	0.00	111.49	246.20
$Si(CCH)_4$	*GS*	919.33	-8090.11	-5814.85	-19.49	-13005.13	9928.32	-4983.46	
	TS	828.34	-7483.12	-6050.21	-19.24	-12724.21	9928.32	-5009.98	
	Δ	-90.99	606.99	-235.36	0.25	280.92	0.00	-26.52	254.40
Germanium									
GeH_4	*GS*	933.48	-9213.81	-5373.76	-3.87	-13657.95	10079.28	1897.21	
	TS	790.16	-9080.72	-4990.84	-4.16	-13285.54	10079.28	1926.55	
	Δ	-143.32	133.09	382.92	-0.29	372.41	0.00	29.34	401.75
GeF_4	*GS*	1074.33	-11025.27	-3548.68	-6.22	-13505.85	10079.28	1179.54	
	TS	941.00	-10743.14	-3607.47	-6.28	-13415.89	10079.28	1261.31	
	Δ	-133.33	282.13	-58.79	-0.06	89.96	0.00	81.77	171.73
$GeCl_4$	*GS*	827.88	-8689.39	-4481.38	-21.40	-12364.27	10079.28	706.21	
	TS	685.00	-8505.58	-4391.09	-21.41	-12233.06	10079.28	773.19	
	Δ	-142.88	183.81	90.29	-0.01	131.21	0.00	66.98	198.19
$GeBr_4$	*GS*	718.66	-7509.10	-5165.61	-26.10	-11982.15	10079.28	509.20	
	TS	595.34	-7404.31	-5018.17	-25.92	-11853.02	10079.28	572.99	
	Δ	-123.32	104.79	147.44	0.18	129.13	0.00	63.79	192.92
GeI_4	*GS*	610.26	-6432.21	-5760.76	-32.84	-11615.56	10079.28	357.75	
	TS	490.02	-6369.69	-5582.67	-32.13	-11494.42	10079.28	426.06	
	Δ	-120.24	62.52	178.09	0.71	121.14	0.00	68.31	189.45
$Ge(OH)_4$	*GS*	1072.81	-9802.20	-4823.05	-12.96	-13565.40	10079.28	-1097.24	
	TS	936.87	-9599.68	-4783.03	-13.01	-13458.86	10079.28	-1083.19	
	Δ	-135.94	202.52	40.02	-0.05	106.54	0.00	14.05	120.59
$Ge(NH_2)_4$	*GS*	1102.04	-9169.08	-5481.43	-19.41	-13567.87	10079.28	-3020.00	
	TS	961.08	-9052.14	-5369.98	-19.38	-13480.40	10079.28	-2940.02	
	Δ	-140.96	116.94	111.45	0.03	87.47	0.00	79.98	167.45
$Ge(CH_3)_4$	*GS*	1140.55	-8460.14	-6073.25	-22.27	-13415.12	10079.28	-4789.56	
	TS	874.85	-8179.02	-5757.07	-22.29	-13083.55	10079.28	-4769.43	
	Δ	-265.70	281.12	316.18	-0.02	331.57	0.00	20.13	351.70
$Ge(CN)_4$	*GS*	985.63	-8547.00	-4660.55	-18.80	-12240.71	10079.28	-4401.84	
	TS	811.93	-8347.23	-4488.84	-18.66	-12042.79	10079.28	-4332.41	
	Δ	-173.70	199.77	171.71	0.14	197.92	0.00	69.43	267.35
$Ge(CCH)_4$	*GS*	1077.33	-8384.16	-5548.54	-20.60	-12875.96	10079.28	-5027.74	
	TS	913.81	-7875.80	-5606.15	-20.27	-12588.38	10079.28	-5038.43	
	Δ	-163.52	508.36	-57.61	0.33	287.58	0.00	-10.69	276.89
Phosphorus									
PF_4^+	*GS*	1268.64	-13747.06	-7421.37	-6.39	-19906.18	16955.80	1448.90	
	TS	1047.47	-13356.33	-7363.56	-6.44	-19678.86	16955.80	1541.91	

	Δ	-221.17	390.73	57.81	-0.05	227.32	0.00	93.01	320.33
PCl_4^+	*GS*	850.72	-10635.28	-8757.21	-23.17	-18564.95	16955.80	859.06	
	TS	666.79	-10488.13	-8511.71	-23.35	-18356.37	16955.80	946.54	
	Δ	-183.93	147.15	245.50	-0.18	208.58	0.00	87.48	296.06
PBr_4^+	*GS*	699.13	-9085.28	-9715.33	-28.75	-18130.22	16955.80	605.35	
	TS	551.48	-9042.45	-9428.82	-28.39	-17948.13	16955.80	689.44	
	Δ	-147.65	42.83	286.51	0.36	182.09	0.00	84.09	266.18
PI_4^+	*GS*	556.32	-7747.01	-10539.51	-36.41	-17766.61	16955.80	419.23	
	TS	432.58	-7741.42	-10266.25	-36.03	-17611.05	16955.80	507.96	
	Δ	-123.74	5.59	273.26	0.38	155.56	0.00	88.73	244.29
$P(OH)_4^+$	*GS*	1277.78	-11810.65	-9582.46	-13.33	-20128.67	16955.80	-904.01	
	TS	1032.77	-11646.39	-9285.71	-13.41	-19912.75	16955.80	-879.58	
	Δ	-245.01	164.26	296.75	-0.08	215.92	0.00	24.43	240.35
$P(CH_3)_4^+$	*GS*	1143.26	-9972.01	-11075.44	-22.72	-19926.92	16955.80	-4725.64	
	TS	956.79	-9608.87	-10758.57	-22.90	-19433.56	16955.80	-4706.53	
	Δ	-186.47	363.14	316.87	-0.18	493.36	0.00	19.11	512.47
$P(CN)_4^+$	*GS*	1045.56	-10458.03	-8910.00	-19.45	-18341.92	16955.80	-4280.75	
	TS	908.50	-10314.00	-8767.30	-19.40	-18192.17	16955.80	-4143.89	
	Δ	-137.06	144.03	142.70	0.05	149.75	0.00	136.86	286.61
$P(CCH)_4^+$	*GS*	1185.19	-9922.87	-10540.52	-21.39	-19299.59	16955.80	-4910.29	
	TS	1057.13	-8982.70	-10966.58	-21.21	-18913.34	16955.80	-4999.65	
	Δ	-128.06	940.17	-426.06	0.18	386.25	0.00	-89.36	296.89
Arsenic									
AsF_4^+	*GS*	1278.67	-13837.95	-6094.07	-7.36	-18660.71	16343.67	1252.72	
	TS	1107.39	-13465.01	-6179.29	-7.41	-18544.32	16343.67	1337.96	
	Δ	-171.28	372.94	-85.22	-0.05	116.39	0.00	85.24	201.63
$AsCl_4^+$	*GS*	953.10	-10816.87	-7777.12	-25.37	-17666.25	16343.67	748.67	
	TS	777.28	-10603.32	-7659.63	-25.40	-17511.03	16343.67	820.72	
	Δ	-175.82	213.55	117.49	-0.03	155.22	0.00	72.05	227.27
$AsBr_4^+$	*GS*	802.60	-9303.40	-8791.99	-31.03	-17323.82	16343.67	533.18	
	TS	659.23	-9194.59	-8611.11	-30.76	-17177.19	16343.67	602.79	
	Δ	-143.37	108.81	180.88	0.27	146.63	0.00	69.61	216.24
$As(OH)_4^+$	*GS*	1297.06	-12182.94	-8078.13	-15.26	-18979.28	16343.67	-1036.82	
	TS	1103.79	-11923.62	-8010.81	-15.32	-18845.97	16343.67	-1023.91	
	Δ	-193.27	259.32	67.32	-0.06	133.31	0.00	12.91	146.22
$As(NH_2)_4^+$	*GS*	1329.43	-11415.89	-9059.84	-22.93	-19169.22	16343.67	-2951.44	
	TS	1196.32	-11494.99	-8796.70	-22.91	-19118.25	16343.67	-2810.39	
	Δ	-133.11	-79.10	263.14	0.02	50.97	0.00	141.05	192.02
$As(CN)_4^+$	*GS*	1159.76	-10642.69	-7928.60	-22.96	-17434.50	16343.67	-4366.44	
	TS	979.33	-10428.35	-7764.37	-22.80	-17236.16	16343.67	-4282.84	
	Δ	-180.43	214.34	164.23	0.16	198.34	0.00	83.60	281.94
$As(CCH)_4^+$	*GS*	1320.63	-10357.97	-9312.34	-25.27	-18374.95	16343.67	-4977.70	
	TS	1136.90	-9610.58	-9546.14	-24.93	-18044.73	16343.67	-5016.47	
	Δ	-183.73	747.39	-233.80	0.34	330.22	0.00	-38.77	291.45

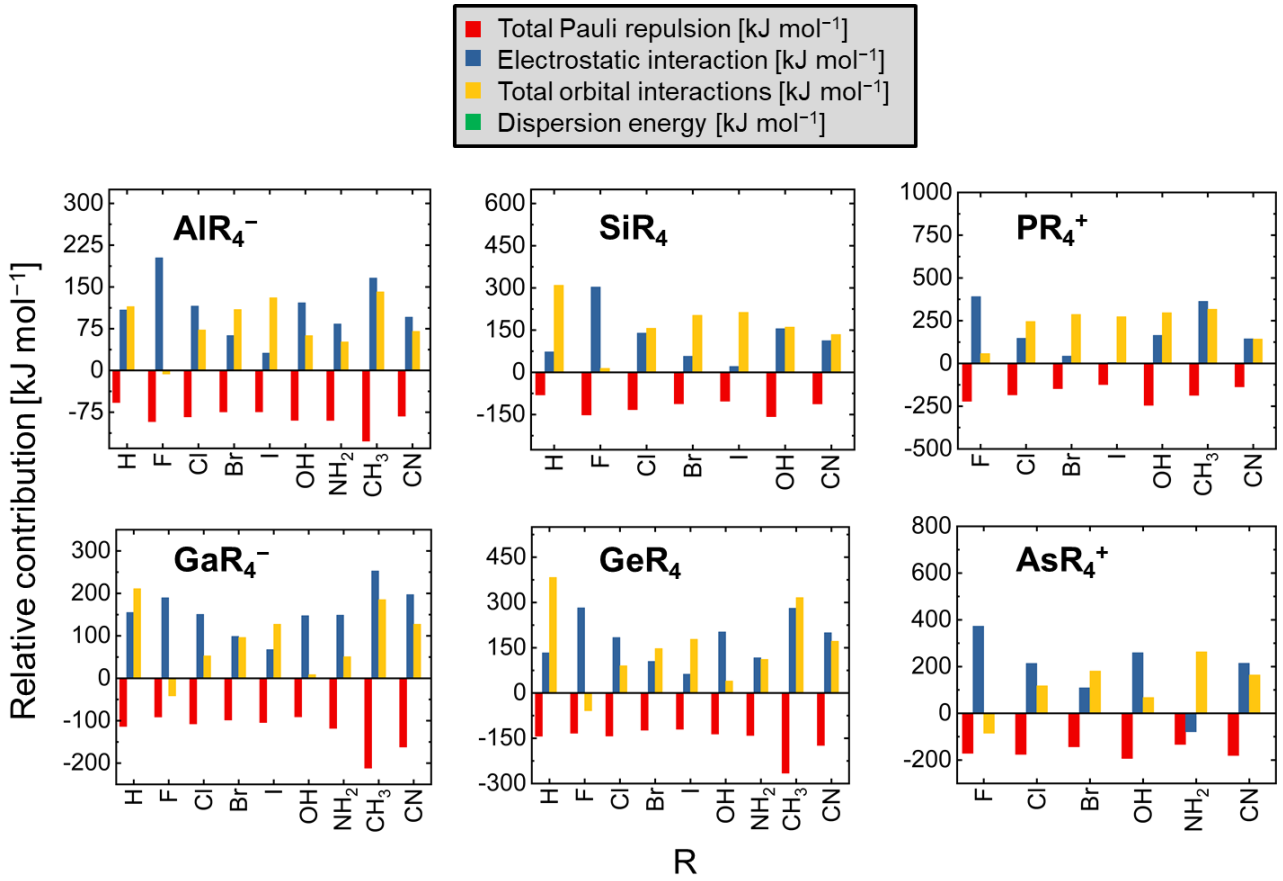

Figure S30: Visualization of the differences (transition state **–** ground state) of the individual components of the interaction energy between region 1 and region 2 (see Figure S29) as obtained by the energy decomposition analyses (Table S12). The contributions of the dispersion energy are too small to be visible in the plots.

Influence of the dissection strategy of the inversion barrier into a radial and an angular contribution

The dissection of the inversion barrier into a radial and an angular portion can be carried out in two different ways when going from the tetrahedral ground to the inversion transition state:

- 1st option: 1) planarization of the system with frozen bond lengths (TS', see Table 2 in the main article) → ***angular part 1***, 2) bond length relaxation → ***radial part 1***
- 2nd option: 1) change of the bond lengths toward those of the transition state (GS' in Table S13) → ***radial part 2***, 2) planarization of the system → ***angular part 2***

We chose the first option and show that both possibilities result in identical conclusions (compare columns six/seven and eight/nine in Table S13). Of note, in all cases of the class of **ER_4^n** compounds a bond elongation occurs when going from the ground to the inversion transition state (see Chapter S4).

Table S13: Results of the energy decomposition analyses (BP86-D3(BJ)/QZ4P) of the ground state (GS), the transition state (TS), a square-planar structure with the bond lengths of the ground state (TS', see Table 2 in the main article), and a tetrahedral structure with the bond lengths of the transition state (GS') of SiH_4 and SiF_4. All numbers are given in kJ mol^{-1}.

	GS	TS'	GS'	TS	Angular 1 (TS' − GS)	Angular 2 (TS − GS')	Radial 1 (TS − TS')	Radial 2 (GS' − GS)	Total (TS – GS)
ΔE_{Pauli}	692.03	709.54	564.28	582.43	17.51	18.15	-127.11	-127.75	-109.60
ΔE_{Coul}	-7847.32	-7807.01	-7831.31	-7795.30	40.31	36.01	11.71	16.01	52.02
ΔE_{Orb}	-6241.34	-6018.76	-6079.89	-5872.73	222.58	207.16	146.03	161.45	368.61
ΔE_{Disp}	-3.61	-3.68	-3.75	-3.82	-0.07	-0.07	-0.14	-0.14	-0.21
ΔE_{Int}	**-13400.24**	**-13119.91**	**-13350.67**	**-13089.42**	**280.33**	**261.25**	**30.49**	**49.57**	**310.82**
$E_{Region2}$	1658.76	1756.17	1619.11	1712.90					

$\Delta\Delta E_{Prep}$					97.41	93.79	-43.27	-39.65	54.14
$\Delta(\Delta E_{Int} + \Delta E_{Prep})$					**377.74**	**355.04**	**-12.78**	**9.92**	**364.96**
ΔE_{Pauli}	957.79	961.89	824.20	831.47	4.10	7.27	-130.42	-133.59	-126.32
ΔE_{Coul}	-10558.30	-10406.27	-10503.38	-10370.15	152.03	133.23	36.12	54.92	188.15
ΔE_{Orb}	-4277.92	-4317.10	-4146.57	-4182.45	-39.18	-35.88	134.65	131.35	95.47
ΔE_{Disp}	-5.81	-5.84	-5.82	-5.86	-0.03	-0.04	-0.02	-0.01	-0.05
ΔE_{Int}	**-13884.24**	**-13767.32**	**-13831.57**	**-13726.99**	**116.92**	**104.58**	**40.33**	**52.67**	**157.25**
$E_{Region2}$	1219.45	1374.23	1170.16	1314.75					
$\Delta\Delta E_{Prep}$					154.78	144.59	-59.48	-49.29	95.30
$\Delta(\Delta E_{Int} + \Delta E_{Prep})$					**271.70**	**249.17**	**-19.15**	**3.38**	**252.55**

Homolytic *versus* heterolytic fragmentation

In addition to the heterolytic fragmentation scheme shown in Figure S29, the corresponding homolytic version was probed for SiH_4 and SiF_4. This was done also with respect to the dissection into a radial and an angular portion (see Table 2 in the main article).

Table S14: Results of the energy decomposition analyses (BP86-D3(BJ)/QZ4P) of the ground state (GS) and the inversion transition state (TS) of SiH_4 and SiF_4 with respect to homolytic or heterolytic fragmentation. Individual angular and radial contributions were derived with help of a D_{4h} symmetric structure with the bond lengths of the ground state (TS', see Table 2 in the main article). All numbers are given in kJ mol^{-1}.

	GS	TS'	TS	Angular contribution (TS' − GS)	Radial contribution (TS − TS')	Total (TS – GS)
SiH_4, homolytic fragmentation						
ΔE_{Pauli}	122.35	102.66	37.15	-19.69	-65.51	-85.20
ΔE_{Coul}	-638.12	-592.56	-554.55	45.56	38.01	83.57
ΔE_{Orb}	-1300.71	-988.06	-956.93	312.65	31.13	343.78
ΔE_{Disp}	-3.61	-3.68	-3.82	-0.07	-0.14	-0.21
ΔE_{Int}	**-1820.09**	**-1481.64**	**-1478.15**	**338.45**	**3.49**	**341.94**
$E_{Region2}$	-328.29	-288.98	-305.26			
$\Delta\Delta E_{Prep}$				39.31	-16.28	23.03
$\Delta(\Delta E_{Int} + \Delta E_{Prep})$				**377.76**	**-12.79**	**364.97**
SiH_4, heterolytic fragmentation						
ΔE_{Pauli}	692.03	709.54	582.43	17.51	-127.11	-109.60
ΔE_{Coul}	-7847.32	-7807.01	-7795.30	40.31	11.71	52.02
ΔE_{Orb}	-6241.34	-6018.76	-5872.73	222.58	146.03	368.61
ΔE_{Disp}	-3.61	-3.68	-3.82	-0.07	-0.14	-0.21
ΔE_{Int}	**-13400.24**	**-13119.91**	**-13089.42**	**280.33**	**30.49**	**310.82**
$E_{Region2}$	1658.76	1756.17	1712.90			
$\Delta\Delta E_{Prep}$				97.41	-43.27	54.14
$\Delta(\Delta E_{Int} + \Delta E_{Prep})$				**377.74**	**-12.78**	**364.96**
SiF_4, homolytic fragmentation						
ΔE_{Pauli}	5994.37	6235.27	5675.81	240.90	-559.46	-318.56
ΔE_{Coul}	-2385.54	-2453.42	-2261.10	-67.88	192.32	124.44
ΔE_{Orb}	-6334.46	-6121.83	-5790.75	212.63	331.08	543.71
ΔE_{Disp}	-5.81	-5.84	-5.86	-0.03	-0.02	-0.05
ΔE_{Int}	**-2731.44**	**-2345.82**	**-2381.90**	**385.62**	**-36.08**	**349.54**

$E_{Region2}$	-340.21	-454.15	-437.21			
$\Delta\Delta E_{Prep}$				-113.94	16.94	-97.00
$\Delta(\Delta E_{Int} + \Delta E_{Prep})$				**271.68**	**-19.14**	**252.54**
SiF_4, heterolytic fragmentation						
ΔE_{Pauli}	957.79	961.89	831.47	4.10	-130.42	-126.32
ΔE_{Coul}	-10558.30	-10406.27	-10370.15	152.03	36.12	188.15
ΔE_{Orb}	-4277.92	-4317.10	-4182.45	-39.18	134.65	95.47
ΔE_{Disp}	-5.81	-5.84	-5.86	-0.03	-0.02	-0.05
ΔE_{Int}	**-13884.24**	**-13767.32**	**-13726.99**	**116.92**	**40.33**	**157.25**
$E_{Region2}$	1219.45	1374.23	1314.75			
$\Delta\Delta E_{Prep}$				154.78	-59.48	95.30
$\Delta(\Delta E_{Int} + \Delta E_{Prep})$				**271.70**	**-19.15**	**252.55**

Fragmentation of one bond *versus* all four bonds

The influence of the chosen fragmentation scheme was considered with regard to whether all four bonds or only one bond is heterolytically dissected during the EDA.

Table S15: Results of the energy decomposition analyses (BP86-D3(BJ)/QZ4P) of the ground state (GS) and the inversion transition state (TS) of SiH_4 and SiF_4 with respect to one bond or four bond fragmentation. All numbers are given in kJ mol^{-1}.

	GS	**TS**	**Total (TS – GS)**
SiH_4, one bond fragmentation			
ΔE_{Pauli}	748.94	995.58	246.64
ΔE_{Coul}	-1124.99	-1112.10	12.89
ΔE_{Orb}	-810.91	-762.14	48.77
ΔE_{Disp}	-1.42	-1.40	0.02
ΔE_{Int}	**-1188.38**	**-880.06**	**308.32**
$E_{Region2}$	-445.99	-389.35	56.64
$\Delta(\Delta E_{Int} + \Delta E_{Prep})$			**364.96**
SiH_4, four bond fragmentation			
ΔE_{Pauli}	692.03	582.43	-109.6
ΔE_{Coul}	-7847.32	-7795.30	52.02
ΔE_{Orb}	-6241.34	-5872.73	368.61
ΔE_{Disp}	-3.61	-3.82	-0.21
ΔE_{Int}	**-13400.24**	**-13089.42**	**310.82**
$E_{Region2}$	1658.76	1712.9	54.14
$\Delta(\Delta E_{Int} + \Delta E_{Prep})$			**364.96**
SiF_4, one bond fragmentation			
ΔE_{Pauli}	769.14	871.27	102.13
ΔE_{Coul}	-1504.84	-1487.90	16.94
ΔE_{Orb}	-587.14	-587.64	-0.50
ΔE_{Disp}	-2.55	-2.46	0.09
ΔE_{Int}	**-1325.39**	**-1206.73**	**118.66**
$E_{Region2}$	-1005.04	-871.19	133.85
$\Delta(\Delta E_{Int} + \Delta E_{Prep})$			**252.51**
SiF_4, four bond fragmentation			
ΔE_{Pauli}	957.79	831.47	-126.32
ΔE_{Coul}	-10558.3	-10370.15	188.15

ΔE_{Orb}	-4277.92	-4182.45	95.47
ΔE_{Disp}	-5.81	-5.86	-0.05
ΔE_{Int}	**-13884.24**	**-13726.99**	**157.25**
$E_{Region2}$	1219.45	1314.75	95.30
$\Delta(\Delta E_{Int} + \Delta E_{Prep})$			**252.55**

S16. References

1. F. Neese, *Wiley Interdiscip. Rev. Comput. Mol. Sci.*, 2012, **2**, 73-78.
2. F. Neese, *Wiley Interdiscip. Rev. Comput. Mol. Sci.*, 2018, **8**, e1327.
3. E. J. Baerends, T. Ziegler, A. J. Atkins, J. Autschbach, D. Bashford, O. Baseggio, A. Brces, F. M. Bickelhaupt, C. Bo, P. M. Boerritger, L. Cavallo, C. Daul, D. P. Chong, D. V. Chulhai, L. Deng, R. M. Dickson, J. M. Dieterich, D. E. Ellis, M. van Faassen, A. Ghysels, A. Giammona, S. J. A. van Gisbergen, A. Goez, A. W. Gtz, S. Gusarov, F. E. Harris, P. van den Hoek, Z. Hu, C. R. Jacob, H. Jacobsen, L. Jensen, L. Joubert, J. W. Kaminski, G. van Kessel, C. Knig, F. Kootstra, A. Kovalenko, M. Krykunov, E. van Lenthe, D. A. McCormack, A. M. Michalak, M., S. M. Morton, J. Neugebauer, V. P. Nicu, L. Noodleman, V. P. Osinga, S. Patchkovskii, M. Pavanello, C. A. Peeples, P. H. T. Philipsen, D. Post, C. C. Pye, H. Ramanantoanina, P. Ramos, W. Ravenek, J. I. Rodrguez, P. Ros, R. Rger, P. R. T. Schipper, D. Schlns, H. van Schoot, G. Schreckenbach, J. S. Seldenthuis, M. Seth and J. G. Snijders, *Journal*, SCM, Theoretical Chemistry, Vrije Universiteit, Amsterdam, The Netherlands, https://www.scm.com, **ADF2019.103**.
4. G. A. Andrienko, *Journal*, https://www.chemcraftprog.com, **Chemcraft 1.8**.
5. S. Grimme, J. Antony, S. Ehrlich and H. Krieg, *J. Chem. Phys.*, 2010, **132**, 154104.
6. S. Grimme, S. Ehrlich and L. Goerigk, *J. Comput. Chem.*, 2011, **32**, 1456-1465.
7. N. Mardirossian and M. Head-Gordon, *J. Chem. Phys.*, 2015, **142**, 074111.
8. A. Najibi and L. Goerigk, *J. Chem. Theory Comput.*, 2018, **14**, 5725-5738.
9. T. H. D. Jr., *J. Chem. Phys.*, 1989, **90**, 1007-1023.
10. D. E. Woon and T. H. D. Jr., *J. Chem. Phys.*, 1993, **98**, 1358-1371.
11. A. K. Wilson, D. E. Woon, K. A. Peterson and T. H. D. Jr., *J. Chem. Phys.*, 1999, **110**, 7667-7676.
12. K. A. Peterson, B. C. Shepler, D. Figgen and H. Stoll, *J. Phys. Chem. A*, 2006, **110**, 13877-13883.
13. F. Neese, A. Hansen and D. G. Liakos, *J. Chem. Phys.*, 2009, **131**, 064103.
14. C. Riplinger and F. Neese, *J. Chem. Phys.*, 2013, **138**, 034106.
15. C. Riplinger, B. Sandhoefer, A. Hansen and F. Neese, *J. Chem. Phys.*, 2013, **139**, 134101.
16. C. Riplinger, P. Pinski, U. Becker, E. F. Valeev and F. Neese, *J. Chem. Phys.*, 2016, **144**, 024109.
17. G. L. Stoychev, A. A. Auer and F. Neese, *J. Chem. Theory Comput.*, 2017, **13**, 554-562.
18. C. Adamo and V. Barone, *J. Chem. Phys.*, 1999, **110**, 6158-6170.
19. F. Weigend and R. Ahlrichs, *Phys. Chem. Chem. Phys.*, 2005, **7**, 3297-3305.
20. L. Zhao, M. von Hopffgarten, D. M. Andrada and G. Frenking, *Wiley Interdiscip. Rev. Comput. Mol. Sci.*, 2018, **8**, e1345.
21. M. v. Hopffgarten and G. Frenking, *Wiley Interdiscip. Rev. Comput. Mol. Sci.*, 2012, **2**, 43-62.
22. T. Ziegler and A. Rauk, *Theor. Chem. Acc.*, 1977, **46**, 1-10.
23. A. D. Becke, *Phys Rev A*, 1988, **38**, 3098-3100.
24. E. Van Lenthe and E. J. Baerends, *J. Comput. Chem.*, 2003, **24**, 1142-1156.
25. E. v. Lenthe, E. J. Baerends and J. G. Snijders, *J. Chem. Phys.*, 1993, **99**, 4597-4610.
26. AIMAll (Version 19.10.12), Todd A. Keith, TK Gristmill Software, Overland Park KS, USA, 2019 (aim.tkgristmill.com)
27. B. O. Roos, P. R. Taylor and P. E. M. Sigbahn, *Chem. Phys.*, 1980, **48**, 157-173.
28. C. Angeli, B. Bories, A. Cavallini and R. Cimiraglia, *J. Chem. Phys.*, 2006, **124**, 054108.
29. C. Angeli, R. Cimiraglia, S. Evangelisti, T. Leininger and J.-P. Malrieu, *J. Chem. Phys.*, 2001, **114**, 10252-10264.
30. C. Angeli, R. Cimiraglia and J.-P. Malrieu, *Chem. Phys. Lett.*, 2001, **350**, 297-305.
31. C. Angeli, R. Cimiraglia and J.-P. Malrieu, *J. Chem. Phys.*, 2002, **117**, 9138-9153.
32. F. Neese and E. F. Valeev, *J. Chem. Theo. Comp.*, 2011, **7**, 33-43.